

ISSN 1913-1844

MODERN APPLIED SCIENCE

Vol. 2, No. 4
July 2008

Editor-in-chief

Daniel Kingst

Managing Editor

Steven Clayer



Canadian Center of Science and Education



Contents

Strength and Setting Times of Low Calcium Fly Ash-based Geopolymer Mortar <i>Djwantoro Hardjito, Chua Chung Cheak & Carrie Ho Lee Ing</i>	3
Experimental Study on Anti-inflammation and Decreasing Pain Effects of Extracts of <i>Periplaneta Americana</i> <i>Xiaoqin Xiao, Shiping Wang, Chen Luo & Xueqin Liu</i>	12
Characterisation of Airborne Particulate Matter in a City Environment <i>Winson Chung, Vida N. Sharifi, Jim Swithenbank, Ogo Osammor & Andy Nolan</i>	17
Manpower Management Benefits Predictor Method for Aircraft Two Level Maintenance Concept <i>Yuanda Wang & Bifeng Song</i>	33
Treatment of Textile Effluent Using Sacrificial Electrode <i>K.Chithra, R.Thilakavathi, A. Arul Murugan, C. Marimuthu & N.Balasubramanian</i>	38
Effects of Microencapsulated Phase Change Materials Granularity and Heat Treat Treatment Condition on the Structure and Performance of Polyurethane Foams <i>Ming You, Xuechen Wang, Xingxiang Zhang & Wei Li</i>	44
Knowledge Extraction from Trained Neural Network Scour Models <i>H. Md. Azamathulla, Aminuddin Ab Ghani, Nor Azazi Zakaria, Chang Chun Kiat & Leow Cheng Siang</i>	52
The Application of the Vector Space Theory to the Limit of Number Sequence <i>Xingxiang Liu & Na Feng</i>	63
Analysis of Heat Transfer Enhancement in Spiral Plate Heat Exchanger <i>Dr. Kaliannan Saravanan & Rangasamy Rajavel</i>	68
The Shapley Value for Stochastic Cooperative Game <i>Ying Ma, Zuofeng Gao, Wei Li, Ning Jiang & Lei Guo</i>	76
Distributed Network in Concave Operating Environment <i>Kam Mun Loong & Gerard Leng</i>	81
Robust Tracking Control of Robot Manipulator Using Dissipativity Theory <i>Hongrui Wang, Zhanfang Feng & Xiuling Liu</i>	95
Forest Road Assessment in Ulu Muda Forest Reserve, Kedah, Malaysia <i>Mohd Hasmadi, I, Kamaruzaman, J. & Muhamad Azizon, J</i>	100
Discussion on Computation of Prestressed Concrete Beam's Bearing Capacity <i>Yingge Wang</i>	109
Study of pH System in Common Effluent Treatment Plant <i>B. Meenakshipriya, Dr.K.Saravanan, R.Shanmugam & S.Sathiyavathi</i>	113
Analysis and Design of Storage Battery Charge/Discharge Equalization Management <i>Jiaqi Wang</i>	122
The Application of MSVC Reactive Power Compensation Device to the High Voltage Power Supply of Coal Mine <i>Zhenbao Zhu & Rui Tian</i>	126
Statistical Perspective and Pollution Indicator in Mengkabong Mangrove Sediment Sabah <i>Miroslav Radojevic, Sarva Mangala Praveena & Mohd Harun Abdullah</i>	131



Contents

Logarithmic Barrier Function Method for Convex Quadratic Programming Problem <i>Xinghua Wang, Wen Liu, Pingping Qin & Lifeng Sun</i>	144
The Properties of Relative Regularity and Compactness <i>Genglei Li & Huidong Wu</i>	148
Determination of Glucose and Fructose from Glucose Isomerization Process by High-performance Liquid Chromatography with UV Detection <i>N.A.Rahman, M.Hasan, M.A.Hussain & J Jahim</i>	151
The Design and Implement of Improvement for Pointer MV-meter Display Mode <i>Yani Gao & Ping Wang</i>	155
Fuzzy Reliability of Two Units of the Cold Storing System <i>Taotao Wang, Xianyun Meng, Yanqin Guan & Jianying Yang</i>	161
Mandible Swing Approach for Excision of Tumors from Parapharyngeal Space <i>Yiwen Ma, Liying Li & Chuanliang Du</i>	167
A Study on the Alteration Tendency of Physical Ability Index and Stress Feature Index of Elite Female Judoists in Intensity Training <i>Ming Chen</i>	171



Strength and Setting Times of Low Calcium Fly Ash-based Geopolymer Mortar

Djwantoro Hardjito, Chua Chung Cheak & Carrie Ho Lee Ing

Department of Civil & Construction Engineering

Curtin University of Technology, Sarawak Campus

CDT 250, 98009, Miri, Sarawak, Malaysia

E-mail: djwantoro.h@curtin.edu.my

Abstract

Geopolymer is a novel binding material produced from the reaction of fly ash with an alkaline solution. In Geopolymer mortar, Portland cement is not utilized at all. In this research, the influence of various parameters on the short term engineering properties of fresh and hardened low-calcium fly ash-based Geopolymer mortar were studied. Tests were carried out on 50 x 50 x 50mm cube Geopolymer mortar specimens. The test results revealed that as the concentration of alkaline activator increases, the compressive strength of Geopolymer mortar also increases. Specimens cured at temperature of 65°C for 1 day showed the highest 28 days compressive strength. The mass ratio of activator/fly ash of 0.4 produced the highest 28 days compressive strength for the specimen. The obtained compressive strength was in the range of 1.6MPa – 20MPa.

Keywords: Geopolymer mortar, Compressive Strength, Setting times

1. Introduction

Portland cement concrete industry has grown astronomically in recent years. It will continue to grow as the result of continuous urban development. However, Portland cement concrete poses problems such as durability and carbon dioxide emission. Many concrete structures have shown serious deterioration, way before their intended service life, especially those constructed in a corrosive environment (Mehta 1997).

Carbon dioxide emission trading is likely to be a critical factor for the construction industry, in particular, the cement and concrete industry. The World Earth Summits in Rio de Janeiro, Brazil in 1992, and Kyoto, Japan in 1997 made it abundantly clear that for long-term sustainability, rate of emission of greenhouse gases to the atmosphere must be prevented from increasing. It has been speculated that one tonne of emission can have a trading value of US\$10 (Malhotra 1999, Malhotra 2004). “Tradeable emissions” refers to the economic mechanisms that are expected to be developed to help countries worldwide meet the stringent emission reduction targets established by the 1997 Kyoto Protocol (Malhotra 1999). The potential trading value after the ratification of Kyoto Protocol is expected to be between US\$20 to US\$30, or more per tonne of carbon dioxide (Malhotra 2002a).

The contribution of ordinary Portland cement production worldwide to greenhouse gas emission is approximately 7% of the total greenhouse gas emission to the atmosphere (Malhotra 2002b). The production of 1 tonne ordinary Portland cement consumes 4GJ energy and produces about 1 tonne of carbon dioxide to the atmosphere (Mehta 2001). About half of the carbon dioxide emissions from Portland cement production are due to calcination of limestone, while the other half are due to combustion of fossil fuel. In the year 1995, the global production of ordinary Portland cement was about 1.4 billion tonne, thus emitting about 1.4 billion tonne of carbon dioxide to the atmosphere (Malhotra 2004).

In 1978, Joseph Davidovits developed Inorganic polymeric materials and coined the term “Geopolymer” for it (1990). Geopolymer has the potential to replace ordinary Portland cement concrete and produce fly ash-based Geopolymer concrete with excellent physical and mechanical properties. Geopolymer is used as the binder to completely replace ordinary Portland cement in producing Geopolymer concrete. In order to produce Geopolymer, low-calcium fly ash needs to be activated by an alkaline solution to produce polymeric Si-O-Al bonds. Geopolymer concrete has the potential to reduce greenhouse emissions from the concrete industry by 80% (Daniel et al 2006).

Many researches have been carried out to study the compressive strength of Geopolymer concrete with different mixing proportion and test variables. However, there are very limited research data on Geopolymer mortar available in the literature. This paper presents the results of a study on the strength and setting times of fly ash-based geopolymer mortar.

2. Past Research on Geopolymer Material

Geopolymer concrete is also known as Alkali-activated concrete or Inorganic polymer concrete. Many researches have been carried out to study the mechanical properties of Geopolymer. From these researches, Geopolymer was shown to possess excellent properties such as a high early strength, low shrinkage, high resistance to freezing and thawing, sulphate attack and corrosion (Davidovits et al 1990, Davidovits 1987, Sofi et al 2006).

Davidovits (1999) conducted researches to investigate the chemical properties of Geopolymers based on silico-aluminates. He used a pure calcined kaolin called KANDOXI (**KA**olinite, **Nac**rite, **Dick**ite **OXI**de) produced from calcinating kaolinitic materials for 6 hours at 750 °C as the source material for geopolymer. A Geopolymer mortar sample (Si/Al ratio = 2) made from PZ-Geopoly ® cement with KANDOXI possesses compressive strength of 20MPa after 4 hours of curing at 20 °C. The final 28 days compressive strength is in the range of 70MPa to 100MPa. From his research, it was discovered that longer curing time will result in higher compressive strength.

In a research conducted by Palomo, Grutzeck, and Blanco (1999), the effects of curing temperature, curing time, the solution / fly ash ratio, and alkali activation of fly ash with high concentration of activator, on the mechanical properties of Geopolymer were studied. Palomo et al. concluded that the amorphous polymer produced in the alkaline activation of metakaolin was a zeolitic precursor. From their research, they concluded that the effect of the activator-fly ash ratio was insignificant and the increase of curing temperature accelerated fly ash activation.

Furthermore, a study was carried out by Alonso and Palomo (2001) to investigate the variables that influences the alkaline activation of metakaolin with the presence of calcium hydroxide. They concluded that the increase in activator solution concentration above 10M induced a delay in the formation of the alkaline polymer due to the stability of ion species and ion mobility, thus resulting in a decrease in flexural strength.

A study was carried out by van Jaarsveld, van Deventer and Lukey (2002) which aimed to investigate the effects of composition of source materials and curing process on the final chemical and physical properties of Geopolymers. They concluded that rapid curing and curing at high temperature resulted in cracking and can impose negative effects on the physical properties of Geopolymer.

A research was conducted by Barbosa, MacKenzie and Thaumaturgo (1999) to study the effects on the polymerization process of the molar composition of the oxides present in the mixture and the water content used. The source material was Kandoxi, which has been prepared by heating kaolinite at 700 °C for 6 hours. In their research, the authors discovered that the optimum formation and curing of sodium poly (sialate-siloxo) polymer occurred when the ratio of Na₂O:SiO₂ was 0.25 and the ratio of H₂O:Na₂O was 10. The sodium content represents a sufficient amount to satisfy the charge balance requirements within the structure, without providing an excess which can form sodium carbonate and may disrupt the polymerization process. The authors claimed that the effect of excess water might be to dilute the reaction or to leach the more soluble components and to transport them away from the reaction zone. The water content of the mixture is also critical for satisfactory polymerization.

Van Jaarsveld, van Deventer, Lukey (2003) conducted a study and stated that the source materials determined the properties of geopolymers especially the CaO content and the water-to-fly ash ratio.

A study was carried out by Daniel, Sanjayan and Sagoe-Crentsil (2006) to study the behavior of fly ash based geopolymer paste and concrete at elevated temperature. In the research, the authors found that when fly ash-to activator ratio decreased, the compressive strength also decreased. The authors found that a longer curing time under elevated temperature did not significantly affect the strength performance of geopolymer paste. The authors drew conclusions that fly ash-to-activator ratio was the most critical parameter for elevated temperature performance following the ratio of sodium silicate-to-potassium hydroxide in activator solution.

3. Experimental Work

Fly ash is the aluminosilicate source material used for the synthesis of geopolymeric binder in this research. In this study, low calcium fly ash (ASTM Class F) from the Sejingkat Power Plant in Kuching, Sarawak, Malaysia was utilized as the source material. The breakdown of the chemical composition of the fly ash as determined by X-Ray Fluorescence (XRF) analysis is shown in Table 1.

The silicon and aluminium oxides constitute 84.6% of the fly ash and the Si to Al molar ratio is 2.06. Davidovits (1999) suggested the molar ratio of Si to Al of about 2 for producing cement and concrete. The fly ash is dark in color which is primarily due to the presence of iron oxide (Fe₂O₃).

A combination of sodium hydroxide solution and sodium silicate solution was used as the alkaline activator. Analytical grade sodium hydroxide in pellets form with 98% purity and sodium silicate with $\text{Na}_2\text{O} = 12\%$, $\text{SiO}_2 = 30\%$, and water = 58% by mass was used in this research. Sodium hydroxide solution was used as alkaline activator because it is widely available and is less expensive than potassium hydroxide solution.

The alkaline activator was prepared in the laboratory. In order to avoid the effect of unknown contaminants, distilled water was used to dissolve the sodium hydroxide pellets. The alkaline activator was prepared by mixing the sodium hydroxide solution with sodium silicate solution together just before the mixing of mortar to ensure the reactivity of solution. The aim of adding sodium silicate is to enhance the formation of Geopolymer precursors or the polymerization process (Xu et al 2000). Locally available fine aggregate (river sand) in saturated surface dry condition was used.

The fly ash and the fine aggregate were first dry mixed together in N50 Hobart Mixer at gear 1 for 2 minutes to ensure homogeneity of the mixture. The Hobart mixer was stopped and the mixture was activated by adding activator solution containing sodium hydroxide and sodium silicate according to the required concentration range of 8 to 16M and mixed for a further 10 minutes. Within the 10 minutes of mixing, the prepared amount of added water was poured into the mixture on two separate times, if necessary. All mixing were conducted in an air conditioned room at temperature of approximately 25 °C. Then, the Geopolymer paste was cast into 50 x 50 x 50 mm cube moulds immediately after mixing in two layers as described in the ASTM C109 standard. Each layer was tamped 25 times with a rod. All the cast specimens were vibrated on a vibrating table for 2 minutes to remove air voids.

All the specimens were transferred to the oven without delay for curing at elevated temperature of 65 °C, 70 °C, and 80 °C for 24 hours. After the oven curing, all the specimens were removed from their moulds and cured undisturbed at room temperature until the day of testing.

The testing method and formulas for volumetric density of Geopolymer mortar was evaluated according to the Archimedes method. The density test was carried out before the compressive test of the specimens.

The Geopolymer mortar specimens were tested for 7, 14, and 28 days compressive strength using the Universal Testing Machine. The specimens were subjected to a compressive force at the rate of 160kN per minute until the specimen failed. The reported strengths were the average results of the three tests.

ASTM Standard C191 for Portland cement paste was modified for measuring the setting times of fly ash-based geopolymer mortar using Vicat needle. The needle used was $1.00 \pm 0.05\text{mm}$ in diameter. In this case, fine aggregates were excluded from the mixture proportion.

The fly ash and activator solution were placed in the mixer bowl. Then, the Hobart mixer was operated at gear 1 for 5 minutes. Within the 5 minutes, the prepared amount of extra water was poured into the mix on two separate times. The Geopolymer paste was cast into the 40 mm height, 80 mm diameter conical mould in two layers. Each layer was tamped with a rod for 25 times.

The specimen was placed into the oven for curing at required elevated temperature, 65 °C, 70 °C, and 80 °C. For every 15 minutes interval, the specimen was placed on the Vicat apparatus to measure the initial setting time. First, the centre of the specimen was placed under the 10mm end of the Vicat needle and the movable rod was lowered until the 1mm needle end makes contact with the Geopolymer paste. The indicator was set to zero. The movable rod was allowed to free fall and the penetration of 1mm needle was recorded. After that, the specimen was returned to the oven for curing at the same elevated temperature.

These procedures were repeated and the penetration for every 15 minutes interval was recorded until a penetration of 25 mm or less was obtained. The time for 25mm penetration was determined by interpolation. This was the initial setting time. The final setting time, defined as the time when the needle did not sink visibly into the Geopolymer paste, was also determined.

4. Results and Discussions

In this section, the experimental results are presented and discussed. Each of the test data points plotted in the figures corresponds to the mean value of the compressive strengths of the three test cubes in a series. The standard deviations are plotted on the test data points as the error bar.

A total of fourteen mixtures were made to study the influence of various parameters on the compressive strength. The details of these mixtures are presented in Table 2. The ratio of sodium silicate to sodium hydroxide solution by mass was 2.5 for all mixture proportion. This ratio was fixed at 2.5 for all mixture because the sodium hydroxide solution is more expensive than the sodium silicate solution. The mass ratio of fine aggregate to fly ash was 2.75 for all mixture.

4.1 Concentration of Sodium Hydroxide Solution

Mixtures 3 to 7 were prepared to study the effects of concentration of sodium hydroxide solution on the compressive strength of Geopolymer mortar. From Figure 1, it was observed that alkaline concentration is proportionate to the

compressive strength of Geopolymer mortar. This is rather unexpected compared to the study conducted by Alonso and Palomo (2001). Their study indicated that when activator concentration increased above 10M, a lower rate of polymer formation was produced resulting in the decrease of flexural strength. This might be due to differences in the type of source materials. Alonso and Palomo (2001) used a high purity metakaolin produced by subjecting the raw kaolin to thermal treatment at 750°C in the air for 24 hours. In contrast, low calcium fly ash (ASTM Class F) was used as the source material in this research. In addition, Alonso and Palomo carried out metakaolin activation in the presence of calcium hydroxide which was not the case in this research.

4.2 Ratio of Alkaline Activator Solution-to-Fly Ash, by Mass

Mixtures 6, 8 and 9 were prepared to study the effects of activator-to-fly ash ratio by mass on the compressive strength of Geopolymer mortar. The concentration of sodium hydroxide solution was fixed at 10M. The curing time was 24 hours at constant curing temperature of 65°C. Figure 3 shows that Mixture 8 with activator-to-fly ash ratio of 0.4 resulted in the highest compressive strength compared to Mixture 6 and Mixture 9.

From Figure 2, it was observed that the optimum activator-to-fly ash ratio is 0.40. As the amount of activator content increases, and consequently increasing the activator-to-fly ash ratio up to 0.40; the compressive strength of geopolymer mortar increases. However, when additional activator content is added, increasing the activator-to-fly ash ratio to 0.45, the compressive strength decreases. This might be due to excess of OH⁻ concentration in the Mixture 9, which will decrease the strength of geopolymer mortar. Excess sodium content can form sodium carbonate by atmospheric carbonation and may disrupt the polymerization process (Barbosa et al 1999).

Palomo, Grutzeck, and Blanco (1999) stated that activator solution-to-fly ash ratio was not a relevant parameter on the compressive strength of geopolymer binder. Current research shows a contradictory result, whereby activator-to-fly ash ratio has influence over the compressive strength of geopolymer mortar. However, this requires further studies to refine the results as the data consist only of three mixtures.

4.3 Curing Temperature

Mixtures 6, 10 and 11 were prepared to study the influence of curing temperature on the compressive strength of Geopolymer mortar. All the other test variables were held constant while the curing temperature varied. The activator-to-fly ash ratio and water-to-geopolymer solids ratio were held constant at 0.35 and 0.324 respectively.

It was observed that the strength increased when the specimens were cured at room temperature of about 25 °C after curing in the oven at elevated temperature for 24 hours. This means that the fly ash activation was incomplete within the introduced curing regime (curing at elevated temperature 65 °C, 70 °C, and 80 °C for 24 hours). From Figure 4, it was observed that the higher curing temperature does not ensure higher compressive strength at 28 days. However, as the curing temperature increases, the early compressive strength increases as well. Figure 4 shows that Mixture 6 cured at 65°C produced the highest compressive strength of 16.1MPa at 28 days. There is a significant increase in the compressive strength at 28 days for Mixture 6 compared to Mixture 10 and Mixture 11. The results shown in Figure 4 indicated that geopolymer mortar cured at curing temperature above 70°C resulted in a decrease in the compressive strength for 24 hours of curing. This results shows that curing temperature plays an important role in the geopolymerisation process of fly ash-based geopolymer mortar.

4.4 Ratio of Water-to-Geopolymer Solids, by Mass

Mixtures 1, 2, 6 and 7 were prepared to study the effects of water-to-Geopolymer solids ratio on the compressive strength of Geopolymer mortar. The total mass of water in the mixture is the sum of the mass of water in the sodium silicate solution, the mass of water in the sodium hydroxide solution and the mass of the extra water. The mass of Geopolymer solids is the sum of the mass of fly ash, the mass of sodium hydroxide solids and the mass of sodium silicate solids (mass of Na₂O and SiO₂ in sodium silicate solution).

Mixtures 1 and 7 have identical mixture composition, but different water-to-Geopolymer solids ratio of 0.273 and 0.333 respectively. The concentration of sodium hydroxide solution was held constant at 8M. The difference is the amount of extra water added to the mixtures. From Figure 5, it was observed that Mixture 1 with lower water-to-geopolymer solids ratio shows higher compressive strength compared to Mixture 7 with higher water-to-geopolymer solids ratio.

Mixtures 2 and 6 have identical mixture composition, but different water-to-geopolymer solids ratio of 0.264 and 0.324 respectively. The concentration of sodium hydroxide solution was held constant at 10M. The difference is the amount of extra water added to the mixtures. From Figure 5, it was observed that Mixture 2 with lower water-to-geopolymer solids ratio shows higher compressive strength compared to Mixture 6 with higher water-to-geopolymer solids ratio.

From Figure 5, Mixture 2 shows higher compressive strength than Mixture 1. Mixture 6 shows higher compressive strength than Mixture 7. This is mainly due to higher concentration of sodium hydroxide solution in Mixtures 2 and 6. As the water-to-Geopolymer solids ratio increases, the compressive strength of geopolymer mortar decreases. The trends of these results were similar to those observed by previous researches (Rangan et al 2006, Barbosa et al 1999,

Hardjito et al 2004). This trend is analogous to the well known effect of water-to-cement ratio on the compressive strength of Portland cement concrete, except that the chemical reaction involved is different.

4.5 Setting Times

The initial and final setting time of Geopolymer is important in practice because it establishes the time available for transport, placing and compaction of Geopolymer. Mixture 6 minus the fine aggregate was used to investigate the setting time of geopolymer paste. The activator-to-fly ash ratio was held constant at 0.35.

The test results on the setting time of geopolymer paste shows that the fresh fly ash based geopolymer mortar could be handled up to 120 minutes without any sign of setting for curing temperature ranging from 65 °C to 80 °C. Similar results were obtained by previous research conducted by Hardjito et. al (2004). Furthermore, it was observed that fresh fly ash-based geopolymer paste did not harden at room temperature for at least one day. From Figures 6 to 8, it is obvious that the geopolymer mortar setting time is much faster when curing temperature increases. This might be due to the increase in curing temperature, which will also increase the rate of chemical reaction.

The initial and final setting time of geopolymer paste at curing temperature of 65 °C was 230 minutes and 270 minutes respectively. The geopolymer paste needed 40 minutes to reach final setting time after the initial setting time. The initial and final setting time of geopolymer paste at curing temperature of 70 °C was 177 minutes and 240 minutes respectively. The geopolymer paste needed 63 minutes to reach final setting time after the initial setting time. The initial and final setting time of geopolymer mortar at curing temperature of 80 °C was 129 minutes and 165 minutes respectively. The geopolymer paste needed 36 minutes to reach final setting time after the initial setting time.

Wang and Cheng (2003) conducted a research to fabricate a coal fly ash based geopolymer for fire resistance purposes. They found that the initial and final setting time of geopolymer paste at curing temperature of 60 °C were 60 minutes and 65 minutes respectively. However, it should be noted that the source material used was metakaolinite which was prepared by calcining kaolinite at 750 °C for 6 hours following the methods proposed by Davidovits (1999). The different source of material yielded different test results compared to the current research (Van Jaarsveld et. al. 2003). Another research conducted by Cheng (2003) to produce a waste serpentine-based geopolymer for fire resistance purpose showed that the initial and final setting time at curing temperature of 60 °C was 79 minutes and 89 minutes respectively. In this research, the initial and final setting time of geopolymer mortar is longer than those reported by Wang and Cheng (2003) and Cheng (2003).

From the test results, it can be concluded that the higher the curing temperature, the higher the rate of geopolymerization process of geopolymer mortar, which eventually accelerates the hardening of Geopolymer mortar.

5. Conclusions

This paper presented the study of geopolymer mortar cured in elevated temperature. From the experimental results reported in this paper, the following conclusions are drawn:

- a) Higher concentration of sodium hydroxide solution results in a higher compressive strength of geopolymer mortar.
- b) The activator-to-fly ash ratio, by mass of 0.40 produced the highest compressive strength.
- c) Curing temperature plays an important role in the geopolymerization process.
- d) As the ratio of water-to-geopolymer solids by mass increases, the compressive strength of geopolymer mortar decreases.
- e) The setting time of Geopolymer mortar due to different curing temperature has been determined. The initial setting time and final setting time ranged from 129 minutes to 270 minutes. The higher the curing temperature, less setting time is required.

References

- Alonso S. and A. Palomo, (2001) *Alkaline Activation of Metakaolin and Calcium Hydroxide Mixtures: Influence of Temperature, Activator Concentration and Solid Ratio*, Material Letters, 47 (1-2): p. 55-62.
- Barbosa, V.F.F., K.J.D. MacKenzie and C. Thaumaturgo, (1999) *Synthesis and Characterisation of Sodium Polysialate Inorganic Polymer Based on Alumina and Silica*, Geopolymer'99 International Conference, France.
- Daniel K., Sanjayan J. and Sagoe-Crentsil K., (2006) *The Behaviour of Geopolymer Paste and Concrete at Elevated Temperatures*, International Conference on Pozzolan, Concrete and Geopolymer, Khon Kaen, Thailand, p. 105 – 118.
- Davidovits J. Comrie D.C., Paterson J.H., and Ritcey D.J., (1990) *Geopolymeric Concretes for Environmental Protection*, ACI Concrete International, 12 (7): p. 30-40.
- Davidovits J., (1987) *Ancient and Modern Concretes: What is the real difference?*, ACI Concrete International, 9(12): p. 23-29.

- Davidovits, J., (1999) *Chemistry of Geopolymeric Systems, Terminology*, Geopolymer'99 International Conference, France.
- Hardjito, D., S.E. Wallah, D.M.J. Sumajouw and B.V. Rangan, (2004) *On the Development of Fly Ash-Based Geopolymer Concrete*, ACI Material Journal, pp. 467-472.
- Malhotra V.M., (2002) *High-Performance High Volume Fly Ash Concrete*. ACI Concrete International, 24 (7): p. 1-5.
- Malhotra V.M., (2002) *Introduction: Sustainable Development and Concrete Technology*, ACI Concrete International, 24 (7): p. 22.
- Malhotra V.M., (1999) *Making Concrete "Greener" With Fly Ash*, ACI Concrete International, 21 (5): p. 61-66.
- Malhotra V.M., (2004) *Role of Supplementary Cementing Materials and Superplasticisers in Reducing Greenhouse Gas Emissions*, ICFRC, Chennai, India: Allied Publishers Private Ltd.
- Mehta P.K., (1997) *Durability – Critical Issues for the Future*, ACI Concrete International, 19 (7): p. 27-33.
- Mehta, P.K., (2001) *Reducing the Environmental Impact of Concrete*, ACI Concrete International, 23 (10): p. 61-66.
- Palomo A., M.W. Grutzeck, and M.T. Blanco, (1999) *Alkali-Activated Fly Ashes, A Cement for the Future*, Cement and Concrete Research, 29 (8): p. 1323-1329.
- Rangan, B.V., S. Wallah, D. Sumajouw and D. Hardjito, (2006) *Heat-cured, Low Calcium Fly Ash-based Geopolymer Concrete*, The Indian Concrete Journal, pp. 47-52.
- Sofi, M., J.S.J. Van Deventer, P.A. Mendis, G.C. Lukey, (2006) *Engineering Properties of Inorganic Polymer Concretes*, Cement and Concrete Research.
- van Jaarsveld J.G.S., J.S.J. van Deventer and G.C. Lukey, (2002) *The Effect of Composition and Temperature on the Properties of Fly Ash and Kaolinite-based Geopolymers*, Chemical Engineering Journal, 89 (1-3): p. 63-73.
- van Jaarsveld, J.G.S., J.S.J. van Deventer, G.C. Lukey, (2003) *The Characterisation of Source Materials in Fly Ash-based Geopolymers*, Materials Letters, 57 (7), p. 1272-1280.
- Xu, H. and J.S.J. van Deventer, (2000) *The Geopolymerisation of Alumino-silicate Minerals*, International Journal of Mineral Processing, 59 (3): p. 247-266.

Table 1. Chemical Composition of Fly Ash as determined by XRF

Oxides	Mass (%)
SiO ₂	59.9
Al ₂ O ₃	24.7
Fe ₂ O ₃	6.3
SiO ₂ + Al ₂ O ₃ + Fe ₂ O ₃	90.8
CaO	2.0
MgO	1.9
TiO ₂	1.0
K ₂ O	2.9
Na ₂ O	0.3
SO ₃	0.1
Loss on Ignition (1000 °C)	0.3

Table 2. Details of mixtures

Mixture No.	Fine Aggregate (kg/m ³)	Fly Ash (kg/m ³)	Sodium Silicate Solution (kg/m ³)	Sodium Hydroxide Solution		Super-plasticiser (kg/m ³)	Added Water (kg/m ³)	Curing Temperature (°C)	Curing Time Hours
				Mass kg/m ³	Concentration				
1	1173	909	228	90	8M		89	65	24
2	1173	909	228	90	10M		89	65	24
3	1173	909	228	90	16M		151	65	24
4	1173	909	228	90	14M		151	65	24
5	1173	909	228	90	12M		151	65	24
6	1173	909	228	90	10M		151	65	24
7	1173	909	228	90	8M		151	65	24
8	1128	909	261	103	10M		151	65	24
9	1082	909	293	116	10M		151	65	24
10	1173	909	228	90	10M		151	70	24
11	1173	909	228	90	10M		151	80	24
12	1173	909	228	90	10M	6.2	151	65	24
13	1173	909	228	90	16M		151	65	48
14	1173	909	228	90	10M		151	60	24

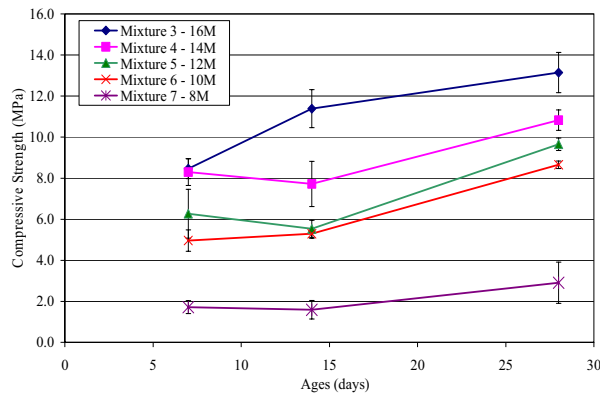


Figure 1. Effect of Concentration of Alkaline Activator on Compressive Strength

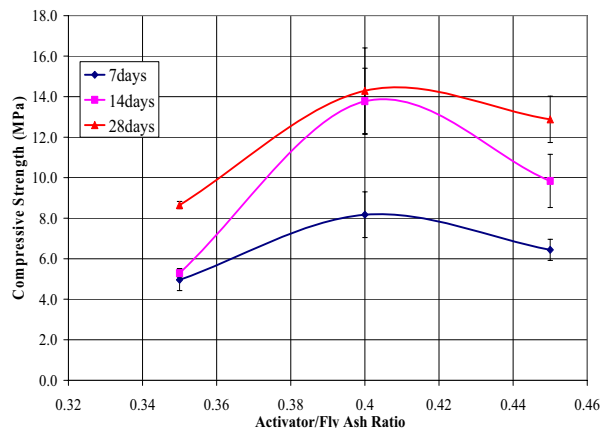


Figure 2. Optimum Activator-to-Fly Ash Ratio

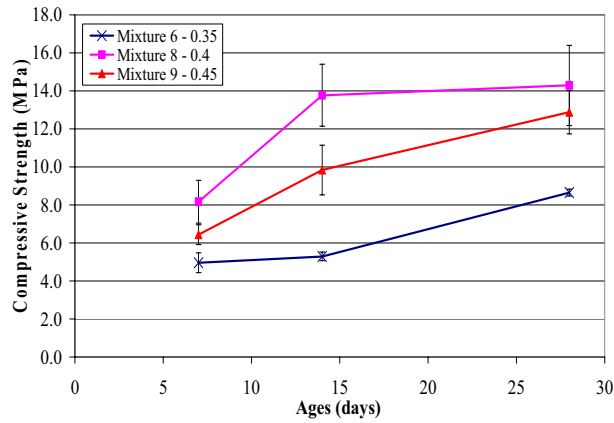


Figure 3. Effect of Activator-to-Fly Ash Ratio on Compressive Strength

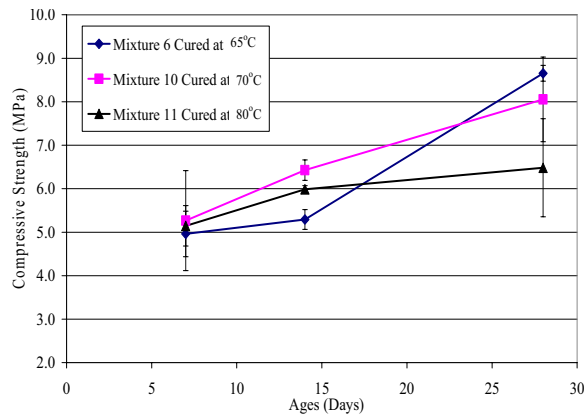


Figure 4. Effect of Curing Temperature on Compressive Strength

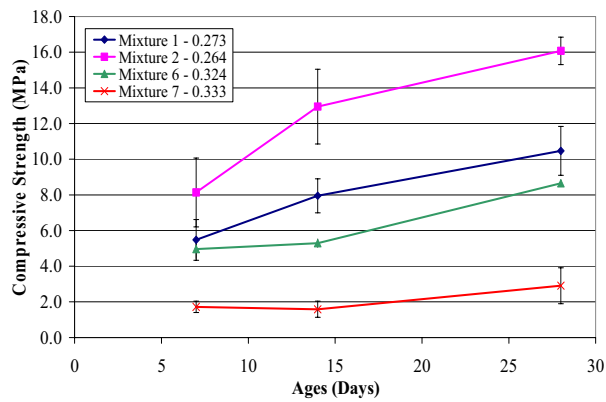


Figure 5. Effect of Water-to-Geopolymer Solids Ratio on Compressive Strength

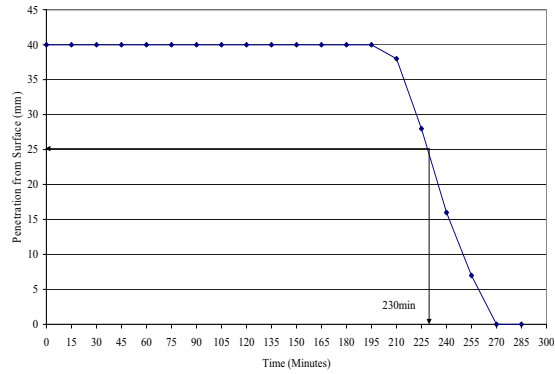


Figure 6. Initial and Final Setting Time of Geopolymer Paste at Curing Temperature of 65oC

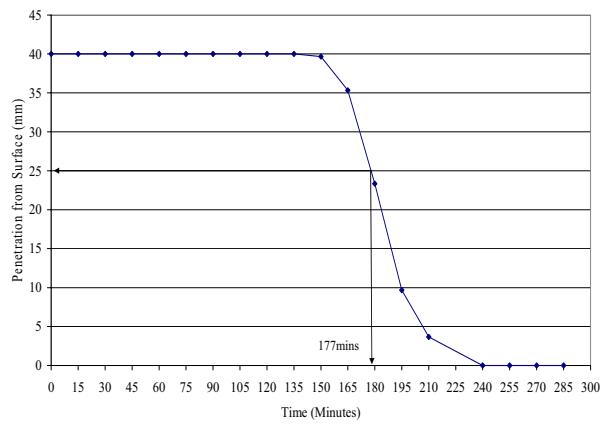


Figure 7. Initial and Final Setting Time of Geopolymer Paste at Curing Temperature of 70oC

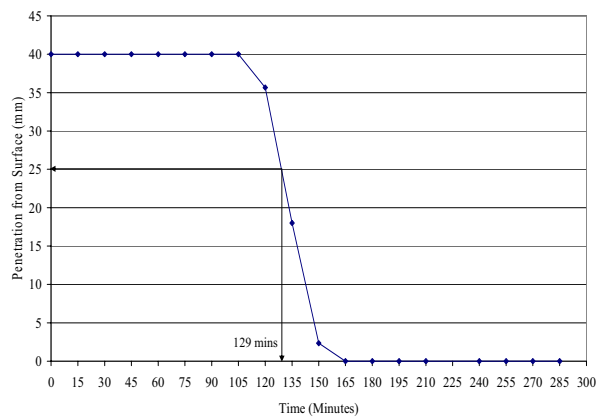


Figure 8. Initial and Final Setting Time of Geopolymer Paste at Curing Temperature of 80oC



Experimental Study on Anti-inflammation and Decreasing Pain Effects of Extracts of *Periplaneta Americana*

Xiaoqin Xiao

Department of Pathogenic Biology, College of Xiangya Basic Medicine

Central South University, Changsha 410078, China

Shaoyang Medical College, Shaoyang 422000, China

E-mail: xiaoxiaoqin@hnsyyz.cn

Shiping Wang

Department of Pathogenic Biology, College of Xiangya Basic Medicine

Central South University, Changsha 410078, China

Chen Luo

Shaoyang Medical College, Shaoyang 422000, China

Xueqin Liu

Department of Pathogenic Biology, College of Xiangya Basic Medicine

Central South University, Changsha 410078, China

Abstract

To investigate the effects of extracts of *Periplaneta Americana* on anti-inflammation and decreasing pain, inhibitive effects of the extracts were investigated in different inflammatory models, for instance, cotton induced-granuloma tissue proliferous inflammation of mice, egg white induced rat paw edema, stress gastric ulcer of rats, acetic acid induced writhing response of mice, and hot metal board induced-pain of mice. Results showed that extracts of *Periplaneta Americana* played important roles in anti-inflammation induced by tumefaction, effusion and hyperplasia, and in decreasing pain. There was obviously statistical difference as compared with control group. It can be concluded that extracts of *Periplaneta Americana* are indeed worthy of further development for potential medicinal value.

Keywords: *Periplaneta americana*, Extracts, Anti-inflammation, Decreasing pain

Periplaneta americana is an insect belonging to *Blattidae*, *Periplaneta*. Its medicinal value was firstly recorded in Shen Nong Ben Cao Jing, "it was salty and cold, lived in rivers and swamps, it could cure blood stasis, cold and heat, destroyed accumulation and cured hypopharynx numbness". It was also recorded in Xin Xiu Ben Cao, Ben Cao Gang Mu, etc. Ben Cao Gang Mu recorded that, firstly, burnt the cockroach dead with boiled water, then dried them by sunshine or roasting, the whole insect could be used as medicine, it had the effect of reliving blood stasis, detoxification and curing malnutrition, inducing diuresis and removing edema, and so on (Li, 2000). Modern medical monograph recorded that cockroach had the effects of "promoting blood circulation, removing blood stasis, eliminating accumulation, curing malnutrition, detoxification, diuresis and detumescence", it could be used to cure furuncle, carbuncle and bite of snake and insect (Group of Medicinal Fauna of China, 1983). In this paper, the breeding *Periplaneta Americana* was used to prepare water extracts, then the extracts' effect of anti-inflammation and decreasing pain were studied in mouse and rat. This study will provide reference for the further study and development of *Periplaneta Americana*.

1. Materials and methods

1.1 Materials

1.1.1 Experimental animals

Kunming mouse, weight, 20-30 grams, female: male, 1:1; Sprague-Dawley (SD) rat, weight, 180-260 grams, female: male, 1:1. All the animals were provided by Department of Experimental Zoology, College of Xiangya Basic Medicine, Central South University.

1.1.2 Reagent and medicine

Nabumetone, Tianjin Smith Kline & French Laboratories Ltd; Cimetidine, Hencer Pharmacy, Aspirin, Hunan Xiangyao

Pharmaceutical co., Ltd.

1.2 Methods

1.2.1 Preparation and dosage of *Periplaneta Americana* extracts

The first generation and second generation of adult *Periplaneta Americana*, coming from pathogenic laboratory of College of Xiangya Basic Medicine, Central South University, were used in the experiment. Adult *Periplaneta Americana* that were less than one month old were transferred to a separated aquarium, they were fed with water but no food for five to six days to defecate the extrinsic factors of intestine, and then kept at -20°C in refrigerator for 30 min to be killed. The wing, feet and antenna of *Periplaneta Americana* were removed and the left part was briefly washed in 75% ethanol to eliminate the external microbes, after that the *Periplaneta Americana* was washed with distilled water for three times, and air dried. After weighing the weight, the *Periplaneta Americana* was put in the mortar in ice bath and whetted for 30 min, and then kept at -20°C for 30 min, the whetting and freezing were repeated for several times until the insects were completely whetted.

Added two volumes 0.02 M PBS (pH 7.4) (Xie, et al., 2003) to the whetted insects and mixed thoroughly, put them at 4°C for 6 hours, mixed them at intervals, then centrifuged at 3000 rpm for 30 min, the supernatant was the extracts of *Periplaneta Americana*, including proteins, polysaccharid and small molecular substances. The dosages of extracts were 125 mg/kg (low dosage group) and 250 mg/kg (high dosage group). The dosage of physiological salt is the same as that of medicine.

1.2.2 The influence of extracts on cotton induced-granuloma tissue hyperplasia of mice (Pan, et al., 2003)

40 Kunming mice, each was sterilized on the skin of back, the midline skin was cut with an ophthalmic scissors, and cut was inserted a blunt forceps toward the neck to isolate the skin and the tissue under the skin, resulting in a 1.5 cm space, then a gobbet of absorbent cotton was put under the skin, and then the cut was sewed. After 24 hours, the mice were separated into 4 groups; one gastric perfusion with extracts, Nabumetone and physiological salt water was done from the mouth every day, totally four times. 24 hours after the last gastric perfusion, mice were killed by breaking the neck. Cut the dorsal skin of the mice, and carefully peel off the granuloma tissue, weighed the wet weight of granuloma and observed the hyperplasia situation of granuloma in each group. Calculated the inhibition rate of the tested substance on granuloma tissue hyperplasia.

1.2.3 The influence of extracts on egg white induced rat paw edema (Huang, et al., 2004)

40 Kunming mice were randomly separated into four groups, one gastric perfusion with medicine or physiological salt water was done from the mouth every day, totally four times. 30 min after the last gastric perfusion, mice were firstly etherized with aether, and then their paws were injected with newly prepared 10 mL 10% egg white. During the injection, the hind leg was put straight, the pinhead was inserted into the tissue under the skin in the middle of paw, part of the egg white was injected upwards, and part of them was injected downwards. The thickness of paw was measured with micrometer calipers at 0 hour after injection and 1 hour after injection (the peak of edema) at the same position. Recorded the time needed to reach the peak and the time for the fade away of peak. The variation of paw thickness compared with that at 0 hour was used to indicate the edema degree. The inhibition rate of tested substance on paw edema was calculated.

1.2.4 The inhibition of extracts on stress gastric ulcer of rats (Lehmann and Stalder, 1998)

40 rats were randomly divided into four groups; one gastric perfusion with medicine or physiological salt water was done from the mouth every day, totally four times. Two days after gastric perfusion, rats were fed with water but no food, and kept in a special iron cage to restrict its free movement, or rats could be gently etherized with aether and fixed by binding its four limbs to wire netting to restrict its free movement, then the rat were vertically soaked into 4°C water with its head upward, until the water comes to the xiphisternum. After 2 hours, the rats were killed by breaking their necks or decollation. Opened the abdominal cavity, ligated the pylorus and took out the whole stomach, injected 10 mL 10% formalin and then soaked the stomach in 10% formalin to fix the interior and exterior layers of the stomach. Cut the stomach along the greater curvature, washed the content inside the stomach with tap water and spread out the stomach on a glass board, cleaned the blood streak on the stomach lining, observed the damage of stomach lining, measured the length of damaged stomach lining under the anatomical microscope to establish the ulcer index, specifically, if the length of the damaged stomach lining was longer than 1mm, each millimeter would be 1 point, if the width was longer than 1mm, it would get double points, and if both the length and width were less than 1mm, it would get 0.5 point. The total points would be the ulcer index of the rat, and then the ulcer inhibition rate was calculated.

1.2.5 The influence of extracts on acetic acid induced writhing response of mice (Xu, et al., 1991)

40 Kunming mice were randomly separated into four groups, one gastric perfusion with medicine or physiological salt water was done from the mouth every day, totally four times. 2 hours after the last gastric perfusion, injected 0.2 mL 0.6% acetate acid into the abdominal cavity, observed the writhing response times within 20 min, calculated the

inhibition rate.

1.2.6 The influence of extracts on hot metal board induced-pain of mice

40 Kunming mice were randomly separated into four groups, firstly numbered the mice, kept the temperature of mental board at $55\pm 0.5^{\circ}\text{C}$ and the room temperature at $15-18^{\circ}\text{C}$, put the mice on the mental board, observed the time for mice to lick their feet for the first time, and determine the basic pain threshold. Then fed the mice normally, and gave one gastric perfusion with medicine or physiological salt water from the mouth every day, totally four times, tested the pain threshold of mice 1 hour, 2 hours 3 hours and 4 hours after the fourth gastric perfusion, recorded the variation of pain threshold.

2. Results

2.1 The influence of extracts on cotton induced-granuloma tissue hyperplasia of mice

As shown in table 1 that the extracts of *Periplaneta Americana* could inhibit the cotton induced-granuloma tissue hyperplasia of mice, it had statistical significance compared with the control ($P<0.01$ or $P<0.05$). The high dosage group showed more obvious effect, indicating that the anti-inflammation effect had positive correlation with dosage of medicine within a certain extent.

2.2 The influence of extracts on egg white induced rat paw edema

It can be seen from table 2 that the high dose group and low dose group showed significant inhibition on the egg white induced rat paw edema of mice, inhibition rate were 48.54% and 54.04% respectively, which were higher than the inhibition rate of Nabumetone (45.78%). And there was significant difference compared with the control group ($P<0.01$).

2.3 The inhibition of extracts on stress gastric ulcer of rats

As shown in table 3 that the extracts had significant effect to inhibit the stress gastric ulcer of rats, moreover, the inhibition rate had correlation with the concentration of extracts, there was statistic significance compared with the control group ($P<0.01$ or $P<0.05$).

2.4 The influence of extracts on acetic acid induced writhing response of mice

After injected with certain amount of acetic acid, the visceral layer and parietal layer of mice would be stimulated, accordingly induce long time phlogistic pain and writhing response, for example, the abdominal wall would sink, the trunk and hind limbs would extend, and the buttocks would rise. Table 4 showed that the extracts of *Periplaneta Americana* could effectively reduce acetic acid induced pain of mice, the writhing times were significantly reduced, and showed statistical significance ($P<0.01$).

2.5 The influence of extracts on hot metal board induced-pain of mice

As shown in table 5 that the extracts of *Periplaneta Americana* could increase the pain threshold of mice, and the effect was the best 2 to 3 hours after taking the medicine. Compared with the basic pain threshold, it had statistical significance, and the effect of decreasing pain was better than that of aspirin.

3. Discussion

The anti-inflammation effects and decreasing pain of extracts of *Periplaneta americana* were studied in animals. Results showed that extracts of *Periplaneta americana* had the effect of anti-inflammation induced by tumefaction, effusion and hyperplasia, and had the effect of decreasing pain. Preliminary tissue pathological observation also supported the anti-inflammation and decreasing pain effects of extracts of *Periplaneta Americana*.

The extract of *Periplaneta Americana* is complex, study shows that it contains protein, polysaccharid, and soluble small molecular substances. Which ingredient functions in the anti-inflammation and decreasing pain is still unclear, but there is no doubt that the *Periplaneta Americana* is a potential resource for anti-inflammation and decreasing pain medicine, further study should be carried out.

References

- Group of Medicinal Fauna of China. (1983). *Medicinal Fauna of China*, book II [M]. Tianjin, Tianjin Science & Technology Publishing House. 93.
- Huang, Lei. Wen, Changfan and Li, Jieliang. (2004). Experimental studies on effects of Sini Granule with additives on anti-inflammation and immunity [J]. *Chinese Journal of Information on Traditional Chinese Medicine*. 11 (2). 120-122.
- Lehmann F S and Stalder G A. (1998). Hypotheses on the role of cytokines in peptic ulcer disease [J]. *Clin Invest*. 28: 511-519.
- Li, Shizhen. (2000). *Ben Cao Gang Mu* [M]. Beijing, People's Medical Publishing House. 1010.
- Pan, Jingqiang. Liu, Huichun. Han, Chao et al. (2003). Pharmacological studies of Yinqiaosan Concentrated Tea Bag on

anti-inflammation, defervescence, acesodyne, bacteriostasis and antiviral [J]. *Guangdong Pharmaceutical Journal*. 13 (1). 359-366.

Xie, Jiangbi. He, Weiguo. Weng, Ning et al. (2003). Extraction and isolation of the anti-tumor protein components from earthworm (*Eisenia fetida andrei*) and the anti-tumor activity [J]. *Chinese Journal of Biochemistry and Molecular Biology*. 19 (3). 359-366.

Xu, Shuyun. Bian, Ruliang and Chen, Xiu. (1991). Methodology of Pharmacological Experiment [M]. Shanghai, Shanghai Science & Technology Press. 528-535.

Table 1. The influence of extracts of *Periplaneta Americana* on cotton induced-granuloma tissue hyperplasia of mice

Group	Dose (mg/kg)	Number of mice	Granuloma Wet weight	Inhibition rate (%)
Low dosage group	125	10	432.73±42.13	15.04
High dosage group	250	10	401.21±35.76	21.22
Nabumetone group	250	10	413.62±28.83	18.79
Physiological salt water group		10	509.32±108.44	

Table 2. The influence of extracts of *Periplaneta Americana* on egg white induced rat paw edema

Group	Number of mice	Dose (mg/kg)	Edema rate (mm)	Inhibition rate (%)
Low dosage group	10	125	8.97±3.58	48.54
High dosage group	10	250	8.01±5.69	54.04
Nabumetone group	10	250	9.45±2.04	45.78
Physiological salt water group	10		17.43±6.34	

Table 3. The influence of extracts of *Periplaneta Americana* on stress gastric ulcer of rats

Group	Number of mice	Dose (mg/kg)	Ulcer index	Inhibition rate (%)
Low dosage group	10	125	34.5±3.34	26.91
High dosage group	10	250	26.2±2.20	44.49
Cimetidine group	10	250	24.8±2.09	47.46
Physiological salt water group	10		47.2±1.61	

Table 4. The influence of extracts on acetic acid induced writhing response of mice

Group	Number of mice	Dose (mg/kg)	Writhing times in 15 minutes	Inhibition rate (%)
Low dosage group	10	125	24.25±15.53	44.06
High dosage group	10	250	22.52±11.21	48.05
Aspirin group	10	100	21.63±14.36	50.10
Physiological salt water group	10		43.35±11.34	

Table 5. The effect of extracts of *Periplaneta Americana* in decreasing hot metal board induced-pain of mice

Group	Low dosage group	High dosage group	Aspirin group	Physiological salt water group
Dose(mg/kg)		250	125	
Basic pain threshold	17.52±3.5	18.53±4.9	17.26±2.3	18.36±4.5
Pain threshold after 1 hour	28.53±3.9	29.32±7.4	27.47±4.1	15.38±5.6
Percent Increased (%)	62.8	58.2	59.2	
Pain threshold after 2 hours	41.56±2.7	42.54±2.5	38.68±6.2	18.33±5.2
Percent Increased (%)	137.2	129.6	124.1	
Pain threshold after 3 hours	43.26±4.3	45.37±7.9	42.26±4.9	19.31±4.3
Percent Increased (%)	146.9	144.9	144.8	
Pain threshold after 4 hours	31.34±7.3	33.24±6.8	27.75±6.7	23.52±3.7
Percent Increased (%)	78.9	79.4	60.8	



Characterisation of Airborne Particulate Matter in a City Environment

Winson Chung (Corresponding author)

Sheffield University Waste Incineration Centre (SUWIC)

Department of Chemical & Process Engineering, The University of Sheffield

Mappin Street, S1 3JD, United Kingdom

Tel: 44-7949-300-101 E-mail: W.Chung@shef.ac.uk

Vida N. Sharifi

Sheffield University Waste Incineration Centre (SUWIC), Department of Chemical & Process Engineering, The University of Sheffield

Mappin Street, S1 3JD, United Kingdom

Tel: 44-114-222-7518 E-mail: v.n.sharifi@shef.ac.uk

Jim Swithenbank

Sheffield University Waste Incineration Centre (SUWIC), Department of Chemical & Process Engineering, The University of Sheffield

Mappin Street, S1 3JD, United Kingdom

Tel: 44-114-222-7518 E-mail: j.swithenbank@shef.ac.uk

Ogo Osammor

Environmental Strategy, Environmental & Regulatory Services, Sheffield City Council

2-10 Carbrook Hall Road, Sheffield, S9 2DB, United Kingdom

Tel: 44-114-273-4655 E-mail: Ogo.Osammor@sheffield.gov.uk

Andy Nolan

Environmental Strategy, Environmental & Regulatory Services, Sheffield City Council

2-10 Carbrook Hall Road, Sheffield, S9 2DB, United Kingdom

Tel: 44-114-273-4655 E-mail: Andy.Nolan@sheffield.gov.uk

The research is financed by the Engineering and Physical Sciences Research Council Pollutants in the Urban Environment (PUrE) Ref: EP/C532651/2.

Abstract

Airborne particulate matter contains a mixture of pollutants. Identifying the source of these particles, their composition and physical/chemical properties would help to provide a clear connection between their impacts on the environment and the human health. Individual particles have a different chemical morphology and this data could provide information on the formation and reaction mechanism of these particles. It also helps to identify the source they originate from as well as their atmospheric history. Over the years, numerous studies have been conducted to characterise PM₁₀ and little work has been carried out on PM_{2.5}. However, there is an emerging interest in identifying the effects of very fine particles such as nano-particles.

The main objective of this research project was to carry out a comprehensive characterisation study of nano-particles

collected from a city environment. Environmental monitoring samples from a local authority monitoring site were collected over a period of 7 months using a tapered element oscillating microbalance technique (TEOM). The sample filters were then analysed for their morphology and elemental compositions using SEM/EDS and LA-ICP-MS. SEM/EDS analysis was able to detect several heavy metal particulate matter while the LA-ICP-MS showed that there were more heavy metals present in the filter samples especially the heavier metals. Some of these heavier elements could have been inhibited by organic or higher amounts of the more common metals found in the EDS such as Fe, Zn, Si and Al. Nano-particles originated from high temperature sources, biological, carbonaceous and road transport were also detected in the samples. It was also found that particles containing more metallic elements tended to have a more defined shape while carbonaceous materials typically had amorphous structures. Tests showed that particles with environmental dust compositions of Ca, Al and Si were abundant. It was observed that the biological particles had very fine sizes.

Keywords: Fine-Particles, Ultrafine-Particles, Environmental Monitoring, Pollutants, Urban Environment, TEOM, SEM

1. Introduction

“Airborne suspended particulate matter may be either primary or secondary in its origins. Primary particles are those directly emitted to the atmosphere from sources such as road traffic, coal burning, industry, windblown soil and dust and sea spray. On the other hand, secondary particles are particles formed within the atmosphere by chemical reaction or condensation of gases, and the major contributors are sulphate and nitrate salts formed from the oxidation of sulphur dioxide and nitrogen oxides respectively” (QUARG, 1996).

Airborne particulate matter (PM) can cause a variety of environmental problems, and can also have a significant impact on human health (Zanobetti et al., 2000). A recent report by Brook et al., (2004) showed that the current airborne PM concentration is sufficient to cause an increased risk for cardiovascular events. Such events usually lead to increased case of hospitalisation due of coronary artery disease, stroke and other atherosclerotic diseases. Ultrafine PM from a few nanometres in diameter ($d_p < 100$ nm) penetrates much deeper into the lungs causing more significant damage compared to fine particles greater than 1 micrometre ($d_p < 2.5$ μm) (Donaldson et al., 1998; Glantz, 2002; Brook et al., 2004; Donaldson et al., 2005). Aerosol particles in the atmosphere can cause light scattering, which has a direct effect on the climate and visibility. It can also indirectly affect the climate by acting as cloud condensation nuclei which other pollutants could react with to produce other toxic and carcinogenic pollutants (Wieprecht et al., 2004). Over the years there have been numerous studies on the significance of particulate matter as a pollutant, however there is still a major need to fully characterise airborne PMs in terms of morphology, chemical composition and their origin in relation to health and environmental impact.

In the UK, the major sources of airborne particulate matter as described by the NAEI are transportation (35%), stationary fuel combustion (34%), processes (16%), agriculture and waste (14%) and others (1%) (Dore et al., 2006). There have been relatively few comprehensive studies of atmospheric particulate matter in the UK, considering the morphology and inorganic composition in detail. Often, more consideration is given to the organic components of the particulate matter, but inorganic compounds may also be significant from a health point of view, with a paper by Baulig et al., (2004) indicating that copper (and possibly iron) were significant contributors to the oxidative stress caused by fine particulate matter (Baulig et al., 2004; Limbach et al., 2005). One of the key tools selected for detailed investigation of the airborne PM samples is electron microscopy. Scanning electron microscopy with energy-dispersed analysis of X-rays (SEM/EDS) have already proven to provide information on the morphology, phase and elemental composition of individual particles (Paoletti et al., 2002; Laskin et al., 2006). The elemental composition of the samples can be analysed using laser ablation coupled with an inductive coupled plasmas mass spectrometer (LA-ICP-MS). The LA-ICP-MS is able to detect very low elemental concentrations while only requiring minute amounts of the sample.

Quantification and characterisation of particles is crucial in assessing their impact on the environment. Although airborne mass concentrations of various sizes of particulate matter are collected routinely, further information can be obtained from shape, size and chemical composition of samples, or even individual particles. Individual particles have different morphology and chemical composition, and these data will provide information on their source, atmospheric history, and their formation and reaction mechanisms. Identifying the source of airborne particles, and their composition, physical and chemical properties will help to provide a clear connection to their impact on the environment and the human health. Nevertheless, over the years, numerous studies have been conducted to characterise PM_{10} and some work on $\text{PM}_{2.5}$. Most of these studies were carried out in terms of the medical effects of particulate matter (Zanobetti et al., 2000; Baulig et al., 2004; Limbach et al., 2005). However, at the moment there is very little information on the origins of PM in the environment.

This paper presents the experimental results obtained for nano-particles collected at a local Authority monitoring site in a UK City.

2. Experimental methodology

2.1 Sampling location

Sheffield is the fourth largest city in the UK with just over half a million population. It is located in South Yorkshire and boundary to the Peak District National Park. Sheffield has a history as a major steel/metal producer in the UK. In the early 1900s, coal burning for steel production and domestic heating was a major contributor to poor air quality in the City which was associated with adverse health effects on the population (Daly and Elleker, 2004). It was the introduction of the Clean Air Act in 1956 that saw the enforcement of smokeless zone and improved air quality for residential as well as industrial areas. The location of the monitoring site used for this study is called "Groundhog 3". The site is located within a residential area and close to an A-road. This PM monitoring unit is situated within an urban commercial/residential area. The possible sources of particulate matter collected from this site are: commercial and residential heating, road transportation, and railway line. There is also a possibility that some of these airborne particulates may have migrated to this region from elsewhere. Sample filters were collected for a period of approximately 7 months (sampling duration ~ 30 to 60 days) from the local environmental monitoring unit.

2.2 Sampling technique

Samples were collected by Sheffield City Council on quartz fibre filters designed for TEOMs using Rupprecht & Patashnick Series 1400A TEOM samplers (R&P Co. Inc., 1998). Monitoring of ambient air PM₁₀ mass concentration was performed using a 15-minute time resolution. The duration of the sampling was approximately 30 to 45 days from April 2006 to January 2007, and the average PM₁₀ concentration during the monitoring period were approximately 24µg/m³ to a max of 35µg/m³.

2.3 Scanning Electron Microscopy

Characterisation of the particles in airborne PM₁₀ samples were performed using scanning electron microscopy (SEM). Morphology images (shape and size) of the particles were obtained using a CamScan Series II SEM. The elemental composition of the particles was analysed using an AN10/85 Energy Dispersive X-ray Spectrometer (EDS). The CamScan SEM was capable of producing images with a resolution of 7 nm for both secondary electron (SE) and back scattered electron (BSE) compositional imaging mode. In addition, the EDS allowed qualitative and quantitative microanalysis and for X-ray mapping. Digital images captured using various image acquisition software packages enabled the images to be obtained digitally. Usage of a Be window detector however limited the ability for the EDS to analyse lighter elements (Na and below). In the EDS mode the equipment was only able to detect concentrations in ppm levels. Six sample filters were analysed and each of these samples corresponded to a monitoring period. Particulates from the sample filters were carefully transferred onto carbon film tape mounted on a SEM specimen holder. Each sample was then carbon coated under vacuum before being analysed by SEM.

2.4 Laser Ablation ICP-MS

For solid sampling technique, Laser ablation has proven to be the most versatile sampling technique to be used in combination with an Inductive Coupled Plasma (ICP) spectrometry. It is often known as Laser Ablation Inductive Coupled Plasma-Mass Spectrometer (LA-ICP-MS). A sufficient amount of energy in the form of a focused laser beam was directed onto the surface of the sample, the material then started to sputter and vaporised. The vapour plume and particles were then transported by an argon gas carrier into the plasma flame for atomisation and ionisation. The interest and use of LA was due to its ability to sample a diverse range of materials from conducting and non-conducting inorganic and organic compounds as solids or powders (Akbar, 1998). In this experiment, PM samples were subjected to laser ablation line rasters using a New Wave RS UP-266 macro laser ablation system. This allows compositional information to be obtained from different sub-regions of the PM sample. The ablated PM was then analysed using an Agilent HP 4500 ICP-MS.

3. Results and discussion

3.1 SEM/EDS Analysis

3.1.1 Groundhog 3 PM₁₀ (25/04/06 – 24/05/06)

In figure 1, the feature particle in the middle, a hollow shaped sphere, has the characteristic of particles from a high temperature source known as cenosphere. Cenospheres are typically found in fly ash and bottom ash samples of particulate matter from thermoelectric power stations (Vallack and Chadwick, 1993; Vassilev and Vassileva, 1996). It is common for particles of this nature to have compositions of alumino-silicate glass, mullite, quartz, calcite, Fe oxides, Ca silicates and sulphates (Vassilev et al., 2004). EDS result for the feature particle gave a high peak of S, which suggests high sulphate content. It also showed minor peaks of Al, Si, Ca, Fe and K. The only difference between the feature particle analysed in this study and the ones reported in the literature is the "size of particle". Typical thermoelectric power station cenospheres have sizes ranging from 5 to 500µm and since the location of particle sampling is next to a busy road with no other major high temperature activities in the surroundings; it can be concluded

that the size of this particle (slightly larger than $3\mu\text{m}$ diameter) is a result of erosion during migration. The nearest thermoelectric power station is a large Coal-fired Power Station which is approximately 40 miles downwind towards the city of Sheffield. There are also crustal materials, which could have been accumulated either during migration or sampling.

Figure 2 is an image of typical particulate matter in another region of the same filter. EDS analysis showed that the rod-like particle is composed of only elemental Fe. All the other amorphous shaped particles are either soot or carbonaceous material. This rod-like particle is around $1\mu\text{m}$ in diameter and $3\mu\text{m}$ long. The morphology of the feature particle suggests that it is a product of metal wear from vehicle tailpipe, breaks etc. It should be noted that A61 road (with an average of 20,000 vehicles using the road per day) is located next to the sampling station (Groundhog 3) (Abu-Allaban et al., 2003).

3.1.2 Groundhog 3 PM_{10} (24/05/06 – 27/06/06)

The particles in black circles in figure 3 have all been subjected to EDS analysis and the results giving varying peaks of S, Ca with moderate amounts of Cl. There were also some small amounts of Si and K present. These particles are around $10\mu\text{m}$ with round edges. The shape of the particle could be a result of accumulation and erosion in the atmospheric environment.

A high magnification of the particle in figure 4 shows evidence of particulate matter accumulation due to its morphology. The EDS analysis gave very similar elemental compositions to particles shown in figure 3.

Particle in figure 5 is around $10\mu\text{m}$ in length with high peaks of Fe and very minute counts of Si, S and Ca. The shape suggests that it is plate-like and could have been a result of brakes abrasion or rust compounds from vehicles.

In an urban environment, there are various types of particles in the form of metal, non-metals and biological particles. Particle in figure 6 is an example of a bacterium or an environmental micro-organism known as bio-film. EDS analysis of the particle surface shows that middle of the particle surface is smoother than the surround dotted surface. The results contained high counts of Cl with lower counts of S and minute amounts of K. There are reports of these particles causing allergies and infectious disease in humans. Since this particle is approximately $7\mu\text{m}$ in diameter, there is a possibility that it will penetrate into the human respiratory system, which could subsequently led to other detrimental health issues.

3.1.3 Groundhog 3 PM_{10} (20/07/06 – 05/09/06)

There are two feature particles in figure 7 labelled as “A” and “B” respectively. EDS analysis on particle A gave only a high peak of Cl. The limitation of the SEM detector as well as the EDS did not allow Na to be detected therefore it could be concluded that the “A” is a salt particle e.g. NaCl. A review of SEM images of NaCl particles from literature has shown that they are similar to the feature particle A in terms of shape and size (around $2\mu\text{m}$) (Ebert et al., 2002; Hoffman et al., 2004).

Feature particle B looks like a $2\mu\text{m}$ diameter spherical particle with amorphous and crustal material stuck onto it. The EDS analysis of the whole particle gave a high peak of Fe and S, which suggests that; it is a product of metal wear from vehicles or combustion processes. Signs of metal wear were further confirmed based on the minor peaks of Cr and Zn, both elements of which are used in the vehicle/steel manufacturing industries for chroming and galvanizing steel. However the shape and appearance along with the high peak in S, seems to suggest that this particle is emitted from a high temperature source such as the metal industry (there is local metal factory northeast of the sampling site). The crustal like deposit on particle B was confirmed by the EDS showing minor peaks of Ca, Cl, K and Si.

The feature particle shown in the middle of figure 8 is comprised of mainly Fe. There is also a high peak in Cl with lower concentrations of Ni and Cr. The particle in question is approximately $3\mu\text{m}$ wide and is surrounded by other amorphous-like particles, which are thought to be non-metal since under the back-scattered mode it did not show any presence of metal elements.

Figure 9 is an image of the TEOM filter fibre. EDS analysis confirms a high concentration of Si with lower concentrations of K, Ca and Ti. This type of filter media is made using silica fibre as the major component along with K, Ca and Ti. This was confirmed by the manufacturer (R&P Co. Inc., 1998).

3.1.4 Groundhog 3 PM_{10} (05/09/06 – 28/09/06)

Particle A shown in figure 10 is composed of mainly Fe with minute quantities of other environmental dust particles such as Ca, Al and Si. Since there are a lot of other smaller amorphous particles settled on top of it, it is not possible to determine the morphology or its true size. Particles B and C are salt crystals which were shown in the EDS as just a Cl peak. In the middle of the image, there is also a cube like particle, which is partially visible along with the smaller square particle on the right hand side of the image. Both particles are salt based on their morphology. Image in figure 11 has similar composition to particles B and C. Therefore based on its EDS analysis and morphology, it can be concluded that this particle is also a salt crystal.

The particles in figure 12 and 13 have a length of around 6 μ m and 12 μ m respectively. EDS analysis performed on both particles gave similar results of Si, Al and K counts with smaller quantities of Fe and Cl. These particles are environmental dust particles.

3.1.5 Groundhog 3 PM₁₀ (23/11/06 – 05/01/07)

The black circle in figure 14 is a burnt spot from the EDS analysis, which gave high peaks of Ca and S along with lower counts of Si, K and Ca. It seems that environmental dust particles and most non-metals will suffer burns when electron beams are being applied. It could be due to the high 15KV energy used for EDS analysis, however under the imaging mode of 8KV the surface of the particle seemed to be melting.

Particles A and B in figure 15 are “salt particle” and “iron particle” respectively. The former particle was smaller than 1 μ m while the latter had a size of around 2 to 2.5 μ m in size.

3.2 LA-ICP-MS Analysis

Most of the elements shown in figure 16 were less than 85ppm with the exception of Pb with a surprising peak of nearly 140ppm in the final sample. Mn, Ni and Cr averaged around 15ppm while a gradual increase in Zn and Fe was observed. In figure 17, the concentrations of Sb, Mo and As were also less than 15ppm throughout the sampling dates. Ca and Na concentrations were expected to be high due to busy roads and high dust concentrations within the vicinity of the sampling location. The toxic metal concentrations of Co, Tl and Hg in figure 18 were all less than 2ppm while Cd concentrations were less than 4.5ppm. Concentration of elements illustrated in figure 19 was lower than 20 ppm except Si, which had a peak of approximately 30ppm in the third sample. From all four figures there were several elements, which exhibit similar concentration trends. One such trend observed was elements of Ca, Al and Si, which are the composition of typical crustal or dust particles.

3.3 Discussion

The SEM analysis of each sample filters showed that there were particles, which could have originated from the surrounding activities and environment but it also showed that some particles could have migrated from high temperature processes further upwind. In most of the images there were some particles, which had an amorphous structure, but EDS analysis did not detect any elemental composition. This could have been due to the sensitivity of the equipment or the Be window detector. However, the appearance and morphology of amorphous particles suggests that they could be soot particles produced from the combustion of petrol and diesel in internal combustion engines (Moreno et al., 2004). It was not unusual to find high amounts of carbonaceous or soot particles since the monitoring location is within the vicinity of a busy A-road with an approximate traffic of 20000 vehicles/day. There were also some particles, which were biological in nature. These micro-organisms are known as bio-films. Crustal material was also one of the major components found in this analysis. The sources of these crustal materials are industrial fly ash, dust from transportation and soil. The compounds usually exist naturally as oxides of aluminium, silica, calcium, titanium, iron, magnesium, sodium and potassium with moisture contributing to more than 80% of the soil sediments (Chan et al., 1997; Suzuki, 2006). However, the high content of Fe, Cr, Zn and other heavy metals detected by the EDS analysis could have been released by the steel and metal industries or wear and tear metals parts of vehicles. The majority of the chlorine found in the EDS analysis was thought to be sea salt particles, which could have travelled inland from the oceans or from road gritting during the winter seasons. Generally chlorine was detected more in PM₁₀ samples since marine aerosols are much more dominant in the coarse particle range (Kouimtzis and Samara, 1995).

Analysis from the elemental composition of all the filters showed that the concentrations of Cd, Co, Tl and Hg were lower than 4.5ppm. Concentrations of Mn, Ni, Cr, Sb, Mo and As were less than 15ppm. All these heavy/toxic metal elements are highly regulated due their effects on human health. It was expected that the concentrations of Al, Na and Ca would be very high since they exist in the environment as crustal material (dusts, soil, sand etc) and salt. Some elements such as Pb, Zn and Fe were found to be very high such as Pb at nearly 140ppm, but these could have originated from wear of vehicles or from high temperature processes in the North-east region of Sheffield. The metals detected in the samples such as Ni, Zn, Fe, Mn, Mo, Pb and Cu are all the known metallic elements which are widely used in the metal/steel industries. Some of trends exhibit in the figures also proved that some metals tend to condense or agglomerate close to each other.

4. Conclusions

The main findings from this research project are as follows:

- SEM/EDS analysis was only able to detect some heavy metal particulate matter while the LA-ICP-MS showed that there were other heavy metal elements present in the filter sample. Some of these heavier elements could have been inhibited by organic or higher amounts of the more common metals found in the EDS such as Fe, Zn, Si and Al.
- However, SEM analysis was able to show the characteristics and morphology of individual particles and thus

enabled one to understand its origin and airborne activity.

- Individual particles could have originated from high temperature sources, biological, carbonaceous and road transportation were detected in the samples. It was also found that particles containing more metallic elements tended to have a more defined shape while carbonaceous material typically had an amorphous structure.
- Some metals and their elemental compositions detected in the samples were traced back to the common metallic-elements widely used in the steel and metal industries.
- The analytical techniques used in this study were able to provide valuable information on the morphology and elemental composition of the samples collected. This information was used to identify the sources of origin of the particle emission.

5. Acknowledgements

The authors would like to thank the following organisation and individuals for their financial and technical support for this research project: Engineering & Physical Science Research Council (EPSRC Pollutants in the Urban Environment (PurE) Consortium), Sheffield City Council, Dr David Poole (CORUS Ltd), Alan Cox (CAS, Chemistry Department, Sheffield University) and Sorby Centre (Dept of Materials Engineering, Sheffield University).

References

- Abu-Allaban, M., Gillies, J.A., Gertler, A.W., Clayton, R. & Proffitt, D. (2003). "Tailpipe, resuspended road dust, and brake-wear emission factors from on-road vehicles". *Atmospheric Environment*, 37 (37), 5283-5293.
- Akbar, M. (1998). *Inductively Coupled Plasma Mass Spectrometry*. Wiley.
- Baulig, A., Poirault, J.J., Ausset, P., Schins, R., Shi, T., Baralle, D., Dorlhene, P., Meyer, M., Lefevre, R., Baeza-Squiban, A. & Marano, F. (2004). "Physicochemical Characteristics and Biological Activities of Seasonal Atmospheric Particulate Matter Sampling in Two Locations of Paris". *Environ. Sci. Technol.*, 38 (22), 5985-5992.
- Brook, R.D., Franklin, B., Cascio, W., Hong, Y., Howard, G., Lipsett, M., Luepker, R., Mittleman, M., Samet, J., Smith, S.C., Jr. & Tager, I. (2004). "Air Pollution and Cardiovascular Disease: A Statement for Healthcare Professionals From the Expert Panel on Population and Prevention Science of the American Heart Association". *Circulation*, 109 (21), 2655-2671.
- Chan, Y.C., Simpson, R.W., McTainsh, G.H., Vowles, P.D., Cohen, D.D. & Bailey, G.M. (1997). "Characterisation of chemical species in PM_{2.5} and PM₁₀ aerosols in Brisbane, Australia". *Atmospheric Environment*, 31 (22), 3773-3785.
- Daly, M. & Elleker, A. (2004) (Ed, Environmental Protection Service, S.C.C.) Sheffield City Council, pp. 127.
- Donaldson, K., Li, X.Y. & MacNee, W. (1998). "Ultrafine (nanometre) particle mediated lung injury". *Journal of Aerosol Science*, 29 (5-6), 553.
- Donaldson, K., Mills, N., MacNee, W., Robinson, S. & Newby, D. (2005). "Role of inflammation in cardiopulmonary health effects of PM". *Toxicology and Applied Pharmacology*, 207 (2, Supplement 1), 483.
- Dore, C.J., Watterson, J.D., Murrells, T.P., Passant, N.R., Hobson, M.M., Baggott, S.L., Thistlethwaite, G., Goodwin, J.W.L., King, K.R., Adams, M., Walker, C., Downes, M.K., Coleman, P.J., Stewart, R.A., Wagner, A., Sturman, J., Conolly, C., Lawrence, H., Li, Y., Jackson, J., Bush, T., Grice, S. & Brophy, N. (2006). "UK Emissions of Air Pollutants 1970 to 2004". *UK Emissions Inventory Team, AEA Energy & Environment*.
- Ebert, M., Inerle-Hof, M. & Weinbruch, S. (2002). "Environmental scanning electron microscopy as a new technique to determine the hygroscopic behaviour of individual aerosol particles". *Atmospheric Environment*, 36 (39-40), 5909-5916.
- Glantz, S.A. (2002). "Air pollution as a cause of heart disease: Time for action". *Journal of the American College of Cardiology*, 39 (6), 943.
- Hoffman, R.C., Laskin, A. & Finlayson-Pitts, B.J. (2004). "Sodium nitrate particles: physical and chemical properties during hydration and dehydration, and implications for aged sea salt aerosols". *Journal of Aerosol Science*, 35 (7), 869-887.
- Kouimtzis, T. & Samara, C. (1995). *The Handbook of environmental chemistry Vol.4, Airborne particulate matter*. Berlin ; London: Springer.
- Laskin, A., Cowin, J.P. & Iedema, M.J. (2006). "Analysis of individual environmental particles using modern methods of electron microscopy and X-ray microanalysis". *Journal of Electron Spectroscopy and Related Phenomena*, 150 (2-3), 260.
- Limbach, L.K., Li, Y., Grass, R.N., Brunner, T.J., Hintermann, M.A., Muller, M., Gunther, D. & Stark, W.J. (2005). "Oxide Nanoparticle Uptake in Human Lung Fibroblasts: Effects of Particle Size, Agglomeration, and Diffusion at Low

Concentrations". *Environ. Sci. Technol.*, 39 (23), 9370-9376.

Moreno, T., Jones, T.P. & Richards, R.J. (2004). "Characterisation of aerosol particulate matter from urban and industrial environments: examples from Cardiff and Port Talbot, South Wales, UK". *Science of The Total Environment*, 334-335, 337-346.

Paoletti, L., De Berardis, B. & Diociaiuti, M. (2002). "Physico-chemical characterisation of the inhalable particulate matter (PM10) in an urban area: an analysis of the seasonal trend". *The Science of The Total Environment*, 292 (3), 265.

QUARG (1996). *Airborne Particulate Matter in The United Kingdom*. Department of the Environment. Third report of the Quality of Urban Air Review Group Report No.

R&P Co. Inc. (1998). "TEOM Series 1400A Ambient Particulate Monitor". In: Inc., R.P.C. (ed.). Cheltenham: ETI Group Ltd.

Suzuki, K. (2006). "Characterisation of airborne particulates and associated trace metals deposited on tree bark by ICP-OES, ICP-MS, SEM-EDX and laser ablation ICP-MS". *Atmospheric Environment*, 40 (14), 2626-2634.

Vallack, H.W. & Chadwick, M.J. (1993). "Monitoring airborne dust in a high density coal-fired power station region in North Yorkshire". *Environmental Pollution*, 80 (2), 177-183.

Vassilev, S.V., Menendez, R., Diaz-Somoano, M. & Martinez-Tarazona, M.R. (2004). "Phase-mineral and chemical composition of coal fly ashes as a basis for their multicomponent utilization. 2. Characterization of ceramic cenosphere and salt concentrates". *Fuel*, 83 (4-5), 585-603.

Vassilev, S.V. & Vassileva, C.G. (1996). "Mineralogy of combustion wastes from coal-fired power stations". *Fuel Processing Technology*, 47 (3), 261-280.

Wieprecht, W., Acker, K., Muller, K., Spindler, G., Bruggemann, E., Maenhaut, W., Chi, X., Hitzemberger, R., Bauer, H. & Brink, H.t. (2004). "INTERCOMP2000: ionic constitution and comparison of filter and impactor". *Atmospheric Environment*, 38 (38), 6477.

Zanobetti, A., Schwartz, J. & Dockery, D.W. (2000). "Airborne particles are a risk factor for hospital admissions for heart and lung disease". *Environmental Health Perspectives*, 108 (11), 1071-1077.

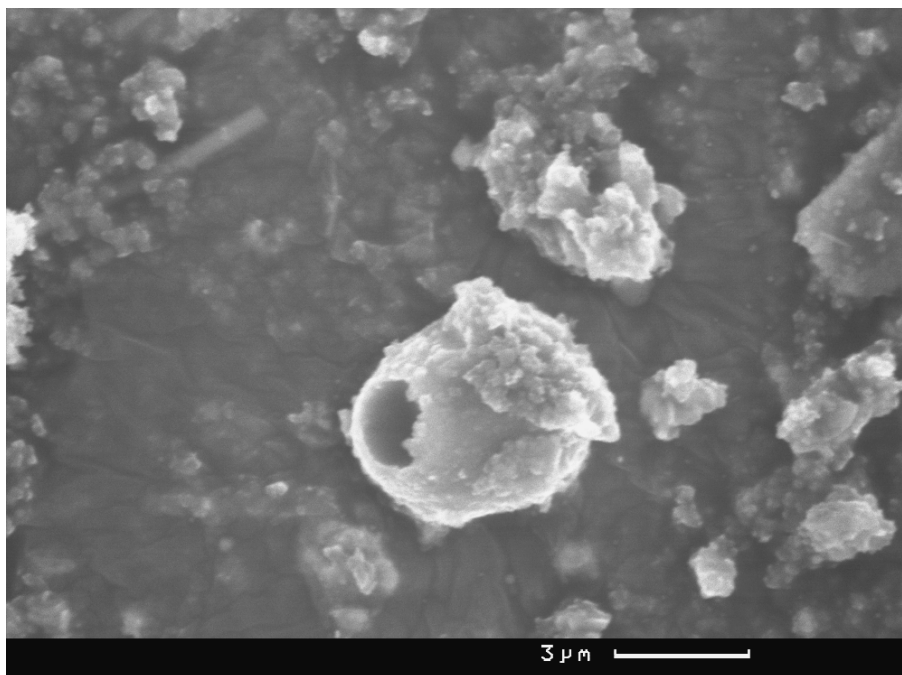


Figure 1. SEM image of PM at 3µm

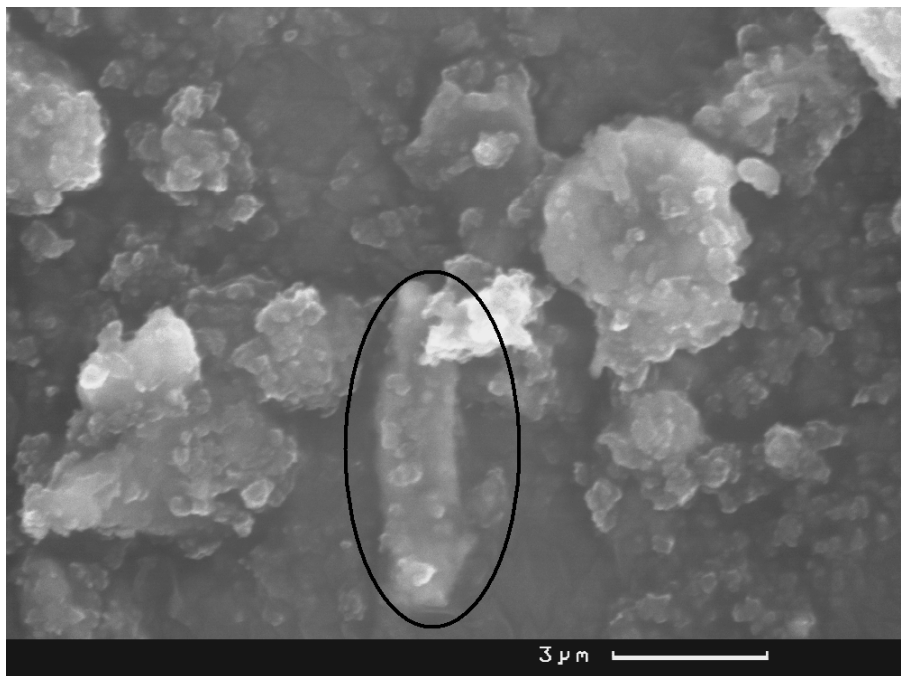


Figure 2. SEM image of PM at 3µm

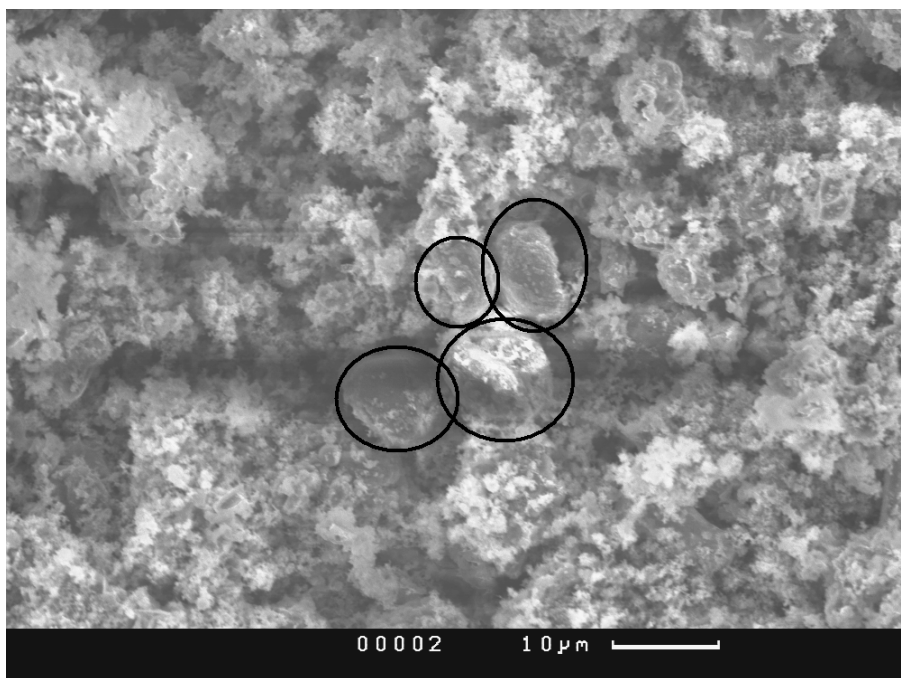


Figure 3. SEM image of PM at 10µm

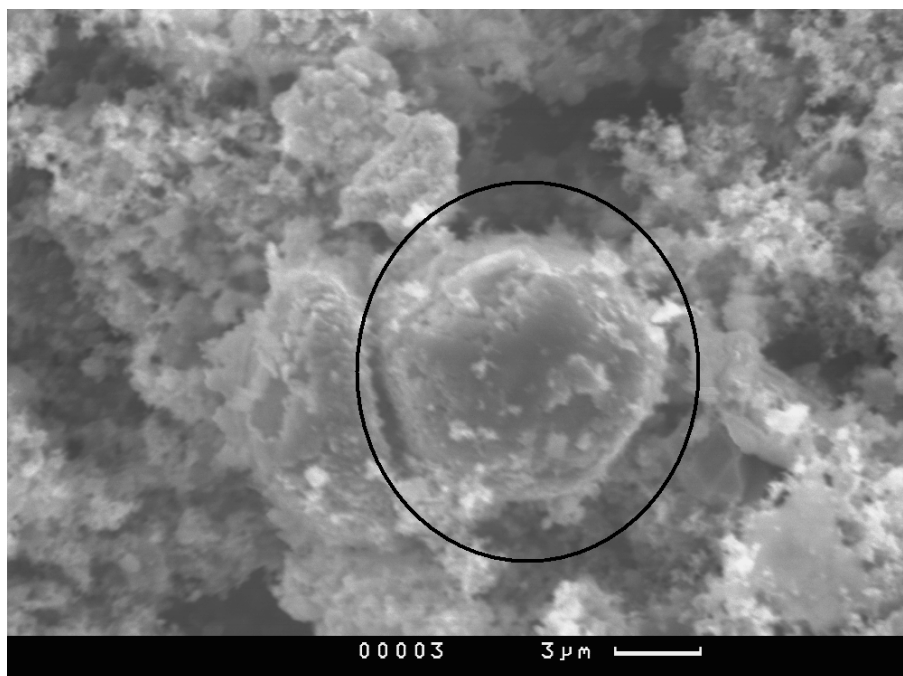


Figure 4. SEM image of PM at 3µm

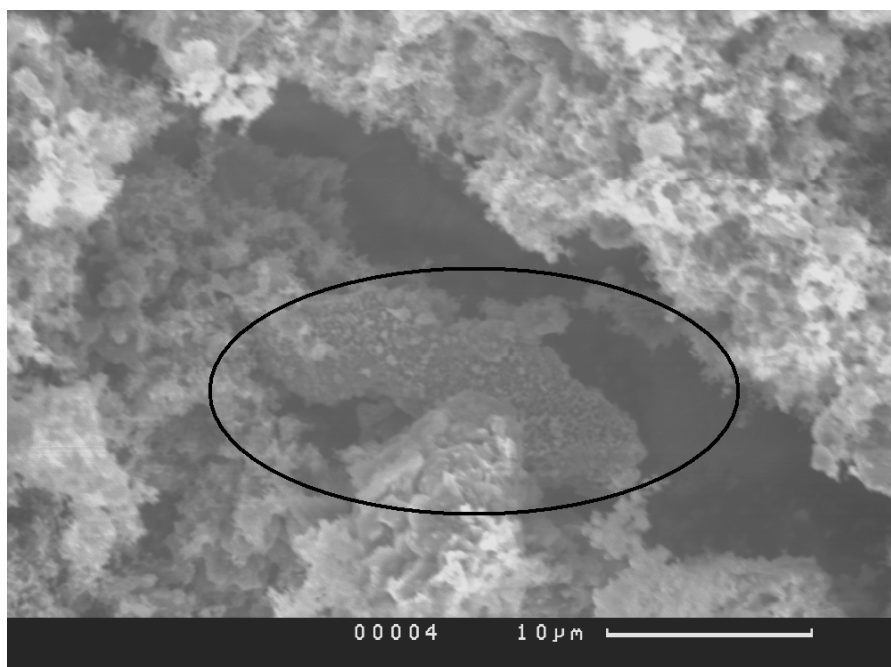


Figure 5. SEM image of PM at 10µm

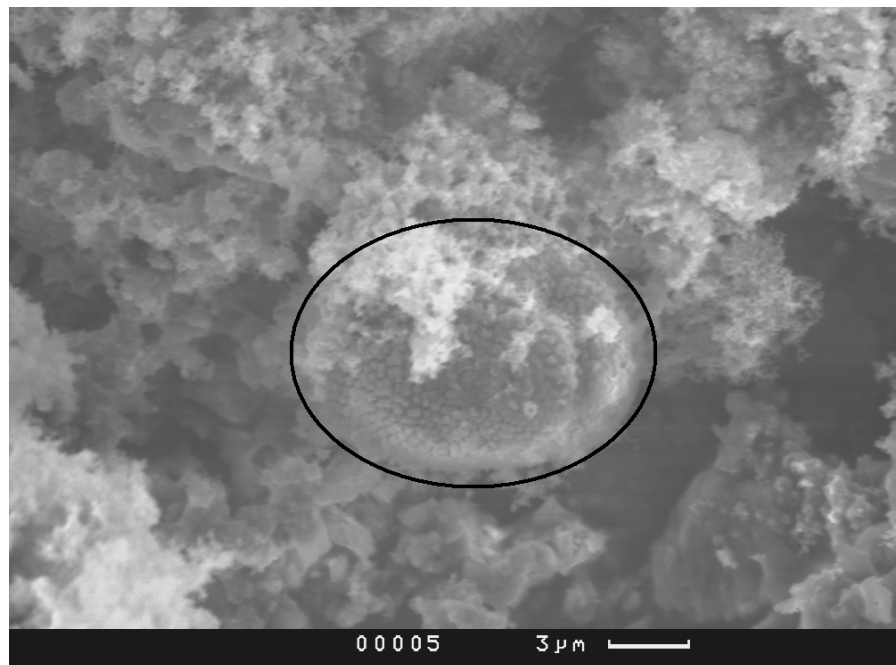


Figure 6. SEM image of PM at 3µm

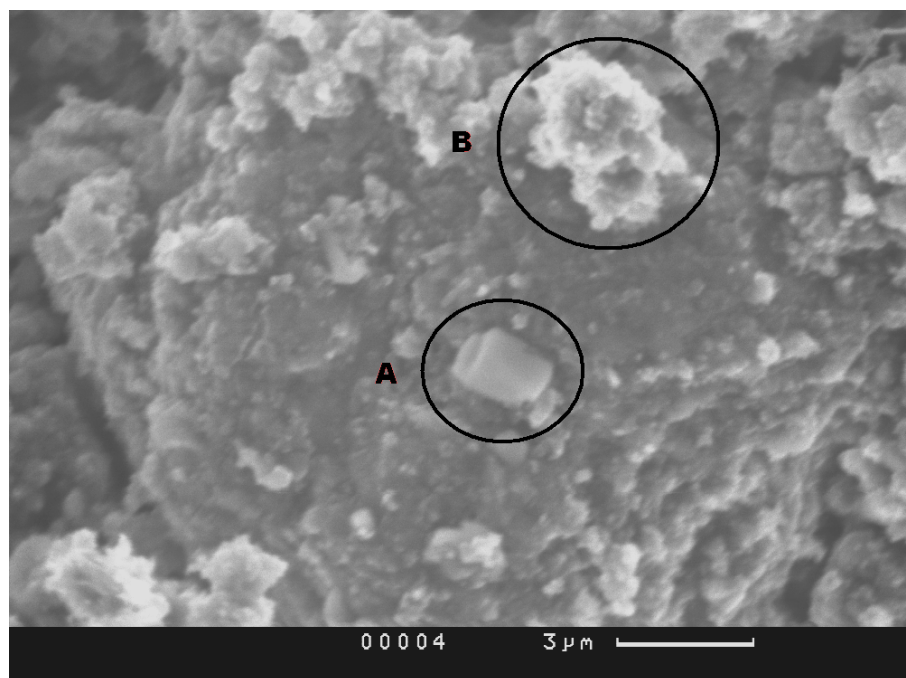


Figure 7. SEM image of PM at 3µm

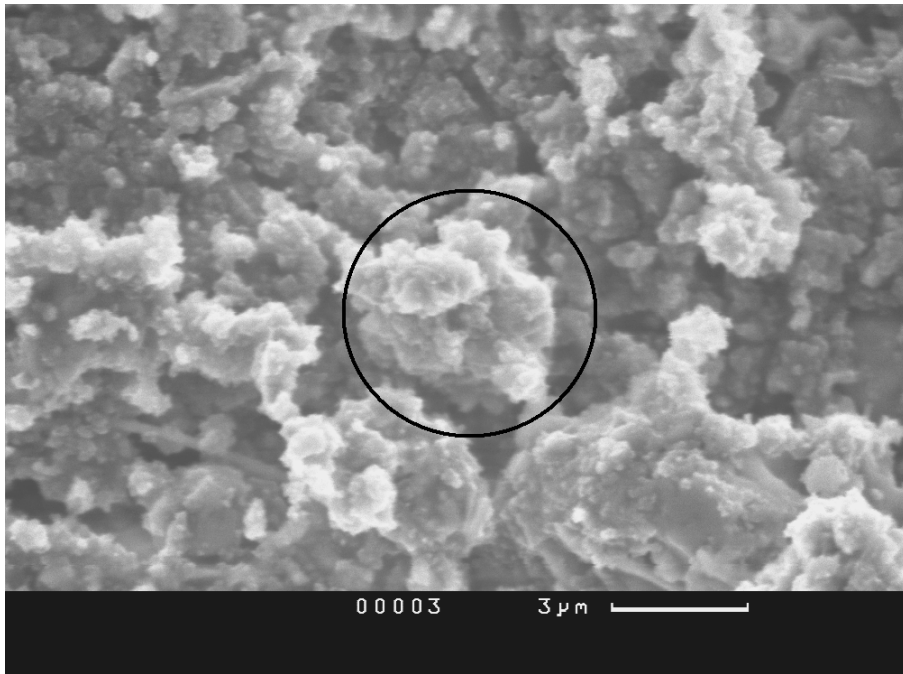


Figure 8. SEM image of PM at 3µm

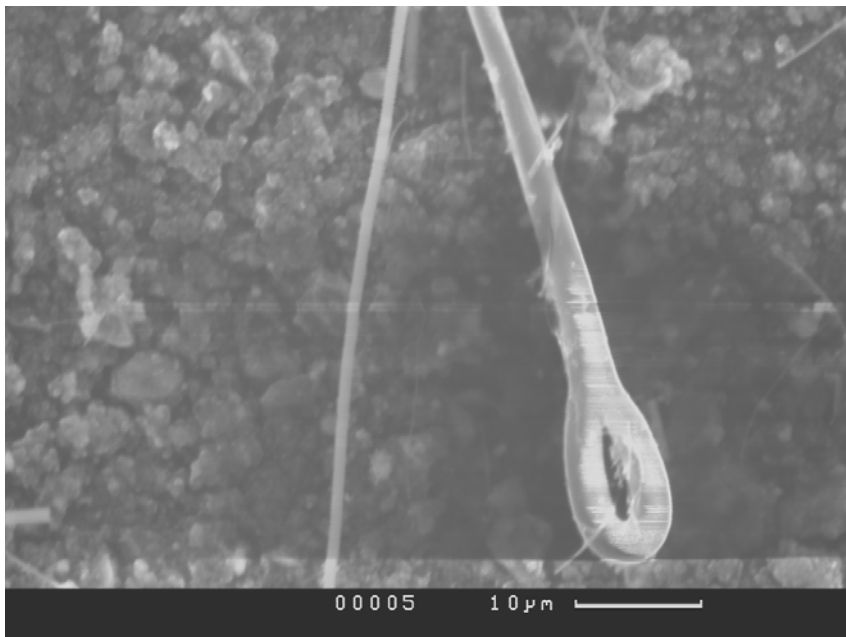


Figure 9. SEM image of PM at 10µm

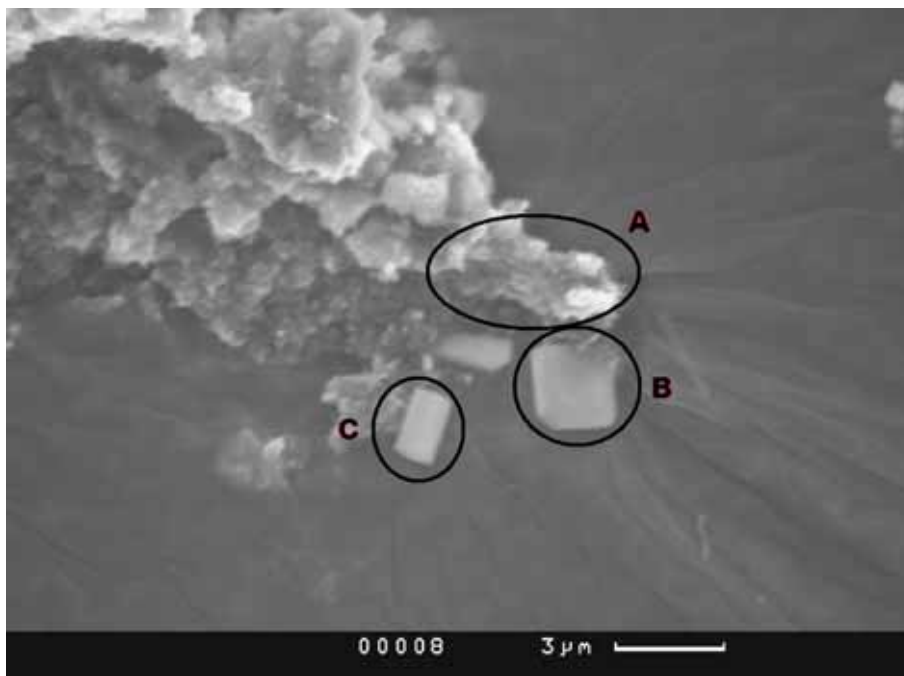


Figure 10. SEM image of PM at 3µm

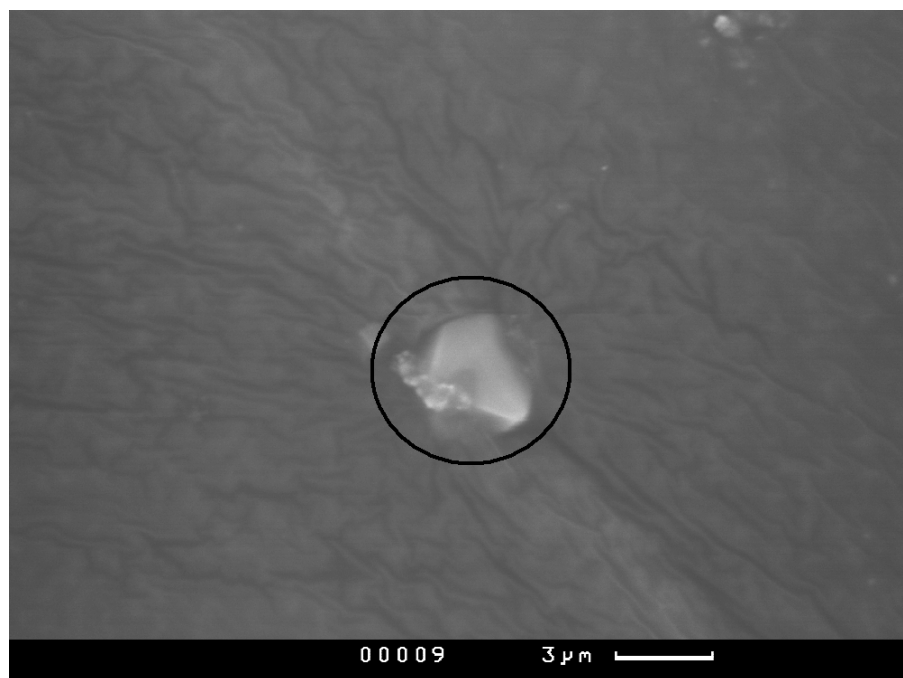


Figure 11. SEM image of PM at 3µm

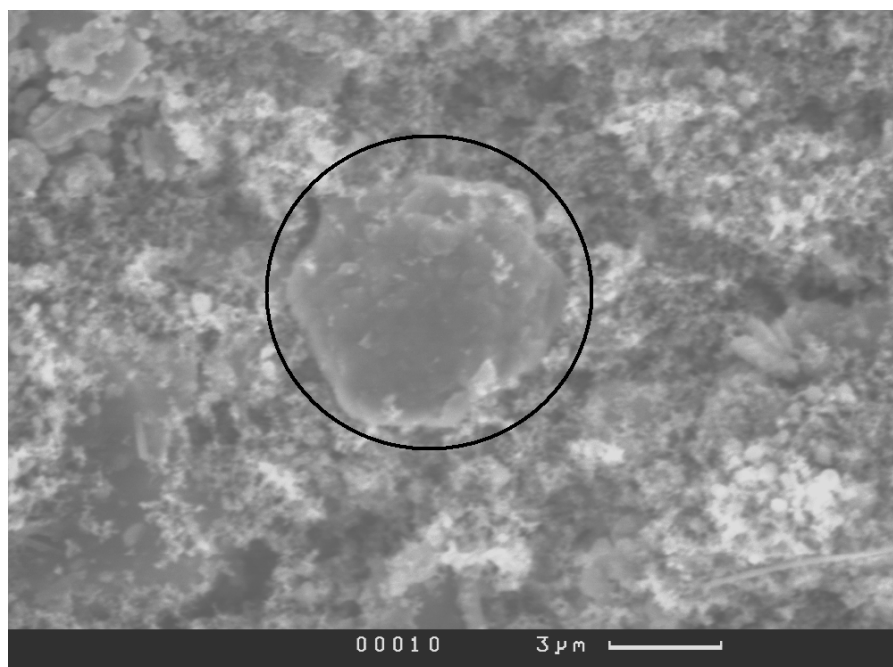


Figure 12. SEM image of PM at 3µm

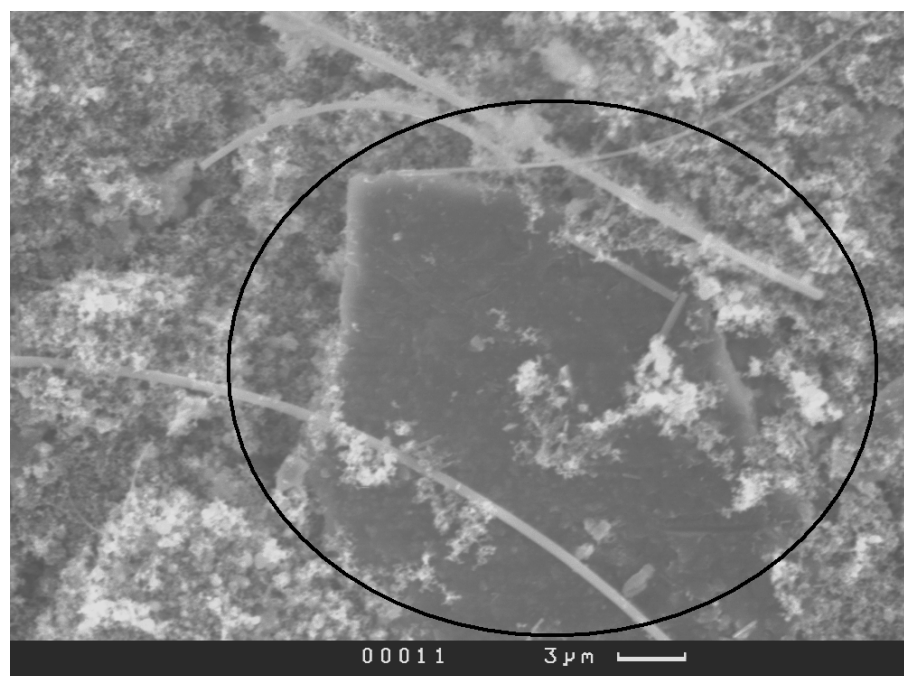


Figure 13. SEM image of PM at 3µm

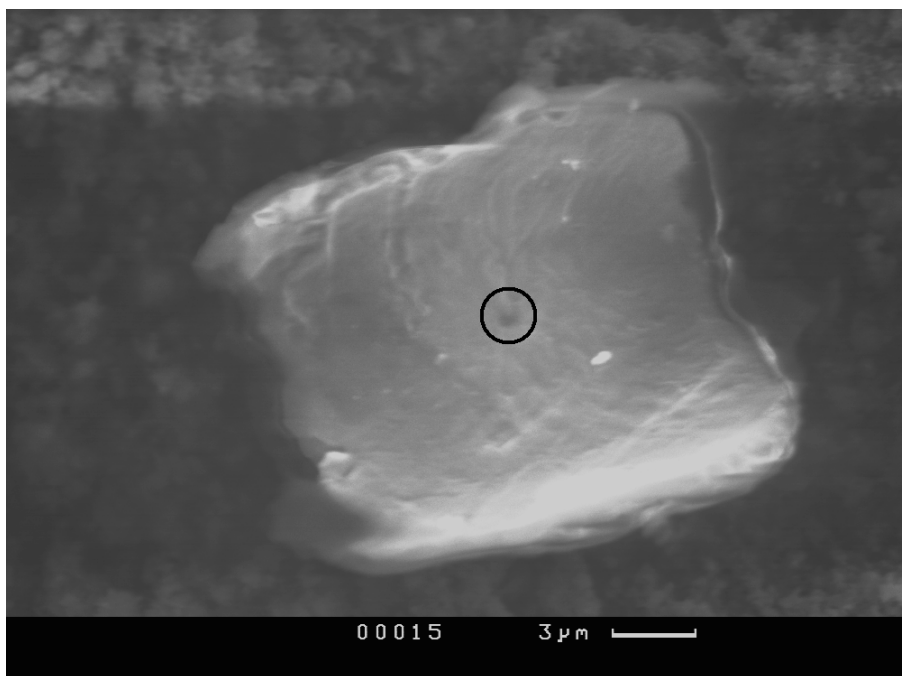


Figure 14. SEM image of PM at 3µm

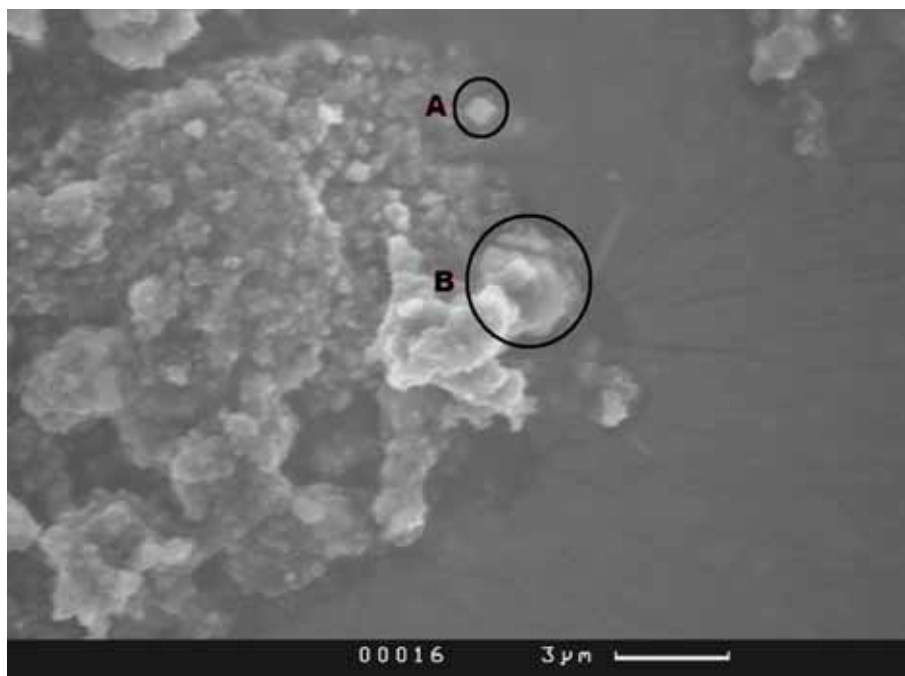


Figure 15. SEM image of PM at 3µm

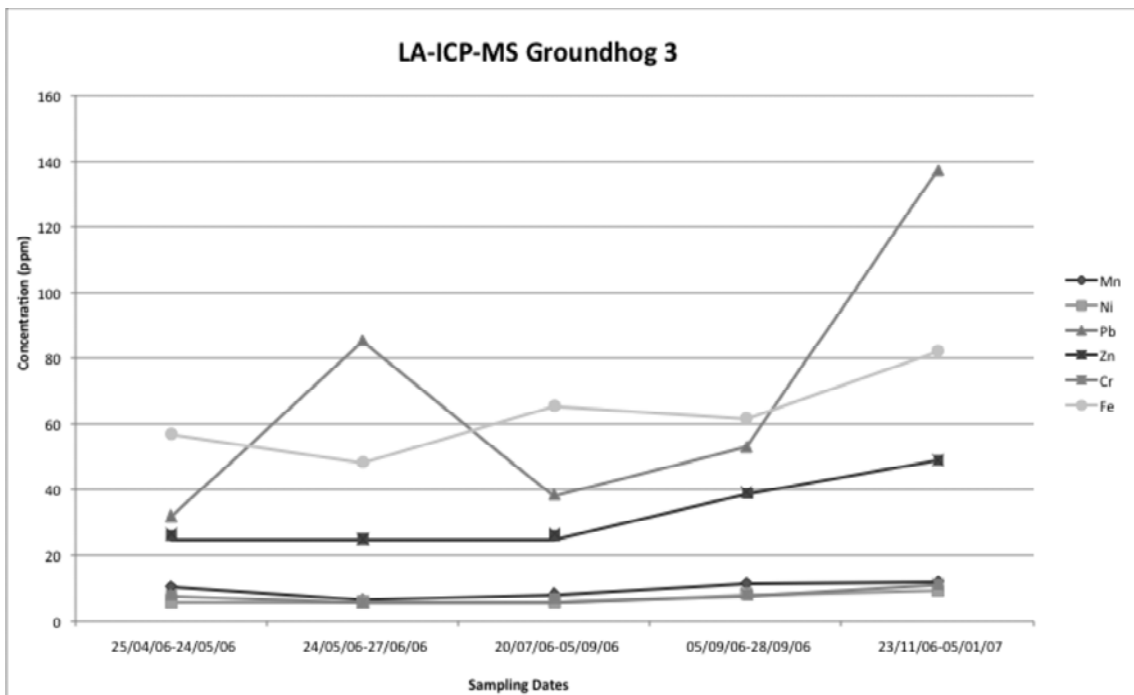


Figure 16. LA-ICP-MS Groundhog 3 for Mn, Ni, Pb, Zn, Cr and Fe

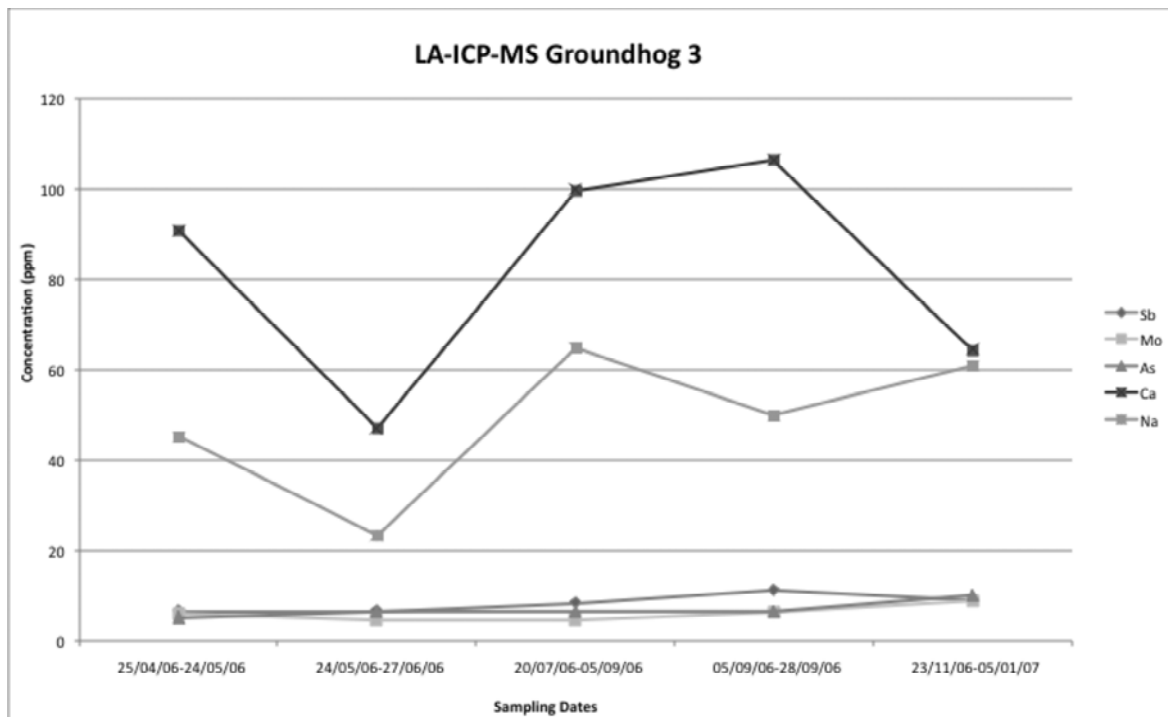


Figure 17. LA-ICP-MS Groundhog 3 for Sb, Mo, As, Ca and Na

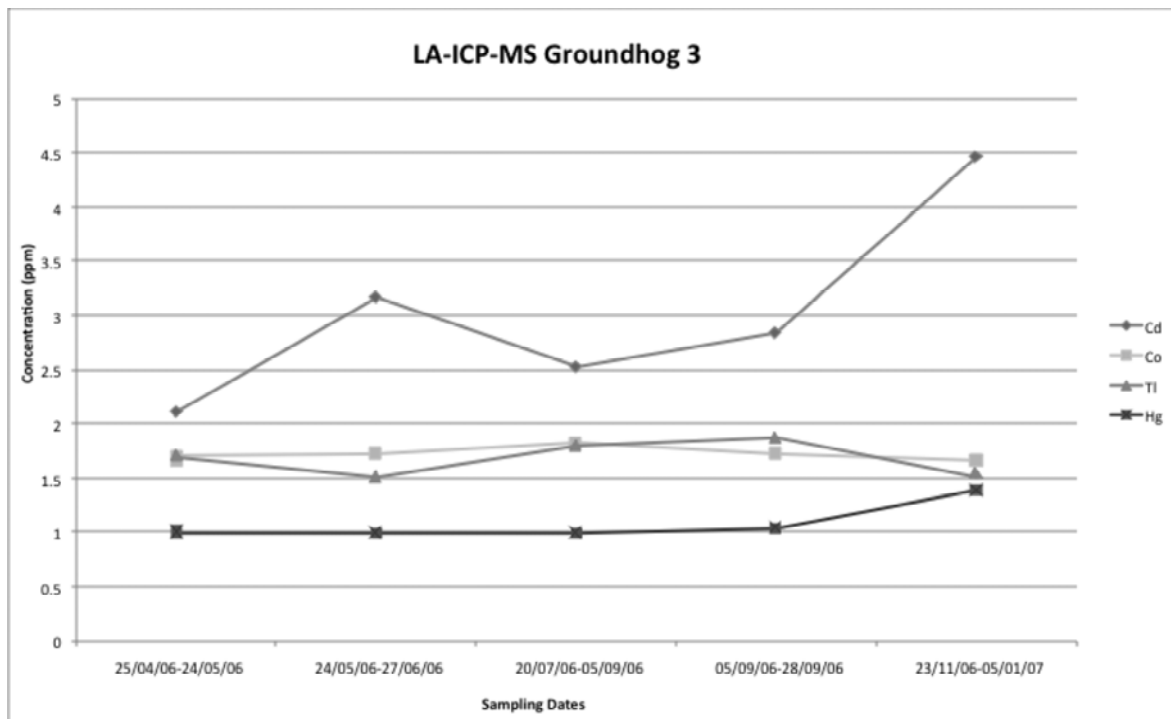


Figure 18. LA-ICP-MS Groundhog 3 for Cd, Co, Tl and Hg

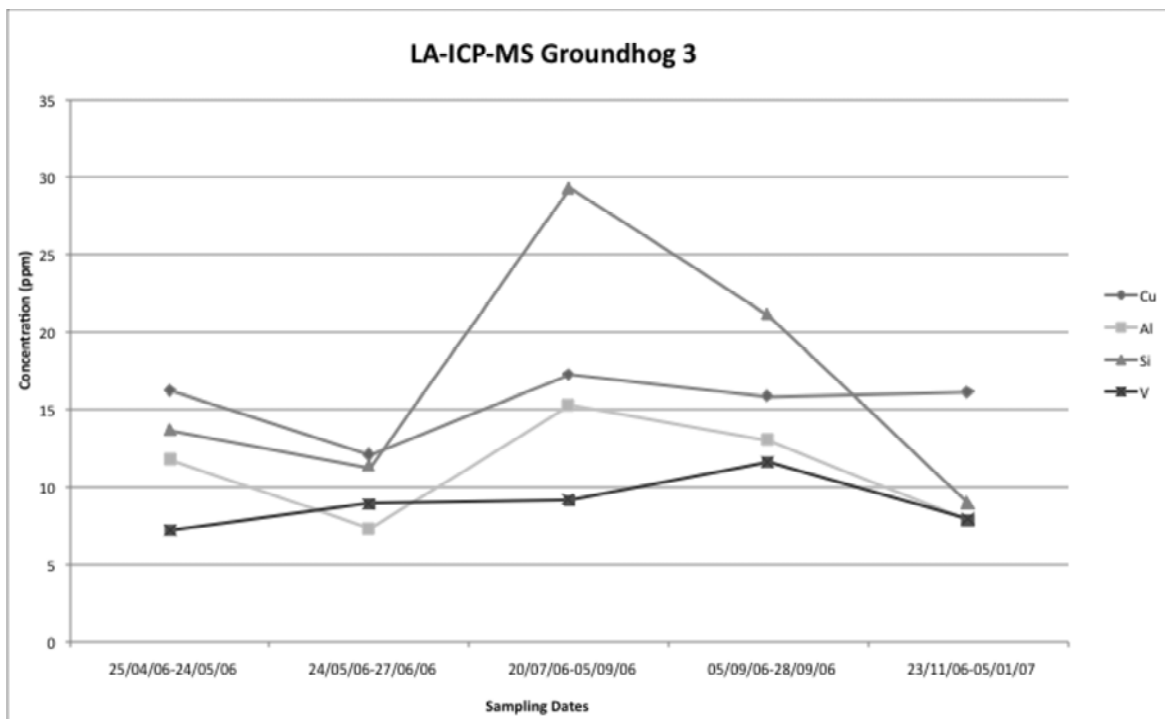


Figure 19. LA-ICP-MS Groundhog 3 for Cu, Al, Si, and V



Manpower Management Benefits Predictor Method for Aircraft Two Level Maintenance Concept

Yuanda Wang (Corresponding author)

College of Aeronautics, Northwestern Polytechnical University

PO box 120, 127 Youyi xi road, Xi'an 710072, China

E-mail: ilabus807@126.com

Bifeng Song

College of Aeronautics, Northwestern Polytechnical University

PO box 120, 127 Youyi xi road, Xi'an 710072, China

Abstract

In maintenance management process of aircraft, how to use the lesser maintenance manpower to get in return the higher maintenance Benefits, it is a problem that the management specialists pay more attention to, so, manpower management and cost estimate are the important compose parts of aircraft Life Cycle Costs (LCC) management. Via improve the maintenance level of aircraft, predigesting maintenance system from three level to two level maintenance (TLM) could save manpower, improve readiness, achieve the goal of bring favorable maintenance management Benefits. We imported gray system Verhulst model theory, established the manpower management forecast model for transforming maintenance system, and predicted according to the actual save manpower data of the United State Air Force. It is proved that the creditability of the prediction model is higher, has certain practical value.

Keywords: Aircraft, Gray Verhulst model, Two level maintenance concept, Manpower management Benefits, Predictor Method

1. Introduction

Military aircraft perform three level maintenance system for a long time. With the increasingly complex in airborne system and great advance in technologies, aircraft's Life Cycle Costs (LCC) especially servicing support costs went on improving, logistical supply line is too long, manpower costs and maintenance costs are too high, there has a biggest conflict between increasing aircraft readiness and reducing LCC, we could buy but cannot afford. So the aircraft maintenance management specialists were trying to find an efficient path of costs saving. With the fast development of avionics and engine technologies and foundation of maintenance system engineering conception, it provides a necessary condition of predigesting maintenance level. In October 1993, the United States Air Force implied two Level maintenance (TLM) concept, transformed Organizational level, Intermediate level and Depot level to Organizational level and Depot level. By the verification of several local wars, TLM have gained magnificent martial and economic Benefits.

Maintenance systems include maintenance production system and maintenance management system. In the maintenance management process, maintenance manpower Benefits estimate is the research emphases. There are some models described calculating procedure, but we have no model, which can calculate TLM manpower costs. USAAF AFH 21-130 gave the total saving manpower costs estimate formula:

Total estimated savings = (base manpower savings) - (increased depot manpower costs) - (increased transportation costs) + or - change in inventory requirement + or - change in RSP cost.

From the upper formula we can see, if we want to calculate manpower Benefits accurately, many practice running data are needed, it is impossible achieved in the beginning of researching maintenance system transform period. So we must find the useful models for reference and practice calculate.

Base on the coming into being manpower Benefits of USAAF implied TLM, we import gray prediction theory, get a prediction model, and solve the above problem preferably.

2. Basic conception of gray prediction theory

The existing system statistical analysis usually use the mathematics statistics method, and the sample are the more and the better, distribution rule is known, thus this method isn't fit the condition of unknown distribution rule. Partial information is known and partial information is unknown, we called such system as gray system. This system regards the random variable as the gray variable which is varying in a certain range, regards the random process as the gray process which is varying in a certain range and a certain time period, use the original data to accumulating generator operator (AGO), and attenuate it's random factors, then establish the whitenization form differential equation for the making sequence of numbers, find out the equation's solution sequence of numbers, finally through the inverse accumulating generator operator (IAGO), we find out the predicted value.

The characteristics of grey prediction theory are as follow:

- (1) Though the grey prediction, we can establish the differential equation. This equation is a differential equation type model, which established by the viewpoints and methods of relational degree convergence theory, generator number, and grey differential equation, it has a wide range of use.
- (2) By the method of data processing, it can put the disorderly and unsystematic original data in order, and become a rule generator sequence of numbers.
- (3) Though the residual test, posterior error test, and relational degree test, we can test the precision.
- (4) According to the predict precision, we also topology predict model, establish the all data GM model, new information GM model, residual model and adjust predict model (include GM model), so as to increase predict precision.
- (5) Because grey prediction establishes model is a generator data model, the results calculate value by the GM model must be dealt with inverse generator to revert prediction value.

3. Verhulst model

3.1 Verhulst model introduction

For non-monotonous swing sequence or saturated S shape sequence, GM (2,1), DGM and Verhulst model can be established.

We use grey prediction to establish GM (1,1) power model for generator sequence of numbers, and use accumulating generator operator processing procedure to deal with the original sequence of numbers.

Suppose there is an original sequence of numbers $X^{(0)}$:

$$X^{(0)} = [x^{(0)}(1), x^{(0)}(2), \dots, x^{(0)}(n)] \quad (1)$$

Make 1 time accumulating generator operator (1-AGO) for $X^{(0)}$, we can gain the generator sequence of numbers $X^{(1)}$.

In here,

$$x^{(1)}(k) = \sum_{m=1}^k x^{(0)}(m) \quad (2)$$

$Z^{(1)}$ is $X^{(1)}$ proximate mean generator sequence, we call $Z^{(1)}$

$$x^{(0)}(k) + az^{(1)}(k) = b(z^{(1)}(k))^\alpha \quad (3)$$

as GM (1,1) power model.

Establish whitenization differential equation for $X^{(1)}$,

$$\frac{dx^{(1)}}{dt} + ax^{(1)} = b(x^{(1)})^\alpha \quad (4)$$

in equation, when $\alpha=2$, this model is called grey Verhulst model.

Verhulst model mainly used to describe the process, which has saturation state, which is S shape process. This model usually used to population projection, biology growth, breeding prediction and product economy life prediction, etc.

Suppose parameter column vector $\hat{a} = \begin{bmatrix} a \\ b \end{bmatrix}$

From relation formula $Y = B\hat{a}$, we can get parameter calculate formula:

$$\hat{a} = (B^T B)^{-1} B^T Y \tag{5}$$

Among this formula:

$$B = \begin{bmatrix} -z^{(1)}(2) & (z^{(1)}(2))^2 \\ -z^{(1)}(3) & (z^{(1)}(3))^2 \\ \vdots & \vdots \\ -z^{(1)}(n) & (z^{(1)}(n))^2 \end{bmatrix}, Y = \begin{bmatrix} x^{(0)}(2) \\ x^{(0)}(3) \\ \vdots \\ x^{(0)}(n) \end{bmatrix}$$

Solve for this whitenization differential equation, we get the time response formula of Verhulst model:

$$\hat{x}^{(1)}(k+1) = \frac{ax^{(1)}(0)}{bx^{(1)}(0) + (a - bx^{(1)}(0))e^{ak}} \tag{6}$$

Make 1 time inverse generator operator (1-IAGO), and revert it, we get prediction-estimated value:

$$\hat{x}^{(0)}(k) = \hat{x}^{(1)}(k) - \hat{x}^{(1)}(k-1) \tag{7}$$

3.2 Model precision test

The precision degree test methods for prediction value commonly have 3 types:

(1) Residual magnitude test.

It is a count test through model precision point.

(2) Posterior error test.

It is a statistical test through probability distribution of residual.

(3) Relating degree test.

It is a geometric test through model curve behavior data curve.

According to the result of different test, we can judge whether the model is fit, or correct the model. In this article, we use the conventional residual magnitude test method.

Residual is $\varepsilon(k) = x^{(0)}(k) - \hat{x}^{(0)}(k)$,

and relative error is $\Delta_k = \frac{|\varepsilon(k)|}{x^{(0)}(k)}$.

4. Calculation of USAAF TLM manpower Benefits

Table 1 gives the saving maintenance manpower data of USAAF maintenance system from three level to two level.

Apply table 1 data, we establish Verhulst model. Because the 1994 and 1995 year are the maintenance system adjustment initial period, these two year's data were insufficient to reflect the matter of question, so we omit it, and calculate from 1996 year.

Because the original data curve is approximate to S shape, we choose

$$x^{(1)} = (5820, 5680, 5962, 5888),$$

it's 1-IAGO sequence is

$$x^{(0)} = \{x^{(0)}(k)\}_1^4 = (5820, -140, 282, -74),$$

it's proximate mean generator sequence is

$$z^{(1)} = \{z^{(1)}(k)\}_2^4 = (5750, 5686, 5790).$$

According to (5), (6) formulas, we get a= 0.067369, b=0.000012.

The predictive model of manpower Benefits is

$$\hat{x}^{(1)}(k+1) = \frac{392.0876}{0.0698 - 0.0024e^{0.067369k}}$$

Thereout, we can simulate and predict the saving manpower after the USAAF implied TLM concept:

$$\hat{x}^{(1)}(1) = 5820, \hat{x}^{(1)}(2) = 5842.588, \hat{x}^{(1)}(3) = 5866.882, \hat{x}^{(1)}(4) = 5893.127, \\ \hat{x}^{(1)}(5) = 5921.462942.$$

In here, $\hat{x}^{(1)}(5)$ is the saving manpower predicted value of USAAF in 2000, and that actual data of 2000 year $x^{(1)}(5) = 5925$.

Residual is

$$\varepsilon(k) = x^{(1)}(5) - \hat{x}^{(1)}(5) = 3.537058,$$

Relative error is

$$\Delta_5 = \frac{|\varepsilon(5)|}{x^{(1)}(5)} = 0.6\%,$$

Predictive precision is 99.4%, so we consider that the simulate effect is better.

5. Conclusions

By establishing and applying Verhulst model, we get the predictive value. Residual test shows that the predictive value is close to the actual value. It proved this model is very suitable to describe the saving manpower Benefits after maintenance system predigested from three level to two level. It provides a means of maintenance manpower management Benefits for some countries air force, we can use this model in the field of demonstration and conversion for two level maintenance concept.

But we must notice that the model can only be predicted the former 8~10 years condition after predigested maintenance system, because once TLM ran normally, it is no meaning to compare TLM with three level maintenance.

References

- Air Force Handbook 21-130. (1998). Technical Analysis to Determine Criterion for 2 vs. 3 Level Repair.
- Air Force Instruction 21-102. (1994). Depot Maintenance Management.
- Air Force Instruction 21-123. (1999). Air Force Gold Program.
- Air Force Instruction 21-129. (1998). Two Level Maintenance and Regional Repair of Air Force Weapon Systems and Equipment.
- Air Force Two Level Maintenance, Materiel Readiness & Maintenance Policy, <http://www.acq.osd.mil>.
- David Snipes. (1993). Data collection in a two level maintenance environment, *In: IEEE, AUTOTESTCON*. pp. 305-307.
- Deng, Julong. (1986). *Grey prediction and decision (in Chinese version)*, Huazhong university of science and technology press. pp. 120-122.
- Duanmu, Jingshun, Zhang, Zhengmin, Wu, Weixin and Wang, Chuanhong. (2003). *Materiel maintenance technology economy (book style with Chinese)*, National industrial press. pp. 135-140.
- George L. Daugherty. (1991). Two level maintenance: How do you get there. *In: Proceedings annual reliability and maintainability symposium*. pp. 397-399.
- John T. Schiefen. (1990). Cost effectiveness of two vs. three levels of maintenance for turbine engines in the Air force inventory thesis. ADA229622.
- Kevin C. Judge. (1989). Two level maintenance for advanced avionics architectures. *In: IEEE, AUTOTESTCON*. pp. 75-79.
- Li, Ruiqian and Wang, Shangren. (2005). *Air force aviation maintenance study (book style with Chinese)*. Defence university press. pp. 21-22.
- Liu, sifeng, Dang, yaoguo and Fang, Zhigeng. (2004). *Grey system theory and application (in Chinese Version)*. Science press. pp. 150-160.
- National Security and International Affairs Division. (1996). Two level maintenance program assessment, United States general accounting office. AD-A307070.
- PLA Air Force Materiel Office. (1988). Air force aeronautical engineering dictionary (dictionary style with Chinese). China science technology press. pp. 11-12.
- Robert L. Mason. (1999). Inside logistics – exploring the heart of logistics. Stealth fighter avionics: 2LM versus 3LM. *Department of the air force air force journal of logistics*, ADA369422.

- Stephen W. Dallas. (1989). Two level maintenance for missile system. *In: IEEE, AUTOTESTCON*. pp. 347-350.
- Stuart Kornreich. (1989). The two level maintenance – I level dilemma. *In: IEEE AUTOTESTCON*. pp. 63-66.
- U.S. Army Missile Command. (1988). Remotely piloted vehicle (RPV) two versus three level maintenance support concept study. ADA200665.
- Wallace Hughes. (1989). Two levels vs. three levels of maintenance: the Cost. *In: IEEE, AUTOTESTCON*. pp. 19-25.
- William J.Ames. (2000). Logistical effectiveness of two Level Maintenance, Air command and staff college air university.
- Yang, Weimin. (1995). *Reliability maintainability supportability pandect (in Chinese Version)*. National industrial press. pp. 100-102.

Table 1. a USA AF unit saved manpower after changing maintenance

Year	1994	1995	1996	1997	1998	1999
Data	996	2048	5820	5680	5962	5888



Treatment of Textile Effluent Using Sacrificial Electrode

K.Chithra

R.Thilakavathi

A. Arul Murugan

C. Marimuthu

N.Balasubramanian (corresponding author)

Department of Chemical Engineering, A.C. Tech Campus

Anna University-Chennai, Chennai-600 025, India

Tel: 91-44-2220-3501 E-mail: nbsbala@annauniv.edu

Abstract

Experiments were carried out to treat synthetic Bismarck Brown dye effluent using electro coagulation covering a wide range in operating conditions. The influence of operating parameters on efficiency of the process has been critically examined. The batch experimental results showed that the dye effluent can be effectively treated using electro coagulation. The overall COD removal efficiencies has been obtained 99%, under optimum operating condition. Further it is attempted to fit the experimental data with popular adsorption isotherms Langmuir and Temkin models. The predictions of Langmuir adsorption isotherm model are in good agreement with the experimental data.

Keywords: Electro coagulation, Wastewater treatment, COD removal, Sacrificial electrode

1. Introduction

Effluents with sturdy color and high COD are common in chemical process industries such as textile, paper, leather and mineral processing industries. In textile industries, dyeing and finishing are the two most important process operations which consumes large amount of water and generates considerable amount of wastewater which contains strong color, suspended particles, high pH and high COD and BOD. The textile effluent cannot be treated by chemical methods as these techniques generate considerable amount of sludge, which itself requires further treatment. While the biological methods are cheap and simple to apply, but cannot be applied to textile wastewaters since most of the commercial dyes are non-biodegradable and toxic to the organisms resulting in sludge bulking. On the other hand the advanced techniques such as reverse osmosis/ultra-filtration have the disadvantages of high cost and low throughput.

In recent years, there has been increasing interest in the use of electrochemical techniques such as electro coagulation, electro flotation, electro decantation, electrochemical oxidation, catalytic wet air oxidation etc for the treatment of dye house effluent. Among these techniques, electro coagulation emerges as one of the promising techniques for the treatment of organic effluent treatment. Successful electrocoagulation (EC) treatment of various industrial effluents has been reported by several researchers as it is considered to be potentially an effective tool for treatment of wastewaters with high removal efficiency. Electro coagulation has been adopted successfully to treat various industrial effluents such as potable water (Viek *et al.*, 1984); oil mill wastewater (Inan *et al.*, 2004); urban wastewater (Pouet and Grasmick, 1995); heavy metal laden wastewater (Lai and Lin, 2003); nitrite effluent (Koparal and Ogutveren, 2002); defluoridation (Zhu *et al.*, 2007); arsenic removal (Balasubramanian and Madhavan, 2001); textile industries (Can *et al.*, 2003); landfill leachate (Tsai *et al.*, 1997); restaurant wastewater (Chen *et al.*, 2000); salina wastewater (Lin *et al.*, 1998); tar sand and oil shale wastewater (Renk, 1988); laundry wastewater (Ge *et al.*, 2004).

The objective of the present study is to investigate the treatment of Bismarck Brown dye house effluent through electro coagulation under various operating conditions. The mechanism of electro coagulation and the effect of individual parameters on the efficiency of electro coagulation have been critically examined.

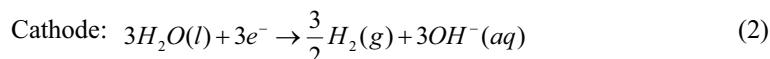
2. Mechanism of Electrocoagulation

It is known fact that electro coagulation is a complex and interdependent process. The sacrificial anode produces coagulating agent to dose the wastewater while electrolytic gases are generated at the cathode. The process of electro coagulation involves three successive steps:

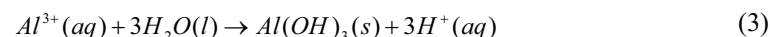
- i. Formation of coagulants by electrolytic oxidation of the 'sacrificial electrode'

- ii. Destabilization of the contaminants, particulate suspension, and breaking of emulsions and
- iii. Aggregation of the destabilized phases to form flocs.

The dissolved Fe/Al in the electrolyte generates corresponding metal ions and hydrolyzes to polymeric iron or aluminum hydroxide, which are excellent coagulating agents. The sacrificial anode continuously produces polymeric hydroxides at the anode and coagulation occurs when these metal cations combine with the negative charge particles carried toward the anode by electro phoretic motion. In the present case aluminum has been used as anode and the electrode reaction can be written as (Chen, 2004)



Al^{3+} and OH^{-} ions generated during the electrochemical reactions react to form various monomeric and polymeric species and transform into $Al(OH)_3$ according to the following reaction.

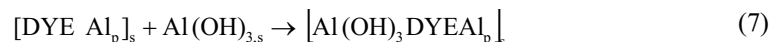
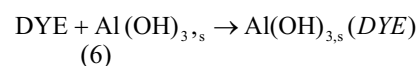


These $Al(OH)_3$ flocs capture the dye molecules present in the solution by the following reaction mechanism

Precipitation:



Adsorption:



In the electro coagulation process, the rate of removal of COD is proportional to the pollutant concentration and the amount of aluminium hydroxide formed.

$$\frac{-d[COD]}{dt} = k[COD][Al(OH)_3] \quad (8)$$

Since the generation of aluminium hydroxide produced can be assumed constant for a given current density, the equation (8) can be simplified to pseudo first order kinetics as

$$\frac{-d[COD]}{dt} = k[COD] \quad (9)$$

The integration of equation (9) results

$$\log \frac{[COD]_t}{[COD]_0} = -kt \quad (10)$$

The slope of the plot $\log [COD]_t / [COD]_0$ versus time gives rate constant.

3. Experimental

Experiments were carried out in a batch electrochemical reactor of 250ml. Aluminium and Stainless Steel of $7 \times 4 \text{ cm}^2$ were used as anode and cathode respectively. The electrodes were washed with dilute acid to remove surface grease/other impurities on the metal surface. The experiments were carried out under potentiostatic conditions covering wide range in operating conditions and samples were collected periodically for analyzed. The anode was weighed before and after the experiment for each experiment run to estimate the electrode consumption. At the end of the each run the solution was centrifuged at 2500 rpm, filtered and the filtrate was analyzed. The pollutant degradations were estimated by Colorimeter by standard estimation procedure for COD estimation.

4. Adsorption Isotherm

As stated earlier, the generated $Al(OH)_3$ flocs remains as a suspension in the electrolyte solution which effectively remove the pollutants by adsorption resulting in charge neutralization by complexation/ electrostatic attraction. It is attempted to extend the adsorption isotherms $Al(OH)_3$ for COD removal. The electrode consumption can be estimated according to Faraday's Law while the amount of flocs can be estimated stoichiometrically. The most widely used adsorption isotherms Langmuir and Temkin isotherms have been attempted in the present investigation to check the adsorption kinetics.

The mathematical expression of Langmuir isotherm can be written as

$$\frac{C_e}{Q_e} = \frac{1}{K_L} + \frac{a_L}{K_L} C_e \quad (11)$$

where the constant K_L refers Langmuir equilibrium constant. A plot of C_e/Q_e versus C_e gives a straight line results a_L/K_L (slope) and $1/K_L$ (intercept).

The Temkin isotherm can be expressed mathematically as

$$Q_e = \frac{RT}{b} \ln A + \frac{RT}{b} \ln C_e \quad (12)$$

$$\frac{RT}{b} = B \quad (13)$$

where A and B are Temkin constants. A plot of Q_e versus $\ln C_e$ enables to determine the constants A and B.

5. Results and Discussion

Experiments were carried out at various pH by adjusting the electrolyte with sodium hydroxide or hydrochloric acid and the observations are given in Figures 1-5. It can be ascertained from the Figure 1 the percentage COD removal increases with increase in the process time. The rate of increase in the percentage COD removal is high in the beginning of the process and approaches monotonical situation beyond 30minutes of process time. This can be explained that the more of coagulation process occurs within 30minutes of process time. This can be explained that the existence of excess colloids for the adsorption at high initial concentrations.

The Figure 2 shows the effect of electrolyte pH on percentage COD removal efficiency. It can be seen from the figure that the percentage COD removal increases with an increase in the electrolyte pH from 3 to 4. However no significant improvement has been observed when the pH increased beyond pH value of 4. A maximum 97% removal efficiency has been observed at a pH value of 4 in the present investigation.

The effect of applied charge on COD removal efficiency is given in Figure 3. It can be seen from the figure that the percentage COD removal efficiency increases with an increase in the applied current density. This can be explained that at high current densities, the extent of anodic dissolution of aluminum increases, resulting in a greater amount of precipitate for the removal of pollutants. In addition, the rate of bubble generation also increases with increasing current density, which enhances the COD removal efficiency.

The reaction rate constant, k, was estimated from a plot of $\ln[\text{COD}_t/\text{COD}_0]$ versus electrolysis time. The influence of operating parameters on the reaction rate constant has been verified and it has been observed that the rate constant, k, is influenced by the applied charge [Figure 4.]. However no significant improvement has been observed with electrolyte pH.

Figure 5 shows the relationship between the amount of COD adsorbed per unit mass of charged hydroxo cationic complexes (Q_e) and final COD in the aqueous phase (C_e). The plots of COD uptake against equilibrium concentration indicate that adsorption increases with concentration and approaches saturation. Based on the correlation coefficient (r^2) shown in Table 1, the adsorption isotherm with hydroxo cationic complexes can be described by the Langmuir equation (11) which gives a better fit of experimental data than the Temkin equation (12).

6. Conclusions

Experiments were carried out to treat dye house effluent using electro coagulation. The influence of initial dye concentration, pH and current density on coagulation efficiency has been critically examined. It has been observed from the present investigation that the percentage of COD reduction is significantly influenced by the initial dye concentration, pH and current density. The adsorption isotherms namely Langmuir and Temkin isotherms were used to check the adsorption kinetics.

7. References

- Balasubramanian, N., Madhavan., K. (2001). Arsenic removal from industrial effluent through electrocoagulation. *Chemical Engineering Technology* 24, 519-521.
- Can, O.T., Bayramoglu, M., Kobya, M. (2003). Decolorization of reactive dye solutions by electrocoagulation using aluminum electrodes, *Ind. Eng. Chem. Res.* 42, 3391–3396.
- Chen, G. (2004). Electrochemical technologies in wastewater treatment, *Sep. Purif. Technol.*, 38, 11–41.
- Chen, X., Chen, G., Yue, P.L. Separation of pollutants from restaurant wastewater by electrocoagulation, *Sep. Purif. Technol.* 19 (2000), pp. 65–76.
- Ge, J., Qu, J., Lei, P., Liu, H., 2004. New bipolar electro coagulation– electro flotation process for the treatment of laundry wastewater. *Sep. Purif. Technol.* 36, 33–39.

Inan, H., Dimoglo, A., Şimşek, H., Karpuzcu, M. (2004). Olive oil mill wastewater treatment by means of electro-coagulation, *Separat. Purif. Technol.* 36, 23–31.

Koparal, A.S., Ogutveren, U.B. (2002). Removal of nitrate from water by electroreduction and electrocoagulation, *J. Hazard. Mater.* 89, 83–94.

Lai, C.L., Lin, S.H. (2003). Electrocoagulation of chemical mechanical polishing (CMP) wastewater from semiconductor fabrication, *Chem. Eng. J.* 95, 205–211.

Lin, S.H., Shyu, C.T., Sun, M.C., (1998). Saline wastewater treatment by electrochemical method. *Water res.* 32, 1059-1066.

Pouet, M.F., Grasmick, A. (1995). Urban wastewater treatment by electrocoagulation and flotation, *Water Sci. Technol.* 31, 275–283.

Renk, R.R., 1988. Electrocoagulation of tar sand and oil shale wastewater. *Energy Prog.* 8, 205–208.

Tsai, C.T., Lin, S.T., Shue, Y.C., Su, P.L., 1997. Electrolysis of soluble organic matter in leachate from landfills. *Water Res.* 31, 3073–3081.

Vik., E, Carlson., D, Eikum., A. (1984). Electrocoagu-lation of potable water. *Water Research*, 11, 1355-1600.

Zhu, J., Zhao, H., Ni, J. (2007). Fluoride distribution in electrocoagulation defluoridation process Separation and Purification Technology, 56, 2, 184-191.

Table 1. Isotherm constants for adsorption of COD on Al(OH)₃

Langmuir	$K_L(Lg^{-1})$	$a_L(Lmg^{-1})$	r^2
	8.1×10^{-6}	0.0059	0.9613
Temkin	B	A (Lg ⁻¹)	r^2
	3×10^5	0.006	0.92

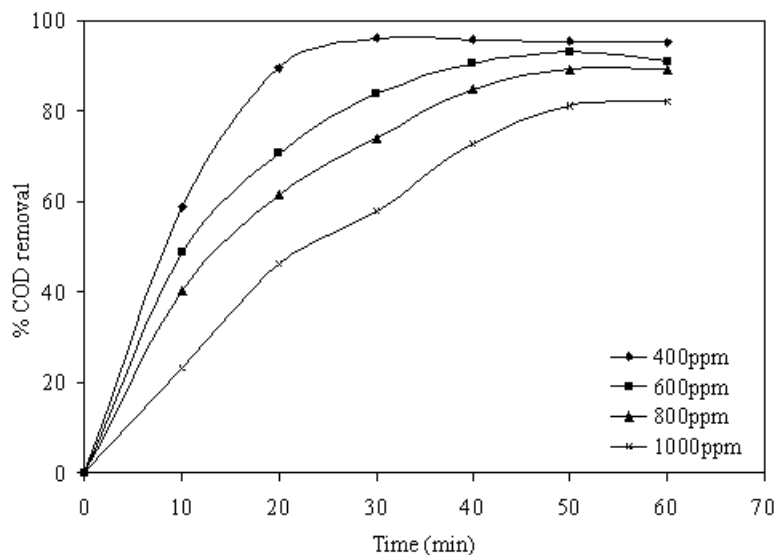


Figure 1. Effect of electrolysis time on percentage COD removal (Current density: 6 mAcm⁻²; Supporting electrolyte concentration: 400ppm).

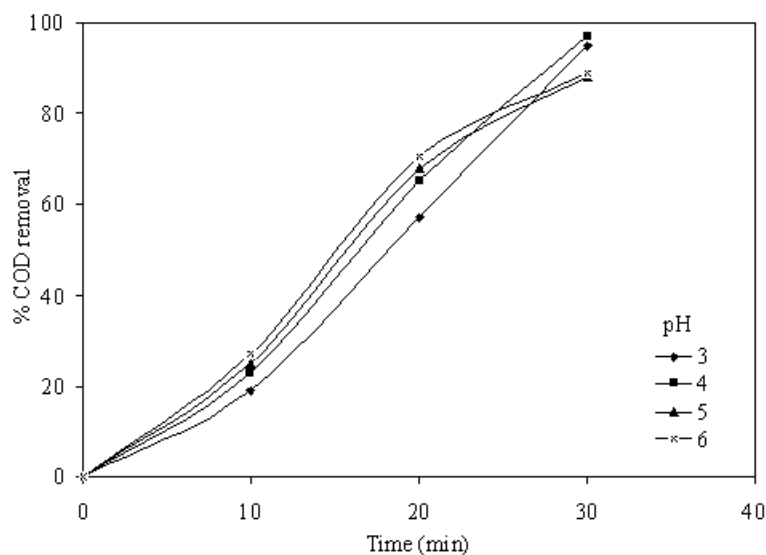


Figure 2. Effect of initial pH on percentage COD removal
(Supporting electrolyte concentration: 400ppm; Current density: 6mAcm⁻²; Electrolysis time: 1hr).

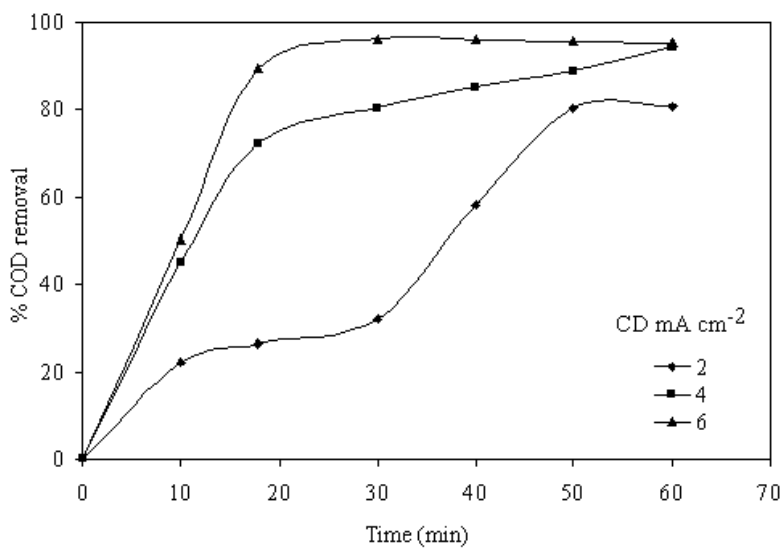


Figure 3. Effect of current density on percentage COD removal
(Electrolysis time: 30min; Supporting electrolyte concentration: 400ppm).

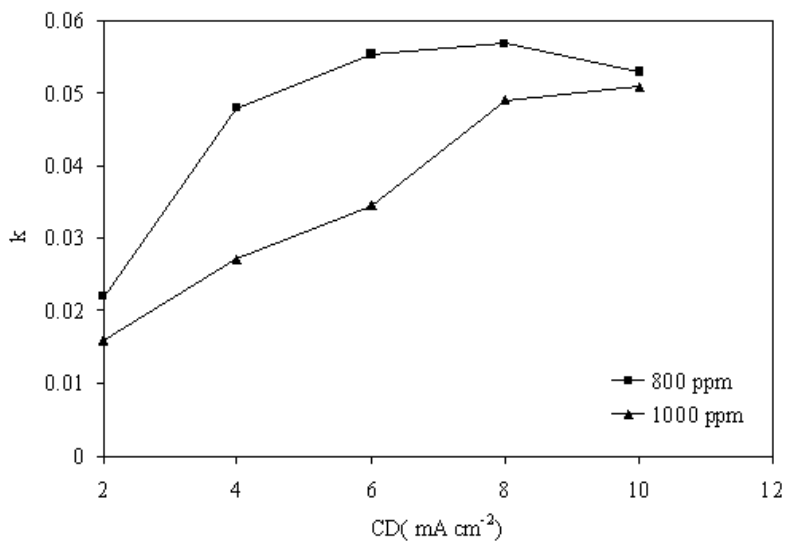


Figure 4. Effect of current density on rate constant k.

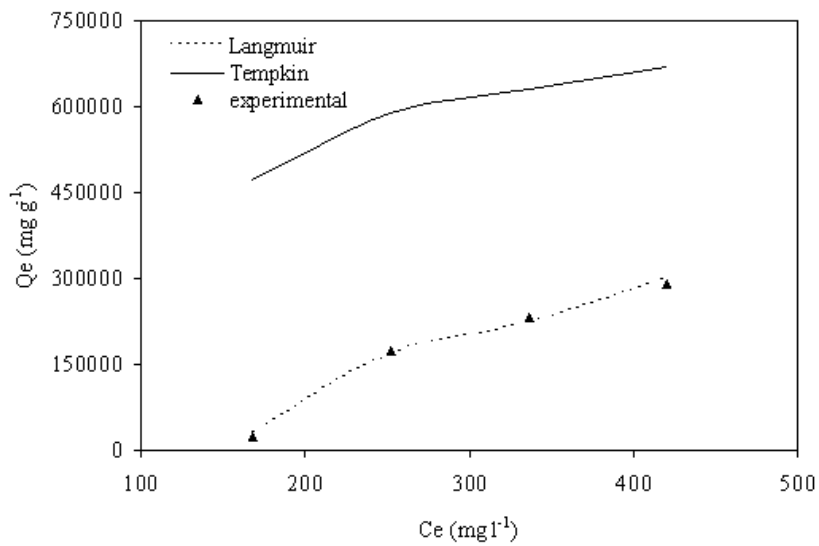


Figure 5. Comparison of isotherm model predictions with the experimental observation.



Effects of Microencapsulated Phase Change Materials Granularity and Heat Treat Treatment Condition on the Structure and Performance of Polyurethane Foams

Ming You, Xuechen Wang, Xingxiang Zhang & Wei Li

Tianjin Municipal Key Lab of Fiber Modification and Functional Fiber

Tianjin Polytechnic University, Tianjin 300160, China

Tel: 86-22-2458-4815 E-mail: yming_21@yahoo.com.cn

Abstract

In this article, we study on the effect of different congregated granularities of microencapsulated n-octadecane on polyurethane foamed system, and the making of the polyurethane foams with high contents of microencapsulated n-octadecane. The results show that, when relative low granularities of microencapsulated phase change materials (MicroPCMs) are used as additives, the remnant water and formaldehyde have adverse effects on the foam, so the MicroPCMs should better be heat-treated which is helpful for removing the residual, and more uniform foam can be obtained when relative low granularities of MicroPCMs are used. The polyurethane foams with maximum contents of 28 parts of n-octadecane can be made when the polyethylene glycol-400 (PEG-400) is interfused in the foamed system to regulate the viscosity of the system. The formed foams absorb heat at about 27°C and dissipate heat at about 25°C, which heat storage is bigger than 18J/g and can be used as thermal insulation materials.

Keywords: Microencapsulated phase change materials, Polyurethane, Foam, Heat-treatment, Granularity

In the phase change process, phase change materials (PCM) can absorb and dissipate heats to control the temperature of the environment (Chaurasia, 1981, p.159). Microcapsule is the tiny “container” with the diameter of 1~1000µm, and it is the MicroPCMs which encapsulates phase change materials in the capsule wall and can realize permanent solid state of phase change materials (Xing, 2004, p.2669–2675). MicroPCMs can absorb or dissipate heats in a certain range, and the temperature is almost changeless in the process of heat absorption or heat dissipation, and this special performance has important applications in fibrous fabrics (Hittle, 2002, p.175 & Bryant, 1994 & Kim, 2002, p.1093 & Zhang, 2005, p.3729) and solar-energy (Chaurasia, 1981, p.159).

Polyurethane foam is the reactive product of isocyanate and polymer polyhydric alcohols, which applications come down to many domains (Zhu, 2005). With increasingly enhancement of people living level, the research and development of new soft polyurethane foams are more and more. If the MicroPCMs is added into the polyurethane foamed system, the foam with heat storage can be made, and this foam can store heats and regulate temperature (Bryant, 1996). Through a series of experiments, we study effects of MicroPCMs granularity and heat treat treatment condition on the structure and performance of polyurethane foams and primarily explore how to make polyurethane foams with high contents of MicroPCMs.

1. Experiment

1.1 Materials

(1) Combustion modified high resilience foam made by Jiangyin Yobo Polyurethane Co., Ltd. Specification: A group (combined polyether) YB-5181, B group (isocyanate) YB-6280. Technical data advised by the factory: quality proportion A:B=100:33, material temperature: 25±2°C, model temperature: 60±5°C, mold release time: 300~600s.

(2) Dibutyltin dilaurate (DBTL) and chemical purity made by Tianjin Chemical Reagent First Factory. PEG-400 and chemical purity made by Tianjin Tiantai Fine Chemical Co., Ltd.

1.2 The preparation of MicroPCMs

Take melamine-formaldehyde as the capsule ware, n-octadecane (imported from US. The melting point is at 28.5°C and the phase change heat is 242.4J/g) as the capsule core and adopt the in-situ polymerization method to make MicroPCMs (Zhang, 2004, p.300), and the contents of phase change materials is about 65wt%, the granule diameter of MicroPCMs is about 1~5µm. The microcapsule felts in the process of desiccation and dehydration and forms agglomeration particles,

and the diameter of agglomeration particles can achieve 1mm. Take MicroPCMs pass 80-eyes screen and make the diameter of agglomeration particles $\leq 180\mu\text{m}$.

1.3 The preparation of polyurethane foam with MicroPCMs

Mix MicroPCMs, A material, PEG-400 and DBTL according to their prescriptive quantities around intensely in the beaker, and add B material when MicroPCMs spread around in the system, and beat up quickly in 5~10s, and when the glue liquid blanches, put it in the mold, and after about 1 minute, transfer it to the oven at 60°C to foam. Release the mold when it is solidified, and so the polyurethane foam with MicroPCMs is made.

1.4 Testing and tokens

In the oven with constant temperature, respectively at 110°C , 120°C , 130°C , 140°C , 150°C and 160°C , implement heat treatment to MicroPCMs in 30 minutes, and adopt Perkin Elmer DSC-7 differential scanning calorimeter to implement heat differential analysis to the sample of polyurethane foam, and the testing range is $0\sim 80^{\circ}\text{C}$, and the scanning speed is $\pm 10^{\circ}\text{C}/\text{min}$, and implement the protection with N_2 .

Through the golden sprayed treatment to the sample of the foam, observe the cell structure of the polyurethane foam by the Quanta 200 scanning electron microscope.

Implement the test of the viscosity to A material, MicroPCMs, PEG-400 mixture by the NDJ-1 Revolving Viscosity Tester made by Shanghai Precision & Scientific Instrument Co., Ltd.

2. Results and discussions

2.1 Effects of MicroPCMs granularity on foaming

After the filling is added into the polyurethane foaming system, because the initial viscosity and surface strain of the system, the phenomena including volume shrinking, interior break, exterior break, even foam breaking and collapse will occur in the foaming process (Wu, 2005, p.5). And the capsule wall material will contain much hydroxyl group, so the MicroPCMs need to be added into the polyurethane foaming system, and dosages of various group parts, mainly including B material and organic tin activator (DBTL used in this research), need to be regulated to make better foams.

Add MicroPCMs with big granularity and without screening into the foaming system and regulate dosages of various group parts, the better foams can be made, which is show in Table 1.

After take MicroPCMs pass the 80-eyes screen (granularity $\leq 180\mu\text{m}$), foam according to the prescription of Table 1, and the result shows that foam combination and break are very serious in the foaming process and it is hard to make better foam. The reasons may include that a great lot additives such as formaldehyde, antifoam, emulsification and so on are used in the making process of MicroPCMs, and these additives stayed in finished capsules will badly influence foaming. When MicroPCMs don't pass the eyes screen, their granularities are very big, and even some parts will agglomerate, so the remnant additives absorbed on the surface are few, which has little influences to foam, and better foams can be made through the regulation of the prescription, but because some MicroPCMs agglomerations are too big (which diameter can achieve 1mm) to enter in the polyurethane foam evenly, and they will spread in the foam, which will produce limitations in the foam and decrease the performance of the polyurethane. Therefore, to improve the performance of the polyurethane foam, MicroPCMs with small granularity should fully enter into the polyurethane body. When MicroPCMs pass the 80-eyes screen, their granularities will decrease and their surface areas will increase, and the remnant additives absorbed on the surface will comparably increase, which will seriously influence foaming and induce foam combinations and foam breaks.

2.2 Effects of MicroPCMs heat treatment on foaming

Implement heat treatment to MicroPCMs screened by the 80-eyes screen under different temperatures, eliminate remnant formaldehyde and absorbed water (Zhang, 2004, p.300), reduce the diameter of agglomeration particles and regulate the prescription group parts to foam, and the results are shown in Table 2.

From Table 2, we can see that after the heat treatment to MicroPCMs screened by the 80-eyes screen, they can be made better foam materials, and the reason may be that in the process of heat treatment, the volatilizations of remnant formaldehyde and water reduce bad influences to the foaming. When MicroPCMs are treated respectively at 110°C and 120°C , the made foams have bulky apertures because the temperature of heat treatment is too low and the volatilizations of formaldehyde and water are less.

Table 3 shows the heat performance of MicroPCMs after heat treatment. When the temperature of the heat treatment is bigger than 110°C , the performance will be reduced because when the temperature of heat treatment is higher, part of MicroPCMs break and the material (n-octadecane) in the capsule core sublimates. So the condition of heat treatment should be at 130°C and in 30 minutes.

Add MicroPCMs through 80-eyes screen treated at 130°C and in 30 minutes into the polyurethane foaming system, and the foaming prescription is seen in Table 4.

When the additive quantity of MicroPCMs is bigger than 20 parts, the mixture of MicroPCMs and A material presents paste state, and its system viscosity is very high, and MicroPCMs are difficult to evenly spread around in the system, and the ideal foams are difficult to be made however to regulate dosages of various group parts.

2.3 Effects of MicroPCMs granularity on the cell structure and the compressibility of polyurethane foams

Figure 1 shows TEM photos of the polyurethane foam cell structure. When MicroPCMs are added into the foaming system, the cell diameter is generally smaller than it without MicroPCMs, which is induced by the “core formation” function and accords with the rule that general added powder filling will reduce the cell diameter. The polyurethane foams made by adding MicroPCMs through 80-eyes screen into the foaming system have more even cell structure and put up good even characteristic.

2.4 Preparation research of the polyurethane foam with high content of MicroPCMs

Mix MicroPCMs (after heat treatment) with A material (the initial viscosity is 1425mPa) at room temperature, and with the increase of MicroPCMs, the viscosity will rise, which is seen in Figure 2. When additive parts of MicroPCMs are bigger than 20, the system viscosity is too high (for example, when the additive quantity of MicroPCMs is 25 parts, the mixture dynamics viscosity is 9800mPa) to make better foams.

In this experiment, we regulate the system viscosity through interfusing PEG-400 into the mixed system, and the results are shown in Table 5. When PEG-400 is mixed into the mixed system, the system viscosity will decrease and the better foam with maximum content of 28 parts of MicroPCMs can be made. When the additive quantity of MicroPCMs is 30 parts, the foam shrinks seriously, because the content of vesicant in A material (combined polyether) is relative deficient, the foaming gas will reduce. Therefore, when the polyurethane foam with high content of MicroPCMs is made, the system viscosity is a very important factor, and we also can see that if the polyhydric alcohols system with low initial viscosity is used and the prescription ratio of various group parts is regulated, it can further enhance the content of MicroPCMs.

Figure 3 and Figure 4 are respectively DSC temperature rise and drop curves of polyurethane foam with different contents of MicroPCMs. The polyurethane foam without MicroPCMs has not heat adsorption and heat dissipation, and the polyurethane foam with MicroPCMs has heat adsorption and heat dissipation, and with the increase of content of MicroPCMs, its phase change heat will increase, and the measured value is smaller than the theoretical computation value perhaps because of the heat stagnation function of the polyurethane.

3. Conclusions

- (1) It needs to regulate dosages of various group parts to make better foam when adding microencapsulated n-octadecane into the polyurethane foaming system.
- (2) When the microencapsulated n-octadecane with small granularity is added, the proper heat treatment should be implemented to eliminate remnant formaldehyde and water and reduce bad influences for foaming.
- (3) The microencapsulated n-octadecane with small granularity added can enhance the equal character of the foam and make for the equality of the foam.
- (4) When the microencapsulated n-octadecane with small granularity is added, the system viscosity will increase, so the proper decrease of system viscosity can make the foam with higher content of microencapsulated n-octadecane.
- (5) The polyurethane foam with microencapsulated n-octadecane absorbs heat at about 27°C and dissipates heat at about 25°C, and the heat storage can achieve 18J/g.

References

- Bryant, Y G, Colvin D P. (1994). Fabric with Reversible Enhanced Thermal Properties. *US Patent*, 5366801.
- Bryant, YG and Colvin DP. (1996). Moldable Foam Insole with Reversible Enhanced Thermal Properties. *US Patent* 5499460.
- Chaurasia P L B. (1981). Solar-energy Thermal Storage-system Based on Encapsulated Phase Change Material. *Research and Industry*. No.26(3). p.159.
- Hittle, D C and Andre T L. (2002). A New Test Instrument and Procedure for Evaluation of Fabrics Containing Phase Change Material. *ASHRAE Transactions: Research*. No.180(1). p.175.
- Kim, J and Cho G. (2002). Thermal Storage/release, Durability, and Temperature Sensing Properties of Thermostatic Fabrics Treated with Octadecane-containing Microcapsules. *Textile Research Journal*. No.72(12). p.1093.
- Wu, Run-de, Tong X L, Zhang Jia-kai & Liu G B. (2005). Influence of Nano-filler on Mechanical Properties of Soft Polyurethane Foam. *China Elastomerics*. No.15(3). p.5.
- Xing, F B, Cheng G X, Yang B X, et al. (2004). Microencapsulation of Capsaicin by the Complex Coacervation of

Gelatin, Acacia and Tannins. *Journal of Applied Polymer Science*. No.91. p.2669–2675.

Zhang, X X, Fan Y F, Tao X M & Yick K L. (2004). Fabrication and Properties of Microcapsules and Nanocapsules Containing n-octadecane. *Materials Chemistry and Physics*. No.88(2-3). p.300.

Zhang, XX, Wang XC, Tao XM, et al. (2005). Energy Storage Polymer/MicroPCMs Blended Chips and Thermo-regulated Fibers. *Journal of Materials Science*. No.40. p.3729.

Zhu, L M, Liu Y J. (2005). *Polyurethane foam plastics*. Beijing: Chemical Industry Press. 2005.17.

Table 1. Polyurethane foaming prescription with MicroPCMs (without screening)

A material/pphp	B material/pphp	MicroPCMs/pphp	Added DBTL /pphp	Foam
100	33	0	0	better
100	33	5	0.32	better
100	33	7	0.32	better
100	33	10	0.43	better
100	35	12	0.55	better
100	38	15	0.65	better
100	39	17	0.65	better
100	40	20	0.85	good

Note: “pphp” is the quality parts relative to 100 parts of polyhydric alcohols.

Table 2. Effects of MicroPCMs heat treatment on foaming

A material/pphp	B material/pphp	DBTL/pphp	MicroPCMs after heat treatment/pphp	Foam
100	36	0.55	15 (110°C for 30min)	bulky aperture
100	36	0.55	15 (120°C for 30min)	bulky aperture
100	36	0.55	15 (130°C for 30min)	better
100	36	0.55	15 (140°C for 30min)	better
100	36	0.55	15 (150°C for 30min)	better
100	36	0.55	15 (160°C for 30min)	better

Table 3. Heat performance of MicroPCMs after heat treatment

A material/pphp	B material/pphp	MicroPCMs/pphp	Added DBTL /pphp	Foam
100	33	0	0	better
100	33	5	0.32	better
100	33	7	0.32	better
100	33	10	0.43	better
100	35	12	0.55	better
100	38	15	0.65	better
100	39	17	0.65	better
100	40	20	0.85	good

Note: T_m represents the melt point, T_c represents the freezing point, ΔH_m represents the melt enthalpy, ΔH_c represents the crystal enthalpy, and $\Delta H_a = (\Delta H_m + \Delta H_c) / 2$.

Table 4. Polyurethane foaming prescription containing MicroPCMs through 80-eyes screen

A material/pphp	B material/pphp	MicroPCMs /pphp	DBTL/pphp	Foam
100	33	0	0	better
100	33	5	0.32	better
100	33	7	0.32	better
100	33	10	0.32	better
100	34	12	0.55	better
100	36	15	0.55	better
100	38	17	0.65	better
100	38	20	0.85	better

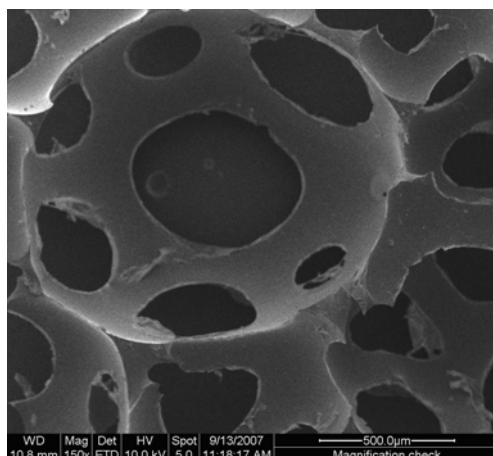
Table 5. Foaming prescription interfused PEG

A material/pphp	PEG-400/pphp	B material/pphp	DBTL/pphp	MicroPCMs/pphp	Dynamics viscosity/ mPa	foam
92	8	36	0.55	22	6600	better
88	14	38	0.65	25	6900	better
80	20	41	0.85	28	7300	good
74	26	43	0.85	30	7600	foam shrinking

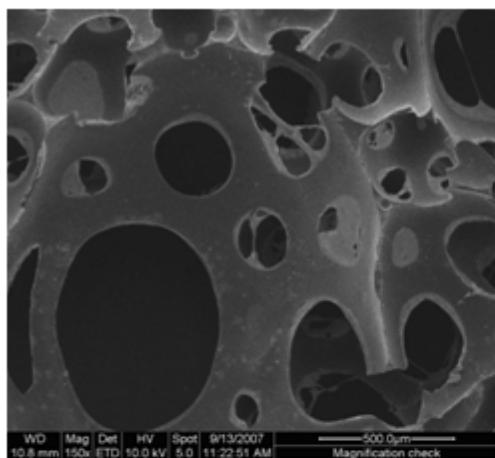
Table 6. Heat performance of polyurethane foam containing MicroPCMs

MicroPCMs/parts	T _m /°C	ΔH _m /J/g	T _c /°C	ΔH _c /J/g	ΔH _a /J/g	ΔH/J/g
0	-	0	-	0	0	0
22	27	16	24	17	16.5	19
25	26	17	24	18	17.5	21
28	27	19	25	18	18.5	23

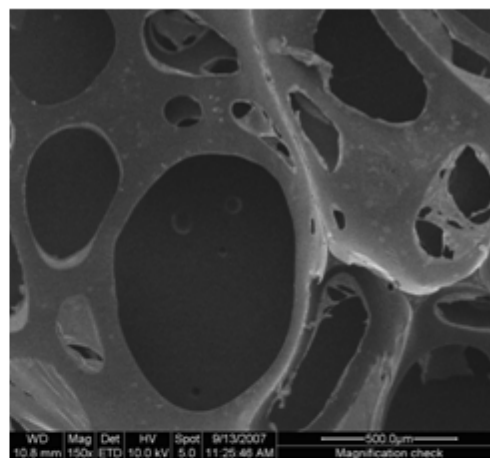
Note: ΔH is the theoretical computation value.



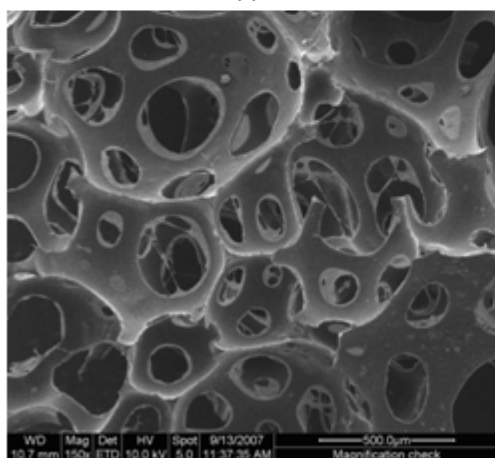
(a)



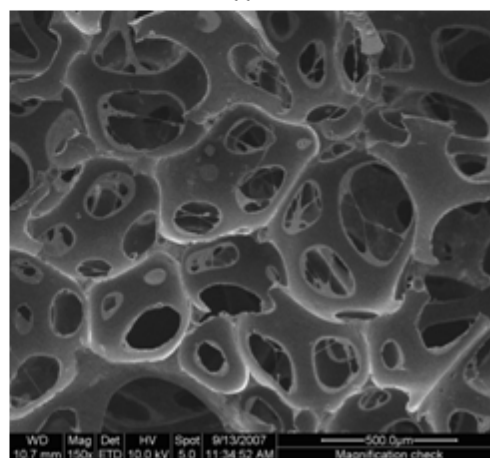
(b)



(c)



(d)



(e)

Figure 1. SEM Photos of Polyurethane Foam Cell Structure ((a) doesn't contain MicroPCMs, (b) contains 15pphp MicroPCMs without screening, (c) contains 20pphp MicroPCMs without screening, (d) contains 15pphp MicroPCMs through 80-eyes screen, (e) contains 20pphp MicroPCMs through 80-eyes screen)

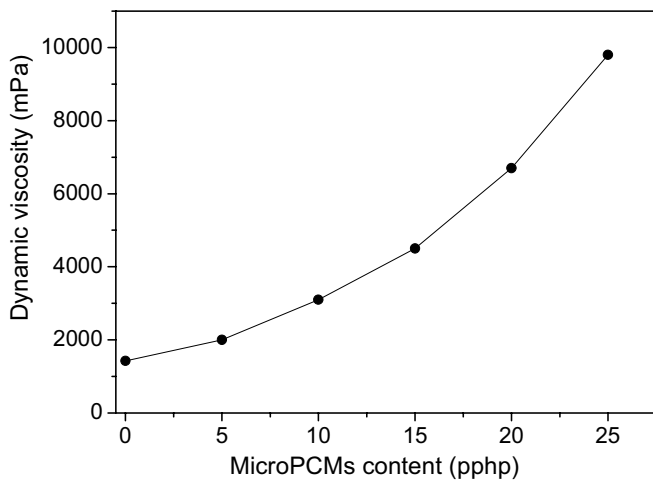


Figure 2. Mixture Dynamics Viscidity: MicroPCMs Content Curve

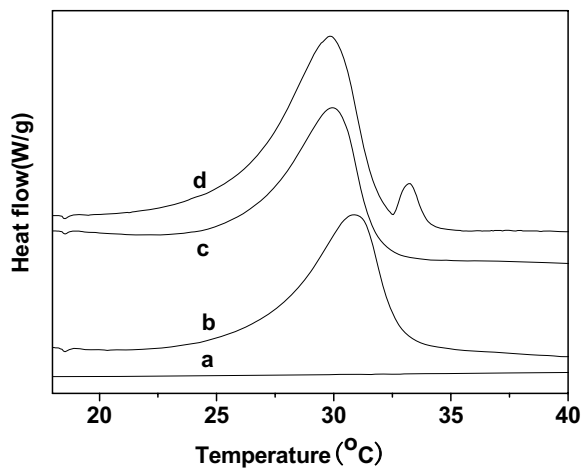


Figure 3. DSC Temperature Rise Curve of Polyurethane Foam with Different Contents of MicroPCMs (a: 0pphp, b: 22pphp, c: 25pphp, d: 28pphp)

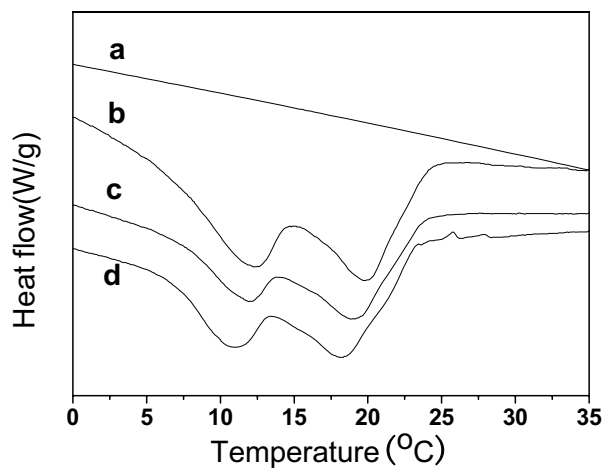


Figure 4. DSC Temperature Drop Curve of Polyurethane Foam with Different Contents of MicroPCMs
(a: 0pphp, b: 22pphp, c: 25pphp, d: 28pphp)



Knowledge Extraction from Trained Neural Network Scour Models

H. Md. Azamathulla (corresponding author)
River Engineering and Urban Drainage Research Centre (REDAC)
Universiti Sains Malaysia, Engineering Campus
14300 Nibong Tebal Pulau Pinang, Malaysia
E-mail: redacazamath@eng.usm.my, mdazmath@gmail.com

Aminuddin Ab Ghani
REDAC, Universiti Sains Malaysia
E-mail: redac02@eng.usm.my

Nor Azazi Zakaria
REDAC, Universiti Sains Malaysia
E-mail: redac01@eng.usm.my

Chang Chun Kiat
REDAC, Universiti Sains Malaysia
E-mail: redac10@eng.usm.my

Leow Cheng Siang
REDAC, Universiti Sains Malaysia
E-mail: redac21@eng.usm.my

The research is financed by Universiti Sains Malaysia for funding a short term grant 304.PREDAC.6035262 (Sponsoring information)

Abstract

This study extends the earlier contribution of Azamathulla et al. in 2005. Artificial neural networks (ANNs), due to their excellent capabilities for modeling complex processes, have been successfully applied to a variety of problems in hydraulics. However, one of the major criticisms of ANNs is that they are just black-box models, since a satisfactory explanation of their behavior has not been offered. They, in particular, do not explain easily how the inputs are related to the output, and also whether the selected inputs have any significant relationship with an output. In this paper, a perturbation analysis for determining the order of influence of the elements in the input vector on the output vector is discussed. The approach is illustrated through networks recommended in Azamathulla et al. 2005 for prediction of scour using neural networks. The analyses of the results suggest that each variable in the input vector (discharge intensity, head, tail water depth, bed material, lip angle and radius of the bucket) influences the depth of scour in different ways. However, the magnitude of the influence cannot be clearly quantified by this approach. Further it adds that the selection of input vector based on linear measures between the variables of interest, which is commonly employed, may still include certain spurious elements that only increase the complexity of the model.

Keywords: Neural Networks, Scour, Spillways

1. Introduction

Artificial neural networks (ANN) technique has been successfully applied across a broad spectrum of problem domains such as pattern recognition and function approximation. Most ANN applications in engineering mainly fall in the

category of prediction, in which an unknown relationship exists between a set of input factors and an output (Jingsheng, 2002). The objective of these studies is to find a formula between the selected input variables and the output based on a representative set of historic examples. The formula is then extended to predict the outcome of any given input. The computational efficiency of ANNs has yielded many promising results in the field of hydraulics and water resources. This interest has been motivated by the complex nature of scour mechanism and the ability of ANNs to model nonlinear relationships (Azamathulla et al. 2005). However, ANNs remain something of a numerical enigma. In particular, they offer end user little or no insight into either the process by which they arrived at a result or, in general, the totality of knowledge actually embedded therein (Tickle et al. 1998). The ANNs possess several significant attributes such as universal function approximation property, robustness, and ability to learn. However, ANNs are also criticized due to their perceived weakness of being black-box models.

This is a significant weakness, for without the ability to produce comprehensible decisions it is hard to trust the reliability of networks addressing real-world problems (Benitez et al. 1997). Therefore, a significant research effort is needed to address this deficiency of ANNs. Some solutions have been proposed to represent the operation of a trained neural network, which deals with classification problems, in terms of symbolic rules (Lozowski et al. 1996; Benitez et al. 1997; Tickle et al. 1998; and Castro et al. 2002). However, most of the hydrologic applications of ANNs fall in the category of function approximation, and knowledge extraction from such models is still a virgin research area. For instance, Lange (1999) states that ANNs are black-box models that only develop the relation between input and output variables without the modeling of any physical processes. However, it must be realized that the data that are employed in developing black-box models contain important information about the physical processes being modeled, and this information gets embedded or captured inside the model. This paper discusses the use of a method similar to perturbation analysis (Ho, 1992) to extract the knowledge embedded in trained ANN models for prediction of scour pattern.

2. Perturbation Analysis

Neural networks (NN) are capable of modeling complex processes, and have been successfully applied to a variety of problems in hydraulic engineering. However, one criticism in this regard is that they are black-box models and do not offer, a satisfactory explanation of their performance. ANN models neither explain how the inputs are related to the output, nor whether the selected inputs have any significant relationship with an output (Sudheer, 2005). In this study, a perturbation analysis for determining the order of influence of the elements in the input vector on the output vector is therefore discussed.

Most NN applications in engineering mainly belong to variable prediction, in which an unknown relationship is assured to exist between a set of input factors and an output (Jingsheng, 2002). The objective of these studies is to find a formula between the selected input variables and the output based on a representative set of historic examples. The formula is then extended to predict the outcome of any given input. However, it must be realized that the data that are employed in developing black-box models contains important information about the physical process being modeled, and this information gets embedded or captured inside the model. This study discusses the use of a method that is similar to perturbation analysis (Ho, 1992) to extract the knowledge embedded in trained NN models for prediction of scour pattern. The main aim of the study was to identify the strength of relationship between individual input variables and the output. The study also aimed at assessing the degree of influence of the individual input variables on the output function. The methodology is illustrated through a FFBP Model-1 for prediction of scour pattern downstream of flip bucket spillway (Azamathulla et al. 2005).

3. Methodology

In NN modeling, the combination of all of the variables (input and output) locates a point in a multidimensional input-output space called phase space (Stewart, 1989). The main idea in the method is that a great deal of information is contained in the sample paths in the phase space of the dynamic system. This is much beyond the usual statistics collected such as the means and variances of various output variables. Rather than looking at the simulation simply as a black box with input parameters and final output results, one can utilize the knowledge on the dynamics of the functional domain and get additional information, such as performance and sensitivity of the model. This can be achieved by studying the effects of small disturbances (perturbation) in the mathematical model of a physical system. This model can be expressed as an algebraic equation, integral equation, and ordinary differential equation, partial differential equation, in isolated or combined form.

Once an NN model is trained for its generalisation properties, it can be assumed that the trained model represents the physical process of the system. The knowledge acquired for the problem domain during the training process is encoded within the NN in two forms: (a) in the network architecture itself (through number of hidden units) and (b) in a set of constants or weights. Since NN models have large degree of freedom in assigning the weights, they can lead to a situation where two different sets of weights can yield identical outputs (Schmitz et al., 1999). A perturbation analysis of NN parameters may, thus, lead to insignificant implications. However, the distributed nature of information

processing in NN implies that a network can be disaggregated in terms of its forecasting inputs, and can still yield outputs. Thus by considering the effects of small disturbances in individual input variables to the network, its relative importance in the total output can be assessed while keeping the network parameters unchanged; or in other words the effect of various inputs on the behavior of the modeled process can be evaluated.

Consider an NN model that represents the functional relationship between attributes inputs x^n and classes outputs y^m and evaluated at a set of points S (input patterns) lying inside the domain D. The magnitudes of the partial derivatives of the function with respect to the inputs are a measure of significance and, it is hence assumed that the variables can change freely and independently from one another. This assumption is valid as the influencing factors can be varied individually. However, if the measured attributes are correlated this assumption is not appropriate, as a change in one input feature may be accompanied by a change in another covariant feature.

Schmitz et al. (1999) showed that these inter-relationships could be taken into account by focusing on the variations of f that actually occur inside the domain D, which is done by measuring the variation of f when moving between points in S. This variation, is computed by a term absolute variation $v(f)$ of the function $f(x)$ between the points i and j , which is defined as the absolute value of the directional derivative of $f(x)$ integrated along a straight line between the two points. Thus, with 'u' as the unit vector in direction x_i to x_j ,

$$v_{ij}(f) = \int_{x_i}^{x_j} |\Delta f(x) \cdot u| dx \quad (1)$$

This variation can be ciphered between all pairs of points in S. If an attribute is insignificant to the function for the domain D, the variation in the function will be unrelated to the variation in the attribute and a measure of significance of an attribute x_i for a function f over a data set S could be the correlation between the absolute variation of the function and the absolute variation of that attribute taken between all possible pairs of points in S. This method is illustrated in the following sections with the help of a FFBP Model-1, NN model. This approach is based on cross-, auto-, and partial auto-correlations between the variables in question.

The sigmoid function is used as the activation function in both hidden and output layers. Therefore, the model output and input were scaled appropriately to fall within the function limits. A standard feed forward back propagation algorithm is employed to estimate the network parameters. The number of hidden neurons in the network, which is responsible for capturing the dynamic and complex relationship between various input and output variables, was identified by various trials (Eberhart and Dobbins, 1990; Maier and Dandy, 2000). The trial-and-error procedure started with two hidden neurons, and the number of hidden neurons was increased to 10 during the trials with a step size of 1 in each trial. For each set of hidden neurons, the network was trained in batch mode to minimize the mean square error at the output layer. In order to check any over-fitting during training, a cross validation was performed by keeping track of the efficiency of the fitted model. The training was stopped when significant improvement in the efficiency was achieved. The model was then tested for its generalization properties.

The final structure of the NN model is: 6 input neurons, 10 hidden neurons, and 3 output neurons. The performance of error measures of the ANN model during testing are presented in Table 2 of Azamathulla et al. 2005. The good correlation between the observed and predicted scour patterns (Table 2 in Azamathulla et al. 2005) even with high levels of perturbation indicates that the NN model is able to capture the information contained in the data very well. The FFBP model-1 performance was very good in terms of the error measures (Azamathulla et al. 2005).

This study discusses an effective technique to distinguish the strength of relationship between input and output variables in an NN model. The results suggested that by performing perturbation analysis, the influence of each individual input variable on the output variable can be assessed. The results indicated that the massively parallel and distributed nature of a trained NN is capable of capturing the dynamics of the physical process being modeled. A careful examination of the important information contained in the trained NN can reveal the nature of the physical processes captured by distributed components of the trained NN.

Furthermore, it adds that the selection of input vector based on linear correlation between the variables of interest, may still include certain spurious elements that will only increase the model complexity.

To ascertain the fault tolerance of the model, the input variables were individually perturbed over the range of validation patterns, and the NN model was used to simulate the forecasts using the perturbed input patterns. Fig. 1 shows the variation of the correlation coefficient between the computed and observed scour during this analysis. As this figure illustrates, an error (perturbation) in the range of -20% to +20 in individual variables does not result in a substantial change in forecasts (see Table. 1). It may be noted that these permissible errors are on the individual values and not the combined effect of errors on all variables. Hence it can be concluded that the trained NN certainly represents the physical behavior of the system through its input variables.

4. Internal Network Structure

As mentioned earlier one of the facts pertaining to the functioning of NNs emunity, is that NN models act as mysterious black boxes and do not provide any clue on how they model the physical process. Some sparse and isolated attempts only have been made in the recent past to overcome this deficiency and to understand the interval structure of trained NN e.g. Castro et al. (2002), Wilby et al. (2003), Jain et al. (2004), Sudheer and Jain (2004). These studies showed that hidden neurons can do piecewise regression and can individually model certain catchment processes while predicting runoff in time series modeling. This section attempts to prove this aspect further and it differs from the previous in that it deals with a causal relationship rather than the earlier temporal ones.

As an example, a trained FFBP-2 network with 5 input nodes and 10 hidden nodes yielding the scour depth was considered. Because the output is obtained by transforming input using the hidden neurons, the two can be simultaneously studied to explore the piecewise processing. The coefficient of correlation, r , between the output of the scour depth was calculated in order to see the transformation made by the hidden nodes affects the network output. This is shown in Table 2. At the same time the output fired from each hidden neuron was listed as in Table 3 for various testing cases.

The hidden neurons H1, H2, H7 are highly correlated with the network output while H3, H4, H8 are not (Table 2). Elimination of these links subsequently was attempted. However, the attempt yielded loose generalization in the results. From Table 2 it can be seen that the neurons H1, H2, H7 produced outputs in the upper half of the total range of the outputs (0,1), while the neurons H3, H4, H8 yielded the outputs in lower tail of the output range. The two tables thus indicated that the influential hidden neurons are H1 H2 and H7. While others (H3, H4, H8) are complimentary, these neurons may be important to take care of the noise in the data. H1, H2, H7 may be modeling the previously known important parameters of head, H1, discharge intensity, q and bucket radius, R while H5, H6, H7, H9, H10 may be modeling other relatively less significant variables like lip angle of bucket, ϕ , sediment size d_{50} . To this extent, present study was in agreement with previous study of time series modeling (Jain et al. 2004). Even in this case of causal relationships, the hidden neurons somehow perform input portioning, transforming it into sub domains with strong hidden neurons. Thus, it is reasonable to assume that the massively parallel components of NN represent different variables of a physical process. A hidden layer thus seems to convert the input domain into another one where the samples become linearly separable and where the data are not forced into a fixed model like regression.

5. Conclusions

A perturbation analysis for determining the order of influence of the elements in the input vector on the output vector was discussed. Present study also identified the strength of relationship between individual input variables and the output. The correlation between the observed and predicted scour patterns (Table 2, Azamathulla et al. 2005) and the high value indicate that the NN model is able to capture the information contained in the data very well.

It was found that the hidden neurons could do piecewise regression and could individually model certain causal relationships. It was also shown that even in this case of causal relationships, unlike earlier observations belonging to time series predictions, the hidden neurons were capable of executing input partitioning, transforming it into sub domains with strong hidden neurons. Hence, it can be assumed that the components of NN represent different variables of a physical process. A hidden layer thus seems to convert the input domain into another one where the samples become linearly separable and where the data are not forced into a fixed model like regression.

6. Acknowledgments

The authors wish to express their sincere gratitude to Universiti Sains Malaysia for funding a short term grant to conduct this on-going research (304.PREDAC.6035262). The authors are also thankful to Prof M C Deo, IIT Bombay for his valuable suggestions.

References

Azamathulla, H. Md., Deo, M. C. and Deolalikar, P. B. (2005). "Neural networks for estimation of scour downstream of ski-jump bucket", *Journal of Hydraulic Engineering*, ASCE, 131(10), 898-908.

- Benitez, J. M., Castro, J. L., and Requena, I. (1997). "Are artificial neural networks black boxes?." *IEEE Trans. Neural Netw.* 8(5), 1156–1164.
- Castro, J. L., Mantas, C. J., and Benitez, J. M. (2002). "Interpretation of artificial neural networks by means of fuzzy rules." *IEEE Trans. Neural Netw.* 13 (1), 101–116.
- Eberhart, R. C., and Dobbins, R. W. (1990). *Neural network PC tools: A practical guide*, Academic, New York.
- Ho, Y. C. (1992). "Perturbation analysis: Concepts and algorithms." Proc., 1992 Winter Simulation Conf., Arlington, Va., J. J. Swain, D. Goldsman, R. C. Crain, and J. R. Wilson, eds., 231–240.
- Jain, A., Sudheer, K. P., and Srinivasulu, S. (2004). "Identification of physical processes inherent in artificial neural network rainfall runoff models." *Hydrolog. Process.*, 118(3), 571–581.
- Jingsheng, J. (2002). "Clustering technique for evaluating and validating neural network performance." *J. Comput. Civ. Eng.* 16(2), 152–155.
- Lange, N. T. (1999). "New mathematical approaches in hydrological modeling-an application of artificial neural networks." *Phys. Chem. Earth*, 24(1&2), 31–35.
- Lozowski, A., Cholewo, T. J., and Zurada, J. M. (1996). "Crisp rule extraction from perceptron network classifiers." *Proc., IEEE International Conf. on Neural Networks. Plenary, Panel, and Special Sessions*, Washington, D.C., 94–99.
- Maier, H.R. Dandy, G.C. (2000). "Neural networks for prediction and forecasting of water resources variables; a review of modeling issues and applications." *Environmental Modelling and Software*, Elsevier, 15, 101-124.
- Schmitz, G. P. J., Aldrich, C., and Gouws, F. S. (1999). "ANN-DT: An algorithm for extraction of decision trees from artificial neural networks." *IEEE Trans. Neural Netw.* 10(6), 1392–1401.
- Stewart (1989). *Does God play dice? The mathematics of chaos*, Blackwell, Cambridge, Mass.
- Sudheer, K. P. (2005). "Knowledge extraction from trained neural network river flow models." *ASCE, J. Hydrologic Eng.*, 10(4), 264-269.
- Sudheer, K. P. and Jain, A. (2004). "Explaining the internal behaviour of artificial neural network river flow models." *Hydrolog. Process.*, 118(4), 833–844.
- Tickle, A. B., Andrews, R., Golea, M., and Diederich, J. (1998). "The truth will come to light: Directions and challenges in extracting knowledge embedded within trained artificial neural network." *IEEE Trans. Neural Netw.* 9(6), 1057–1068.
- Wilby, R. L., Abrahart, R. J., and Dawson, C. W. (2003). "Detection of conceptual model rainfall-runoff processes inside an artificial neural network." *Hydrol. Sci. J.* 48(2), 163–181.

Table. 1 Perturbation analysis for FFBP Model -1

Perturbation	with out perturbation	-5%	-10%	-15%	-20%	+5%	+10%	+15%	+20%
Correlation coefficient of observed to predicted Scour depth	0.97	0.97	0.946	0.934	0.925	0.965	0.956	0.954	0.953
Correlation coefficient of observed to predicted Scour location	0.97	0.965	0.944	0.932	0.927	0.967	0.958	0.956	0.943
Correlation coefficient of observed to predicted Scour Width	0.98	0.975	0.964	0.954	0.954	0.978	0.975	0.968	0.963

Table 2. Ranges of H1,H2, H3H10.

H1	H2	H3	H4	H5	H6	H7	H8	H9	H10
0.755713	0.773763	0.029799	0.098279	0.129731	0.316225	0.748967	0.147867	0.32619	0.327166
0.51793	0.525154	0.035753	0.084581	0.182025	0.235407	0.5091	0.186919	0.242003	0.318382
0.479326	0.455511	0.139226	0.24093	0.243339	0.422084	0.53339	0.211481	0.429642	0.112446
0.64017	0.621656	0.223543	0.330968	0.165308	0.516795	0.685279	0.209114	0.525275	0.11156
0.942169	0.951587	0.04294	0.167201	0.042336	0.512524	0.941037	0.124268	0.526984	0.377622
0.584446	0.564944	0.19469	0.299342	0.175767	0.484028	0.638839	0.177494	0.492225	0.08823
0.467791	0.447847	0.145597	0.24162	0.198986	0.41919	0.538603	0.125766	0.426625	0.054413
0.553207	0.559602	0.039631	0.091556	0.192283	0.247866	0.536713	0.216623	0.254818	0.366087
0.517213	0.524174	0.035603	0.084312	0.185477	0.234474	0.507214	0.190512	0.241048	0.323593
0.83728	0.852083	0.044775	0.133331	0.092169	0.39003	0.832141	0.161744	0.401567	0.370908
0.977077	0.976968	0.809945	0.804581	0.000559	0.868021	0.979715	0.180946	0.873543	0.084741
0.977609	0.981387	0.087993	0.27351	0.025865	0.645305	0.974488	0.237951	0.659523	0.619453
0.870284	0.882283	0.054207	0.153628	0.090285	0.423651	0.861084	0.202013	0.435785	0.44994
0.526459	0.506462	0.168855	0.269578	0.186935	0.45138	0.589641	0.14955	0.459224	0.069231
0.420409	0.414402	0.063666	0.099817	0.227244	0.213875	0.399414	0.207281	0.219037	0.25678
0.834577	0.848652	0.043513	0.130597	0.106269	0.381588	0.824783	0.184798	0.393	0.409948
0.586142	0.566786	0.183105	0.293227	0.184511	0.485937	0.639626	0.202188	0.494231	0.112126
0.680157	0.691165	0.042121	0.106223	0.170018	0.294379	0.660921	0.223154	0.302983	0.409799

Table 3. Correlation coefficient between output of hidden neuron and Outputs (relative scour depth) 'r'

Hidden \ output	d_s/d_w
H1	0.8133
H2	0.8088
H3	-0.0802
H4	0.0632
H5	-0.7636
H6	0.4401
H7	0.8032
H8	0.1937
H9	0.4526
H10	0.7046

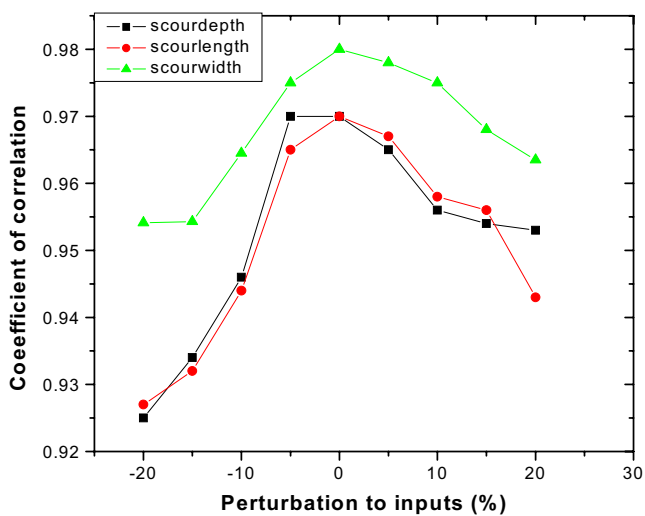


Figure 1. Perturbation to inputs and correlation coefficient for Observed to Predicted Scour

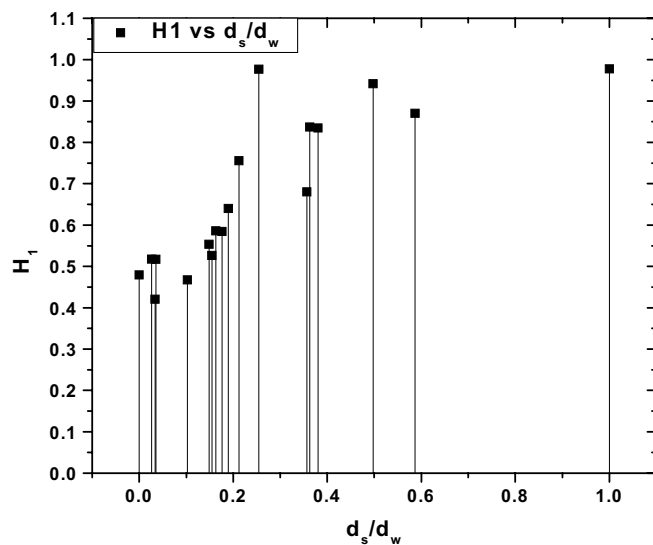


Figure 2. Output from hidden neuron H1 versus relative scour depth

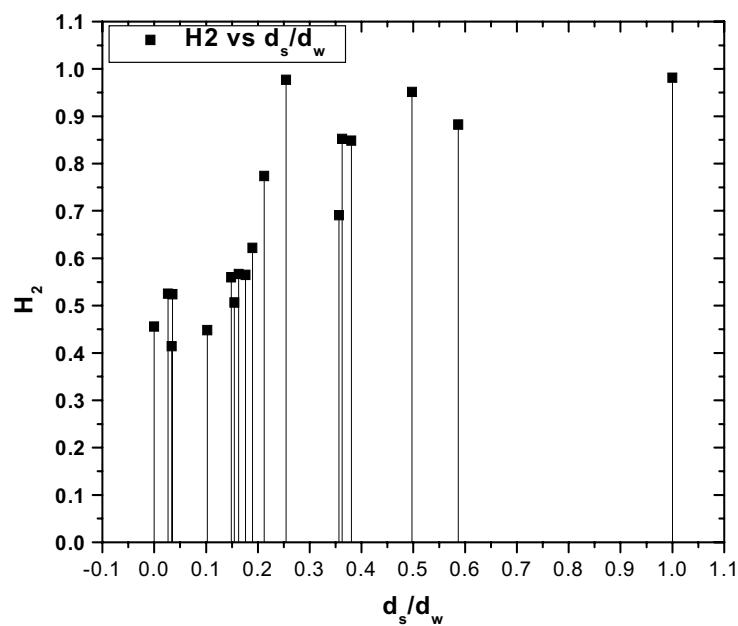


Figure 3. Output from hidden neuron H2 versus relative scour depth

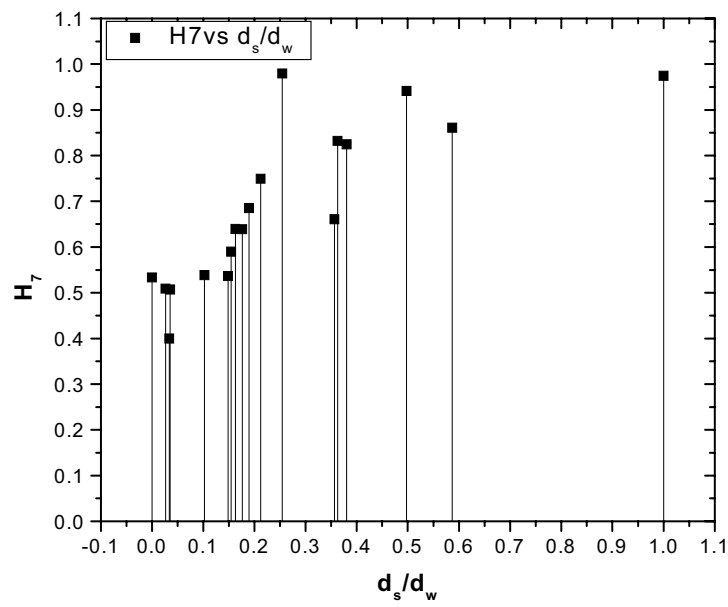


Figure 4. Output from hidden neuron H7 versus relative scour depth

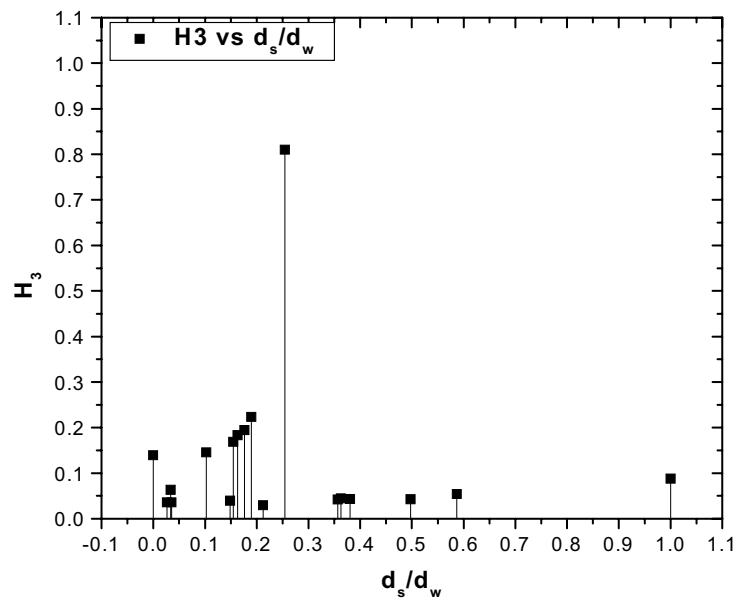


Figure 5. Output from hidden neuron H3 versus relative scour depth

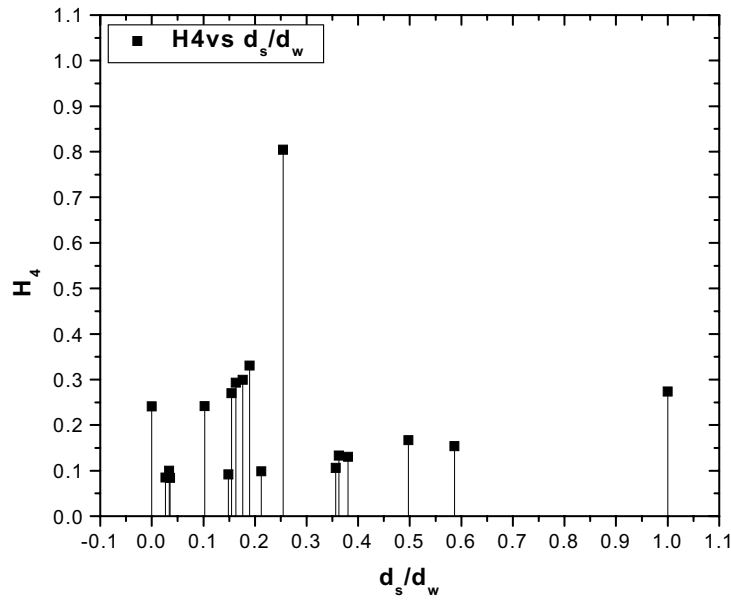


Figure 6. Output from hidden neuron H4 versus relative scour depth

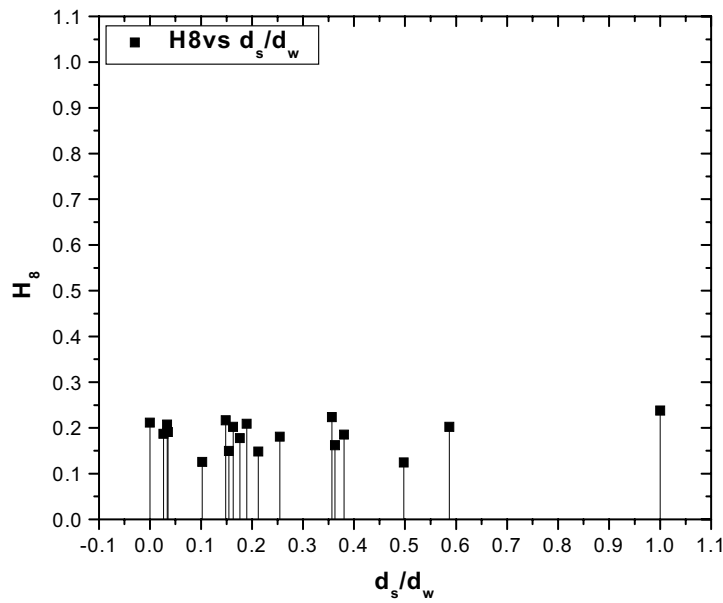


Figure 7. Output from hidden neuron H8 versus relative scour depth



The Application of the Vector Space Theory to the Limit of Number Sequence

Xingxiang Liu & Na Feng

College of Mathematics and Computer Science, Yan'an University, Yan'an 716000, China

Tel: 86-0911-285-9468 E-mail: lxx6407@163.com

Abstract

This article studied the application of vector space theory in the mathematical analysis in order to enhance the teaching and researching levels of the mathematical analysis and strengthen the teaching and researching levels of the higher algebra.

Keywords: Vector space, Base, Limit, Recurrence relations

The mathematical analysis and the higher algebra are two important professional basic lessons in various specialties of the college mathematical department. To a certain extent, any profound mathematical methods are to transform the complex mathematical objective to relative contents of the mathematical analysis and the higher algebra. Though these two lessons are different in the solving method, but they are closely associated and combined each other in many aspects.

The concepts and ideas that utilize the vector space to solve problems (Mi, 2002, p.66-69 & Song, 2004, p.100-101) still have many deficiencies, so in this article, we will further discuss this problem.

Definition 1: suppose $V = \left\{ \{u_n\} \mid u_n = \sum_{k=1}^l a_k u_{n-k}, a_k \in F (k=1, 2, \dots, l), n \geq l+1 \right\}$.

Regulation: (1) $\forall \{u_n\}, \{v_n\} \in V, so, \{u_n\} + \{v_n\} \in V$

(2) $\forall k \in F, \forall \{u_n\} \in V, so, k\{u_n\} = \{ku_n\} \in V$

So, V about Regulation (1) and (2) is the vector space on the number field F.

Lemma 1: suppose $V = \left\{ \{u_n\} \mid u_n = \sum_{k=1}^l a_k u_{n-k}, a_k \in F (k=1, 2, \dots, l), n \geq l+1 \right\}$ and V about Regulation (1) and (2) is the

vector space on the number field F, and $x^l = \sum_{k=1}^l a_k x^{k-1}$ has l single roots, q_1, q_2, \dots, q_l , so

(1) V is l dimensional vector space on F

(2) $\{q_1^n\}, \{q_2^n\}, \dots, \{q_l^n\}$ is a set of base of V

(3) Suppose $u_n = \sum_{k=1}^l b_k q_k^n$, so according to the initial condition u_1, u_2, \dots, u_l , we can confirm $b_k (k=1, 2, \dots, l)$ and obtain the

recurrence relations $u_n = \sum_{k=1}^l b_k q_k^n$.

Certification: Because $x^l = \sum_{k=1}^l a_k x^{k-1}$ has l single roots, and suppose q_1, q_2, \dots, q_l .

Because q_1, q_2, \dots, q_l has l single roots, so $\begin{pmatrix} q_1 \\ q_1^2 \\ \vdots \\ q_1^l \end{pmatrix}, \begin{pmatrix} q_2 \\ q_2^2 \\ \vdots \\ q_2^l \end{pmatrix}, \dots, \begin{pmatrix} q_l \\ q_l^2 \\ \vdots \\ q_l^l \end{pmatrix}$ are linear independent, i.e. the

$$\text{rank} \begin{pmatrix} \begin{pmatrix} q_1 \\ q_1^2 \\ \vdots \\ q_1^l \end{pmatrix}, \begin{pmatrix} q_2 \\ q_2^2 \\ \vdots \\ q_2^l \end{pmatrix}, \dots, \begin{pmatrix} q_l \\ q_l^2 \\ \vdots \\ q_l^l \end{pmatrix} \end{pmatrix} = l.$$

Because the number sequence $\{u_n\}$ is only confirmed by former l items u_1, u_2, \dots, u_l , so the necessary and sufficient

condition that $\{u_n^{(1)}\}, \{u_n^{(2)}\}, \dots, \{u_n^{(l)}\}$ are linear independent is that $\begin{pmatrix} u_1^{(1)} \\ u_2^{(1)} \\ \vdots \\ u_l^{(1)} \end{pmatrix}, \begin{pmatrix} u_1^{(2)} \\ u_2^{(2)} \\ \vdots \\ u_l^{(2)} \end{pmatrix}, \dots, \begin{pmatrix} u_1^{(l)} \\ u_2^{(l)} \\ \vdots \\ u_l^{(l)} \end{pmatrix}$ are linear independent.

Suppose $F^l = \left\{ \begin{pmatrix} u_1 \\ u_2 \\ \vdots \\ u_l \end{pmatrix} \middle| u_i \in F (i=1, 2, \dots, l) \right\}$, so for any $\begin{pmatrix} u_1 \\ u_2 \\ \vdots \\ u_l \end{pmatrix} \in F^l$, $\begin{pmatrix} u_1 \\ u_2 \\ \vdots \\ u_l \end{pmatrix}$ can be linearly presented by $\begin{pmatrix} q_1 \\ q_1^2 \\ \vdots \\ q_1^l \end{pmatrix}, \begin{pmatrix} q_2 \\ q_2^2 \\ \vdots \\ q_2^l \end{pmatrix}, \dots, \begin{pmatrix} q_l \\ q_l^2 \\ \vdots \\ q_l^l \end{pmatrix}$.

So $\{u_n\}$ can be linear presented by $\{q_1^n\}, \{q_2^n\}, \dots, \{q_l^n\}$, so V is the l dimensional vector space on F , and $\{q_1^n\}, \{q_2^n\}, \dots, \{q_l^n\}$ is one set of base of V .

Because $\{u_n\}$ can be linear presented by $\{q_1^n\}, \{q_2^n\}, \dots, \{q_l^n\}$, so $u_n = \sum_{k=1}^l b_k q_k^n$, and according to the initial condition u_1, u_2, \dots, u_l , we can confirm b_1, b_2, \dots, b_l , so $u_n = \sum_{k=1}^l b_k q_k^n$.

Lemma 2: suppose $V = \left\{ \begin{pmatrix} u_n \end{pmatrix} \middle| u_n = \sum_{k=1}^l a_k u_{n-k}, a_k \in F (k=1, 2, \dots, l), n \geq l+1 \right\}$ and V about Regulation (1) and (2) is the

vector space on the number field F , and q_1 is l multiple root of $x^l = \sum_{k=1}^l a_k x^{k-1}$, so

- (1) V is l dimensional vector space on F
- (2) $\{q_1^n\}, \{nq_1^n\}, \{n^2q_1^n\}, \dots, \{n^{l-1}q_1^n\}$ is a set of base of V
- (3) Suppose $u_n = \sum_{k=1}^l b_k n^{k-1} q_1^n$, so according to the initial condition, the values of u_1, u_2, \dots, u_l , we can confirm $b_k (k=1, 2, \dots, l)$ and obtain the recurrence relations $u_n = \sum_{k=1}^l b_k n^{k-1} q_1^n$.

Certification: Because q_1 is l multiple root of $x^l = \sum_{k=1}^l a_k x^{k-1}$, so $\begin{pmatrix} q_1 \\ q_1^2 \\ \vdots \\ q_1^l \end{pmatrix}, \begin{pmatrix} q_2 \\ 2q_1^2 \\ \vdots \\ lq_1^l \end{pmatrix}, \begin{pmatrix} q_2 \\ 2^2q_1^2 \\ \vdots \\ l^2q_1^l \end{pmatrix}, \dots, \begin{pmatrix} q_l \\ 2^{l-1}q_1^2 \\ \vdots \\ l^{l-1}q_1^l \end{pmatrix}$ are linear independent

and the rank $\left(\begin{pmatrix} q_1 \\ q_1^2 \\ \vdots \\ q_1^l \end{pmatrix}, \begin{pmatrix} q_2 \\ 2q_1^2 \\ \vdots \\ lq_1^l \end{pmatrix}, \begin{pmatrix} q_2 \\ 2^2q_1^2 \\ \vdots \\ l^2q_1^l \end{pmatrix}, \dots, \begin{pmatrix} q_l \\ 2^{l-1}q_1^2 \\ \vdots \\ l^{l-1}q_1^l \end{pmatrix} \right) = r$.

So $\{q_1^n\}, \{nq_1^n\}, \{n^2q_1^n\}, \dots, \{n^{l-1}q_1^n\}$ are linear independent, and $\{q_1^n\}, \{nq_1^n\}, \{n^2q_1^n\}, \dots, \{n^{l-1}q_1^n\} \in V$.

Because the number sequence $\{u_n\}$ is only confirmed by former l items u_1, u_2, \dots, u_l of u_n , and when

$\{u_n^{(1)}\}, \{u_n^{(2)}\}, \dots, \{u_n^{(l)}\}$ are linear independent, so $\begin{pmatrix} u_1^{(1)} \\ u_2^{(1)} \\ \vdots \\ u_l^{(1)} \end{pmatrix}, \begin{pmatrix} u_1^{(2)} \\ u_2^{(2)} \\ \vdots \\ u_l^{(2)} \end{pmatrix}, \dots, \begin{pmatrix} u_1^{(l)} \\ u_2^{(l)} \\ \vdots \\ u_l^{(l)} \end{pmatrix}$ are linear independent.

Suppose $F^l = \left\{ \begin{pmatrix} u_1 \\ u_2 \\ \vdots \\ u_l \end{pmatrix} \middle| u_i \in F (i=1, 2, \dots, l) \right\}$, so for any $\begin{pmatrix} u_1 \\ u_2 \\ \vdots \\ u_l \end{pmatrix} \in F^l$, $\begin{pmatrix} u_1 \\ u_2 \\ \vdots \\ u_l \end{pmatrix}$ can be linearly presented

by $\begin{pmatrix} q_1 \\ q_1^2 \\ \vdots \\ q_1^l \end{pmatrix}, \begin{pmatrix} q_2 \\ 2q_1^2 \\ \vdots \\ lq_1^l \end{pmatrix}, \begin{pmatrix} q_2 \\ 2^2q_1^2 \\ \vdots \\ l^2q_1^l \end{pmatrix}, \dots, \begin{pmatrix} q_l \\ 2^{l-1}q_1^2 \\ \vdots \\ l^{l-1}q_1^l \end{pmatrix}$.

So $\{u_n\}$ can be linear presented by $\{q_1^n\}, \{nq_1^n\}, \{n^2q_1^n\}, \dots, \{n^{l-1}q_1^n\}$, so V is the l dimensional vector space on F ,

and $\{q_1^n\}, \{nq_1^n\}, \{n^2q_1^n\}, \dots, \{n^{l-1}q_1^n\}$ is one set of base of V .

Because $\{u_n\}$ can be linear presented by $\{q_1^n\}, \{nq_1^n\}, \{n^2q_1^n\}, \dots, \{n^{l-1}q_1^n\}$, so $u_n = \sum_{k=1}^l b_k n^{k-1} q_1^n$, and according to the initial condition u_1, u_2, \dots, u_l , we can confirm b_1, b_2, \dots, b_l , so $u_n = \sum_{k=1}^l b_k n^{k-1} q_1^n$.

Theorem 1: suppose $V = \left\{ \{u_n\} \middle| u_n = \sum_{k=1}^l a_k u_{n-k}, a_k \in F (k=1, 2, \dots, l), n \geq l+1 \right\}$ and V about Regulation (1) and (2) in

theorem 2 is the vector space on the number field F , and $x^l = \sum_{k=1}^l a_k x^{k-1}$ has roots q_1, q_2, \dots, q_l in which both ones are

different and q_j is k_j multiple root ($k_j \geq 1$) and $k_1 + k_2 + \dots + k_l = l$, so

(1) V is l dimensional vector space on F

(2) $\{q_1^n\}, \{nq_1^n\}, \{n^2q_1^n\}, \dots, \{n^{k_1-1}q_1^n\}, \{q_2^n\}, \{nq_2^n\}, \{n^2q_2^n\}, \dots, \{n^{k_2-1}q_2^n\}, \dots, \{q_l^n\}, \{nq_l^n\}, \{n^2q_l^n\}, \dots, \{n^{k_l-1}q_l^n\}$ is a set of base of V

(3) Suppose $u_n = \sum_{j=1}^l \sum_{i=1}^{k_j} b_{ij} n^{i-1} q_j^n$, so according to the initial condition, the values of u_1, u_2, \dots, u_l , we can

confirm $b_{ij} (i = 1, \dots, k_j; j = 1, \dots, t)$ and obtain the recurrence relations $u_n = \sum_{j=1}^t \sum_{i=1}^{k_j} b_{ij} n^{i-1} q_j^n$.

Example 1: Suppose $x_1 = 1, x_2 = 2, x_3 = 3, x_n = \frac{1}{3}(x_{n-1} + x_{n-2} + x_{n-3}) (n \geq 4)$, find out $\lim_{n \rightarrow \infty} x_n$.

Solution: Suppose $V = \left\{ \{u_n\} \mid u_n = \frac{1}{3}(u_{n-1} + u_{n-2} + u_{n-3}), n \geq 4 \right\}$, so V composes the three-dimensional vector space on the established number field.

From $q^3 = \frac{1}{3}(q^2 + q + 1)$, we can obtain $3q^3 = q^2 + q + 1$, solve it we can obtain $q_1 = 1, q_2 = \frac{1}{3}(-1 + \sqrt{2}i)$

and $q_3 = \frac{1}{3}(-1 - \sqrt{2}i)$, so $\{q_1^n\}, \{q_2^n\}, \{q_3^n\}$ are linearly independent, and $\{q_1^n\}, \{q_2^n\}, \{q_3^n\}$ is one set of base of V, and $\{x_n\}$

can be linearly presented by $\{q_1^n\}, \{q_2^n\}, \{q_3^n\}$, and

$$\begin{aligned} x_n &= aq_1^n + bq_2^n + cq_3^n \\ &= a + b\left(\frac{-1 + \sqrt{2}i}{3}\right)^n + c\left(\frac{-1 - \sqrt{2}i}{3}\right)^n \end{aligned}$$

$$\begin{aligned} \lim_{n \rightarrow \infty} x_n &= \lim_{n \rightarrow \infty} \frac{1}{3}(x_{n-1} + x_{n-2} + x_{n-3}) \\ &= \lim_{n \rightarrow \infty} \frac{1}{3} \left\{ \left[a + b\left(\frac{-1 + \sqrt{2}i}{3}\right)^{n-1} + c\left(\frac{-1 - \sqrt{2}i}{3}\right)^{n-1} \right] \right. \\ &\quad \left. + \left[a + b\left(\frac{-1 + \sqrt{2}i}{3}\right)^{n-2} + c\left(\frac{-1 - \sqrt{2}i}{3}\right)^{n-2} \right] \right. \\ &\quad \left. + \left[a + b\left(\frac{-1 + \sqrt{2}i}{3}\right)^{n-3} + c\left(\frac{-1 - \sqrt{2}i}{3}\right)^{n-3} \right] \right\} \\ &= a \end{aligned}$$

And because
$$\begin{cases} 1 = a + b\left(\frac{-1 + \sqrt{2}i}{3}\right) + c\left(\frac{-1 - \sqrt{2}i}{3}\right) \\ 2 = a + b\left(\frac{-1 + \sqrt{2}i}{3}\right)^2 + c\left(\frac{-1 - \sqrt{2}i}{3}\right)^2 \\ 3 = a + b\left(\frac{-1 + \sqrt{2}i}{3}\right)^3 + c\left(\frac{-1 - \sqrt{2}i}{3}\right)^3 \end{cases}$$
, solve it, we can obtain $a = \frac{14}{6}$, i.e. $\lim_{n \rightarrow \infty} x_n = \frac{14}{6}$.

Example 2: The number sequence, “2, 3, 5, 10, 21 ...”, fulfills $x_n = 4x_{n-1} - 5x_{n-2} + 2x_{n-3} (n \geq 4)$, find out $\lim_{n \rightarrow \infty} \frac{x_n}{x_{n+1}}$.

Solution: Suppose $V = \left\{ \{u_n\} \mid u_n = 4u_{n-1} - 5u_{n-2} + 2u_{n-3}, n \geq 4 \right\}$, so V composes the three-dimensional vector space on the established number field.

From $q^3 = 4q^2 - 5q + 2$, we can obtain $q_1 = q_2 = 1, q_3 = 2$.

Because $q_1 = q_2 \neq q_3$, so $\{q_1^n\}, \{2q_1^n\}, \{q_3^n\}$ are linearly independent, and $\{q_1^n\}, \{2q_1^n\}, \{q_3^n\}$ is one set of base of V, and $\{x_n\}$ can be linearly presented by their linear combination, i.e. $x_n = aq_1^n + b(2q_1^n) + cq_3^n$.

From initial condition, we can obtain
$$\begin{cases} a + 2b + c = 2 \\ aq_1 + 2bq_1 + cq_3 = 3 \\ aq_1^2 + 2bq_1^2 + cq_3^2 = 5 \end{cases}$$
, i.e.
$$\begin{cases} a + 2b + c = 2 \\ a + 2b + 2c = 3 \\ a + 2b + 4c = 5 \end{cases}$$
, solve it, we can get
$$\begin{cases} a + 2b = 1 \\ c = 1 \end{cases}$$
.

$$\begin{aligned}
 x_n &= aq_1^n + b(2q_1^n) + q_3^n \\
 \text{So, } &= (a+2b)q_1^n + q_3^n, \text{ and} \\
 &= q_1^n + q_3^n
 \end{aligned}
 \qquad
 \begin{aligned}
 \lim_{n \rightarrow \infty} \frac{x_n}{x_{n+1}} &= \lim_{n \rightarrow \infty} \frac{q_1^n + q_3^n}{q_1^{n+1} + q_3^{n+1}} \\
 &= \lim_{n \rightarrow \infty} \frac{1+2^n}{1+2^{n+1}} \\
 &= \frac{1}{2}
 \end{aligned}
 .$$

In conclusion, it is hard to use the method of calculus to find the limit for some recurrence relations, but if we consider them from the direction of the vector space theory, the problem will be effectively solved. In this article, we conclude the solutions to find the limit for the recurrence relations with single root, multiple root and several multiple roots, and the key is to find out a set of proper base, so the recurrence relations can be found according to the initial condition.

References

- Mi, Yongsheng & Mi, Dongmei. (2002). Application of the High Algebra Method Problem to Maths Analysis. *Journal of Changchun University*. No.15(2). p.66-69.
- Song, Laimin. (2004). Application of the Method of Linear Algebra in Limit. *Journal of Tongling College*. No. 2. p.100-101.



Analysis of Heat Transfer Enhancement in Spiral Plate Heat Exchanger

Dr. Kaliannan Saravanan

Professor & Head, Department of Chemical Engineering

Kongu Engineering College, Anna University, Erode, Tamilnadu, India-638 052

E-mail: rumisivaesh@yahoo.com

Rangasamy Rajavel (Corresponding author)

Lecturer, Department of Mechanical Engineering

Kongu Engineering College, Anna University, Erode, Tamilnadu, India -638 052

E-mail: rajavel_7@yahoo.com

Abstract

In the present study, the heat transfer coefficients of benzene in a spiral plate heat exchanger are investigated. The test section consists of a Plate of width 0.3150 m, thickness 0.001 m and Mean hydraulic diameter of 0.01 m. The mass flow rate of water (Hot fluid) is varying from 0.5 kg sec^{-1} to 0.8 kg sec^{-1} and the mass flow rate of benzene (cold fluid) varies from 0.4 kg sec^{-1} to 0.7 kg sec^{-1} . Experiments have been conducted by varying the mass flow rate, temperature and pressure of cold fluid, keeping the mass flow rate of hot fluid constant. The effects of relevant parameters on spiral plate heat exchanger are investigated. The data obtained from the experimental study are compared with the theoretical data. Besides, a new correlation for the nusselt number which can be used for practical applications is proposed.

Keywords: Spiral plate heat exchanger, Reynolds number, Nusselt number, Heat transfer coefficient, Mass flow rate

1. Introduction

A spiral plate heat exchanger consists of two relatively long strips of sheet metal, normally provided with welded studs for plate spacing, wrapped helically around a split mandrel to form a pair of spiral channels for two fluids. Alternate passage edges are closed. Thus each fluid has a long single passage arranged in a compact package. To complete the exchanger, covers are fitted at each end. It can handle viscous, fouling liquids and slurries more readily because of a single passage. If the passage starts fouling, the localized velocity in the passage increases. The fouling rate then decreases with increased fluid velocity. The fouling rate is very low compared to that of a shell-and-tube unit. It is more amenable to chemical, flush and reversing fluid cleaning techniques because of the single passage. Mechanical cleaning is also possible with removal of the end covers. Thus, maintenance is less than with a shell-and-tube unit. Considerable research is being pursued in spiral and helical heat exchanger in heat transfer and flow areas.

Heat transfer for pulsating flow in a curved pipe was numerically studied by Chung and Hyun (Chung, J. H. and J. M. Hyun., 1994) for strongly curved pipes with substantial pulsation amplitudes. Local Nusselt numbers were developed based on the Womersley number [ratio of transient inertial to viscous forces], which is a function of the pipe radius, the kinematic viscosity, and the frequency of the pulsation. It was found that the strength of the Womersley number affected the distribution of the Nusselt number around the periphery. Dry-out characteristics were studied experimentally by Kaji et al. (Kaji, M., K. Mori, S. Nakanishi, K. Hirabayashi and M. Ohishi., 1995). for a two-phase flow through helical coils. Their work also studied wall temperature fluctuations and compared the results to straight tube experiments. Mori and Nakayama (Mori, Y. and W. Nakayama., 1965) studied the fully developed flow in a curved pipe with a uniform heat flux for large Dean Numbers. Flow and temperature fields were studied both theoretically and experimentally. They assumed that the flow was divided into two sections, a small boundary layer near the pipe wall, and a large core region making up the Remaining flow. Kubair and Kuloor (Berg, R. R. and C. F. Bonilla., 1950) offered pressure drop and heat transfer for laminar flow of glycerol for different types of coiled pipes, including helical and spiral configurations. Reynolds numbers were in the range of 80 to 6000 with curvature ratios in the range of 10.3 to 27. The number of turns varies from 7 to 12.

Outside-film and inside-film heat transfer coefficients in an agitated vessel were calculated by Jha and Rao (Jha, R. K. and M. R. Rao., 1967). Five different coils were studied, along with different speeds and locations of the agitator. They derived an equation to predict the Nusselt number based on the geometry of the helical coil and the location of the agitator. Kalb and Seader (Kalb, C. E. and J. D. Seader., 1972). performed Numerical studies for uniform wall heat flux with peripherally uniform wall temperature for Dean numbers in the range of 1-1200, Prandtl numbers of 0.005-1600, and curvature ratios of 10 to 100 for fully developed velocity and temperature fields. They found that the curvature ratio parameter had insignificant effect on the average Nusselt number for any given Prandtl number. Bai et al (Bai, B., L. Guo, Z. Feng, and X. Chen., 1999) experimentally studied turbulent heat transfer from horizontal helical coils. They concluded that as the Reynolds number is increased, the contribution of secondary flow to the heat transfer diminished and the heat transfer approaches that of a straight tube. This is due to the fact that as the Reynolds number increases the boundary layer becomes smaller. It is the large boundary layer that is shed off into the center of the tube by the secondary flow that increases the heat transfer coefficient, and this effect decreases with increasing Reynolds number Bai et al (Bai, B., L. Guo, Z. Feng, and X. Chen., 1999). The local heat transfer coefficient on the outer wall can be 3 to 4 times that of the inner wall. They developed a correlation of the Nusselt number as a function of the location on the periphery. They also developed a Nusselt number correlation; however it did not contain the Dean number as only one size of coil was used in the experiment. Comparisons for the heat transfer coefficients between straight tubes and helically coiled tubes immersed in a water bath were performed by Prabhanjan et al (Prabhanjan, D. G., G. S. V. Raghavan, and T. J. Rennie., 2002). Findings showed that the heat transfer coefficient were greater in the helically coiled system.

Using a method of fractional steps for a wide range of Dean [10 to 7000] and Prandtl [0.005 to 2000] numbers, laminar flow and heat transfer were studied numerically by Zapryanov et al (Zapryanov, Z., Christov, C. and E. Toshev. ,1980). Their work focused on the case of constant wall temperature and showed that the Nusselt number increased with increasing Prandtl numbers, even for cases at the same Dean number. They also presented a series of isotherms and streamlines for different Dean and Prandtl numbers. The effect of buoyancy on the flow field and heat transfer was considered numerically by Lee et al (Lee, J. B., H. A. Simon, and J. C. F. Chow. ,1985). for the case of fully developed laminar flow and axially steady heat flux with a peripherally constant wall temperature. They found that buoyancy effects resulted in an increase in the average Nusselt number, as well as modifying of the local Nusselt number allocation. It was also found that the buoyancy forces result in a rotation of the orientation of the secondary flow patterns. Havas et al (Havas, G., A. Deak, and J. Sawinsky. ,1987) performed the study of the heat transfer to a helical coil in an agitated vessel and a correlation was developed for the outer Nusselt number based on a modified Reynolds number, Prandtl number, viscosity ratio, and the ratio of the diameter of the tube to the diameter of the vessel. Acharya et al. (Acharya, N., Sen, M., and H. C. Chang., 1992, Acharya, N., Sen, M., and H. C. Chang., 2001) experimented the heat transfer enhancements due to chaotic particle paths for coiled tubes and alternating axis coils. They developed two correlations of the Nusselt number, for Prandtl numbers less than and greater than one, respectively. Lemenand and Peerhossaini (Lemenand, T. and H. Peerhossaini., 2002) developed a Nusselt number correlation based on the Reynolds number, Prandtl number and the number of bends in the pipe. For the same Reynolds and Prandtl numbers, their work showed that the Nusselt number slightly drops off with increasing number of bends.

Guo et al (Guo, L., Chen, X., Feng, Z., and B. Bai., 1998). studied the heat transfer for pulsating flow in a curved pipe for fully developed turbulent flow in a helical coiled tube. In their work they examined both the pulsating flow and the steady state flow. They developed the correlation for steady turbulent flow for the Reynolds number range of 6000 to 1 80 000. They found that the Reynolds number was increased to very large values [$>1\ 40\ 000$], the heat transfer coefficient for coils began to match the heat transfer coefficient for straight tubes. They also presented correlations of the peripheral local heat transfer coefficients as a function of the average heat transfer coefficients, Reynolds number, Prandtl number, and the location on the tube wall. Inagaki et al (Inagaki, Y., Koiso, H., Takumi, H., Ioka, I., and Y. Miyamoto., 1998) studied the outside heat transfer coefficient for helically coiled bundles for Reynolds numbers in the range of 6000 to 22 000.

Heat transfer and flow characteristics in the curved tubes have been studied by a number of researchers. Although some information is currently available to calculate the performance of the spiral plate heat exchanger, however the study of heat transfer and flow characteristics in spiral plate heat exchanger has not received as much of consideration. This is because the heat transfer and flow characteristics of spiral plate heat exchanger have been studied. In the present study, the heat transfer and flow characteristics of benzene for spiral plate heat exchanger have been experimentally studied, in addition to the development of a new correlation for nusselt number.

2. Experimental Setup

The experimental setup consists of spiral plate heat exchanger, thermocouple, manometers, pumps and tanks as shown in Figure. 2.1. The parameters of heat exchanger are shown in the Table 2.1. The hot fluid inlet pipe is connected at the center core of the spiral heat exchanger and the outlet pipe is taken from periphery of the heat exchanger. The hot fluid

is heated by pumping the steam from the boiler to a temperature of about 60-70° C and connected to hot fluid tank having a capacity of 1000 liters then the hot solution is pumped to heat exchanger using a pump. Thus the counter flow of the fluid is achieved. The cold fluid inlet pipe is connected to the periphery of the exchanger and the outlet is taken from the centre of the heat exchanger. The cold fluid is supplied at room temperature from cold solution tank and is pumped to the heat exchanger using a pump.

3. Experimental Procedure

The heat transfer and flow characteristic of benzene is tested using an Alfa Laval; Model P5-VRB, Spiral plate heat exchanger as shown in Figure. 2.1. The inlet hot fluid flow rate is kept constant and the inlet cold fluid flow rate is varied using a control valve. The flow of hot and cold fluid is varied using control valves, C1 and C2 respectively. Thermometers T1 and T2 are used to measure inlet temperature of cold and hot fluids respectively; T3 and T4 are used to measure the outlet temperature of cold and hot fluids respectively. For different cold fluid flow rate the temperatures at the inlet and outlet of hot and cold fluids are recorded, after achieving the steady state. The same procedure is repeated for different hot fluid flow rates and the data related to temperatures, the corresponding temperatures and mass flow rates are recorded. The mass flow rate is determined by using the Rotometer fitted at the outlet of the corresponding fluids. Table 3.1 shows the experimental conditions.

4. Results and Discussion

4.1 Length from spiral center Vs Heat transfer coefficient

Figure 4.1, 4.2, 4.3 and 4.4. Shows the variation of the length from spiral center and heat transfer coefficient of benzene for different mass flow rates. It is clear that the heat transfer coefficient is varying with mass flow rates. When the mass flow rate is increased the heat transfer coefficient is also increased. On the other hand, the heat transfer coefficient is decreased when the length of spiral plate is increased.

4.2 Length from spiral center Vs Liquid Reynolds number

Figure 4.5 and 4.6 shows the variation of the length from spiral center and Reynolds number of water and benzene for different mass flow rates. It should be noted that the Reynolds number is varying with mass flow rates. When the mass flow rate is increased the Reynolds number is also increased. On the other hand the Reynolds number is decreased when the length of spiral plate is increased.

4.3 Comparison of Nusselt number (Experimental) Vs (predicted)

Figure 4.7 shows the comparisons of the Nusselt numbers obtained from the experiment conducted with those calculated from theoretically. It can be noted that the experimental and Predicted Nusselt numbers fall within $\pm 3\%$. The major discrepancy between the measured data and calculated results may be due to the difference in the configuration of test sections and uncertainty of the correlation.

The proposed Nusselt number correlation (1) for spiral plate heat exchanger is expressed as follows.

The correlation is obtained by fitting a total of 129 experimental data. ($R^2=0.98$)

$$Nu = 0.1868 Re^{0.708} Pr^{-0.371} \quad (1)$$

$$6000 < Re < 11000 \quad 4.7 < Pr < 5.9$$

4.4 Comparison of experimental Nusselt number with Holger Martin correlation

Holger martin correlation (2)

$$Nu = 0.04 Re^{0.74} Pr^{0.4} \quad (2)$$

$$4.10^2 < Re < 3.10^4$$

Comparisons of the Nusselt numbers obtained from the present experiment with those calculated from the existing correlation are shown in Figure 4.8. It can be noted that the values obtained from the correlation are slightly consistent with the experimental data and lie within $\pm 14\%$ for the Holger martin correlation.

5. Conclusion

This paper presents new experimental data from the measurement of the heat transfer coefficient of benzene flows in a spiral plate heat exchanger. The effects of relevant parameters are investigated. The data obtained from the present study are compared with the theoretical data. In addition, a new correlation based on the experimental data is given for practical applications.

6. Acknowledgement

The authors are grateful to the Management and the Principal of Kongu Engineering College, Erode, Tamilnadu, India, for granting permission to carryout the research work.

7. Nomenclature

Nu- Nusselt number

Re-Reynolds number

Pr-Prandtl number

h- Heat transfer coefficient [$\text{W m}^{-2} \text{K}^{-1}$]

U-Over all heat transfer coefficient [$\text{W m}^{-2} \text{K}^{-1}$]

Mh-Mass flow rate of hot fluid [Kg Sec^{-1}]

Mc-Mass flow rate of cold fluid [Kg Sec^{-1}]

References

- Acharya, N., Sen, M., and H. C. Chang. (1992). Heat transfer enhancement in coiled tubes by chaotic mixing. *International Journal of Heat and Mass Transfer*, Vol.35 (10):2475-2489.
- Acharya, N., Sen, M., and H. C. Chang. (2001). Analysis of heat transfer enhancement in coiled-tube heat exchangers. *International Journal of Heat and Mass Transfer*, Vol.44: 3189-3199.
- Bai, B., L. Guo, Z. Feng, and X. Chen. (1999). Turbulent heat transfer in a horizontally coiled tube. *Heat Transfer-Asian Research*, Vol. 28:395-403.
- Berg, R. R. and C. F. Bonilla. (1950). *Trans. N. Y. Acad. Sci.* Vol. 13:12 (as cited in Kubair and Kuloor, 1966).
- Chung, J. H. and J. M. Hyun. (1994). Heat transfer from a fully-developed pulsating flow in a curved pipe. *International Journal of Heat and Mass Transfer*, Vol. 37:43-52.
- Guo, L., Chen, X., Feng, Z., and B. Bai. (1998). Transient convective heat transfer in a helical coiled tube with pulsating fully developed turbulent flow. *International Journal of Heat and Mass Transfer*, Vol. 41:2867-2875.
- Havas, G., A. Deak, and J. Sawinsky. (1987). Heat transfer to helical coils in agitated vessels. *The Chemical Engineering Journal*, Vol. 35:61-64.
- Holger Martin., Heat exchangers, *Hemisphere publishing corporation*, London,(1992).
- Inagaki, Y., Koiso, H., Takumi, H., Ioka, I., and Y. Miyamoto. (1998). Thermal hydraulic study on a high-temperature gas-gas heat exchanger with helically coiled tube bundles. *Nuclear Engineering and Design*, Vol. 185:141-151.
- Jha, R. K. and M. R. Rao. (1967). Heat transfer through coiled tubes in agitated vessels. *International Journal of Heat and Mass Transfer*, Vol. 10:395-397.
- Kaji, M., K. Mori, S. Nakanishi, K. Hirabayashi and M. Ohishi. (1995). Dryout and wall temperature fluctuations in helically coiled evaporating tubes. *Heat Transfer – Japanese Research*, Vol. 24[3]:239-254.
- Kalb, C. E. and J. D. Seader. (1972). Heat and mass transfer phenomena for viscous flow in curved circular tubes. *International Journal of Heat and Mass Transfer*, Vol. 15:801-817.
- Lee, J. B., H. A. Simon, and J. C. F. Chow. (1985). Buoyancy in developed laminar curved tube flows. *International Journal of Heat and Mass Transfer*, Vol. 28(2):631- 640.
- Lemenand, T. and H. Peerhossaini. (2002). A thermal model for prediction of the Nusselt number in a pipe with chaotic flow. *Applied Thermal Engineering*, Vol. 22:1717-1730.
- Mori, Y. and W. Nakayama. (1965). Study on forced convective heat transfer in curved pipes (1st report, laminar region). *International Journal of Heat and Mass Transfer*, Vol. 8:67-82.
- Prabhanjan, D. G., G. S. V. Raghavan, and T. J. Rennie.(2002). Comparison of heat transfer rates between a straight tube heat exchanger and a helically coiled heat exchanger. *International Communications in Heat and Mass Transfer*, Vol. 29:185-191.
- Zapryanov, Z., Christov, C. and E. Toshev. (1980). Fully developed laminar flow and heat transfer in curved tubes. *International Journal of Heat and Mass Transfer*, Vol. 23:873-880.

Table 2.1 Dimensions of the Spiral plate Heat Exchanger

Parameters	Dimensions (P5-VRB plate)
Plate width, m	0.3150
Plate thickness, m	0.0010
Mean channel spacing, m	0.0050
Mean hydraulic diameter, m	0.0100
Heat transfer area, m ²	2.2400

The above table gives the dimensions and the parameters of the Spiral Plate Heat Exchanger

Table 3.1 Experimental Conditions

Sl.No	Variables	Range
1	Hot water temperature	65-50 °C
2	Cold Water temperature	30-50 °C
3	Mass flow rate of hot water	0.5-0.8 kg sec ⁻¹
4	Mass flow rate of cold Water	0.4-0.7 kg sec ⁻¹
5	Reynolds Number of Cold Fluid	6000-11 000

The table above provides the experimental conditions of the hot and cold water temperature, mass flow rate of hot and cold water, Reynolds number of cold fluid

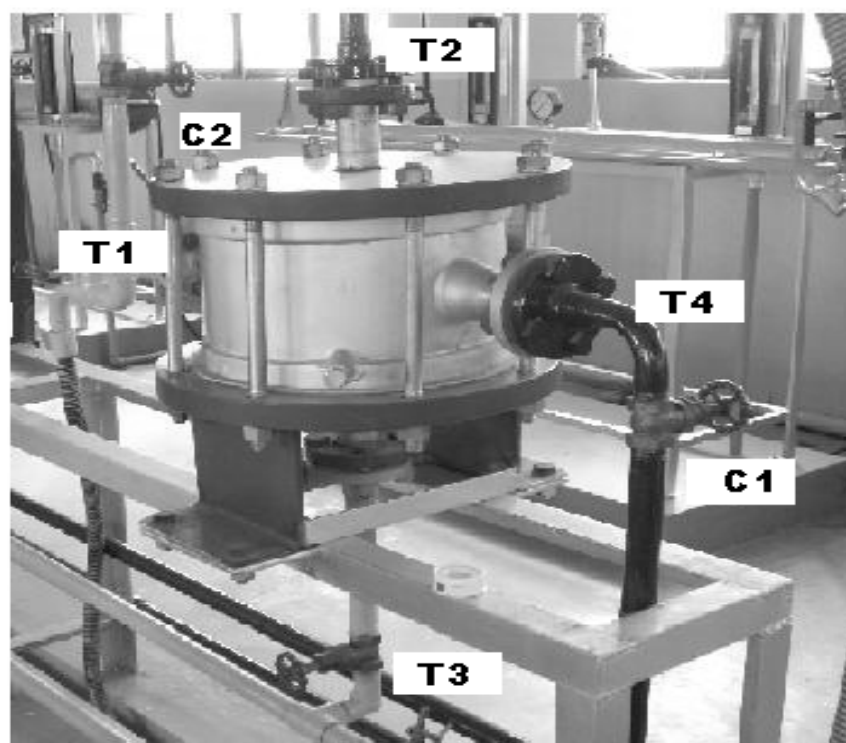


Figure 2.1 Schematic diagram of experimental apparatus C1&C2-Control Valves ,T1,T2,T3&T4-Thermocouples

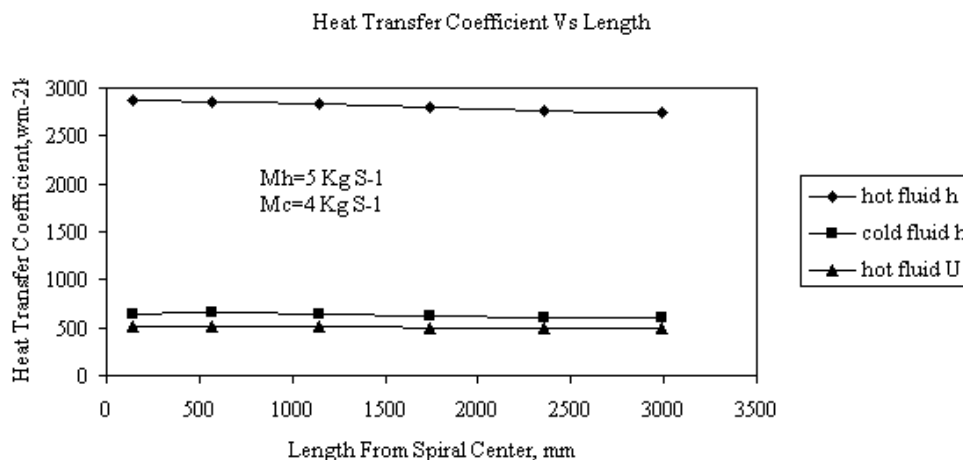


Figure 4.1 Heat transfer coefficient vs length from spiral center

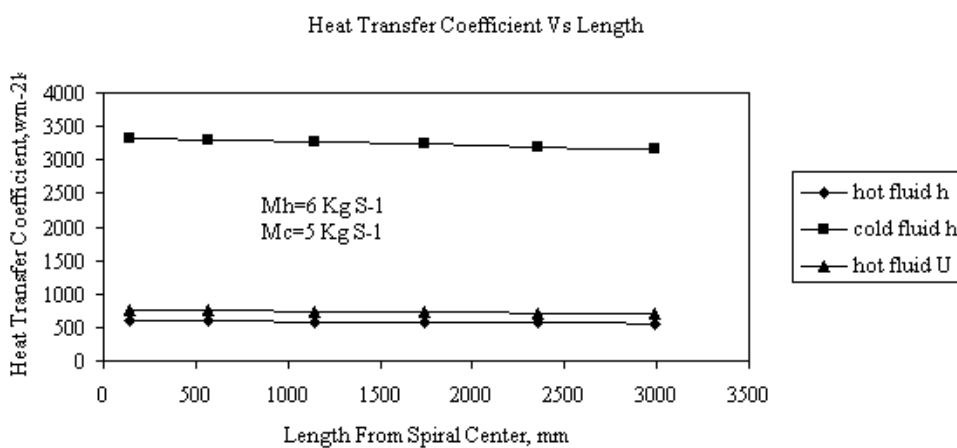


Figure 4.2 Heat transfer coefficient vs length from spiral center

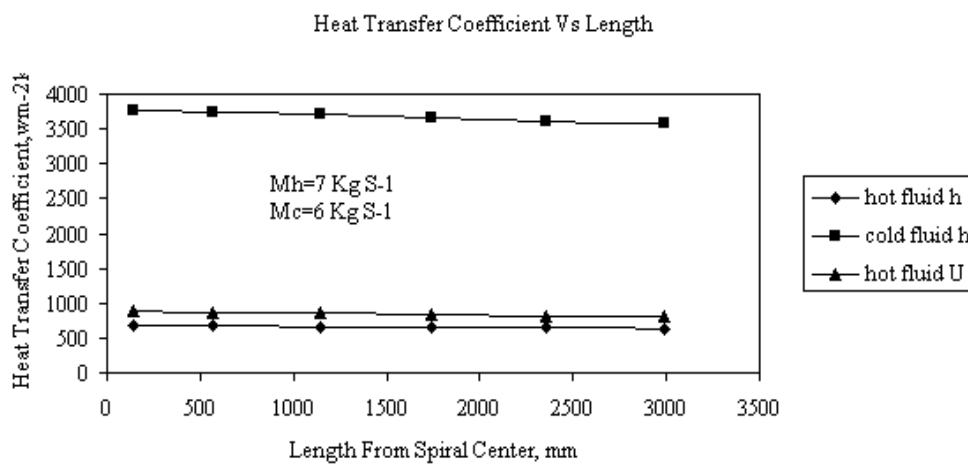


Figure 4.3 Heat transfer coefficient vs length from spiral center

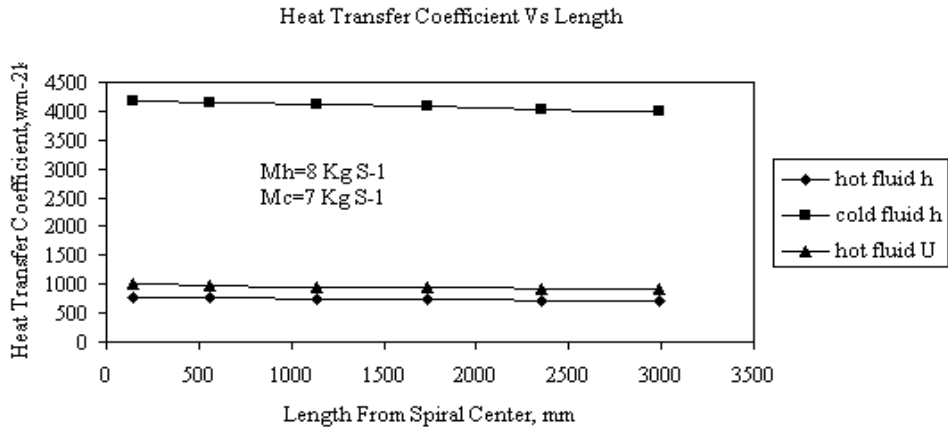


Figure 4.4 Heat transfer coefficient vs length from spiral center

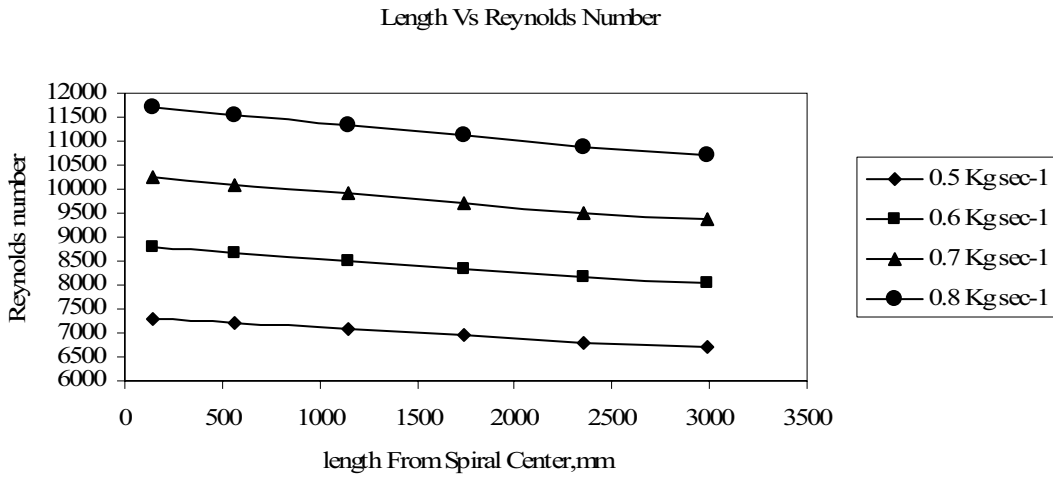


Figure 4.5 Reynolds number (water) vs. length from spiral center

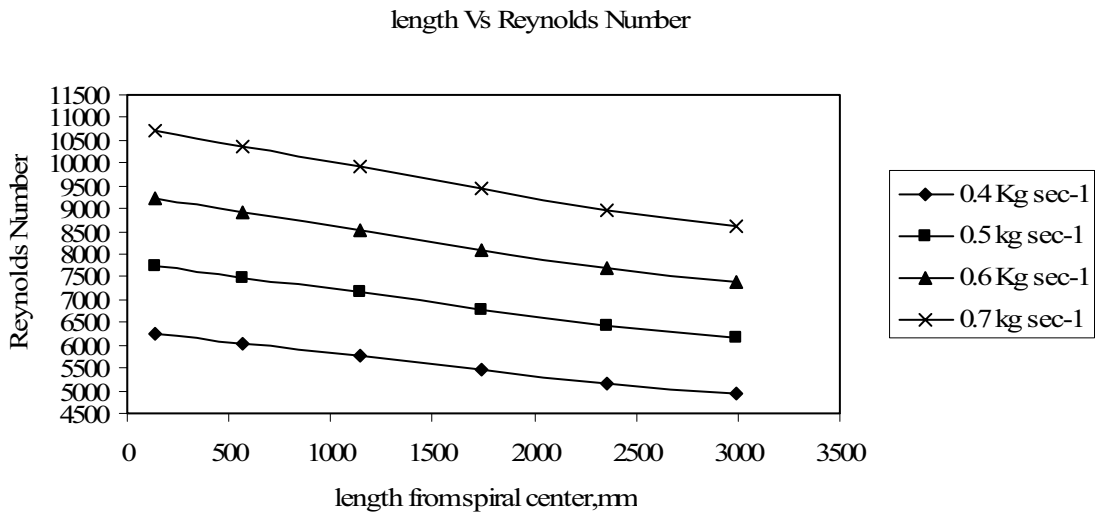


Figure 4.6 Reynolds number (benzene) vs. length from spiral center

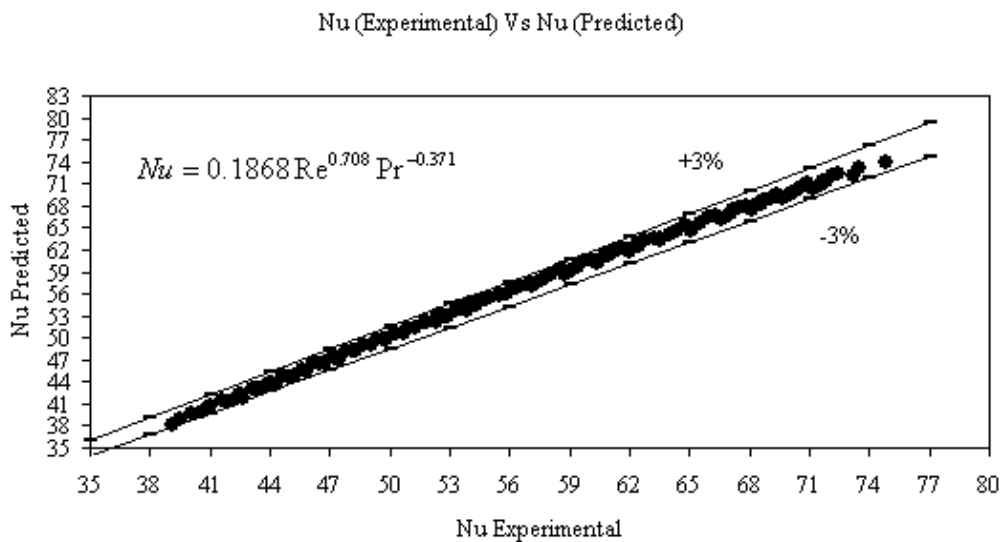


Figure 4.7 Comparison of Nusselt number (Experimental) with Nusselt number (Predicted)

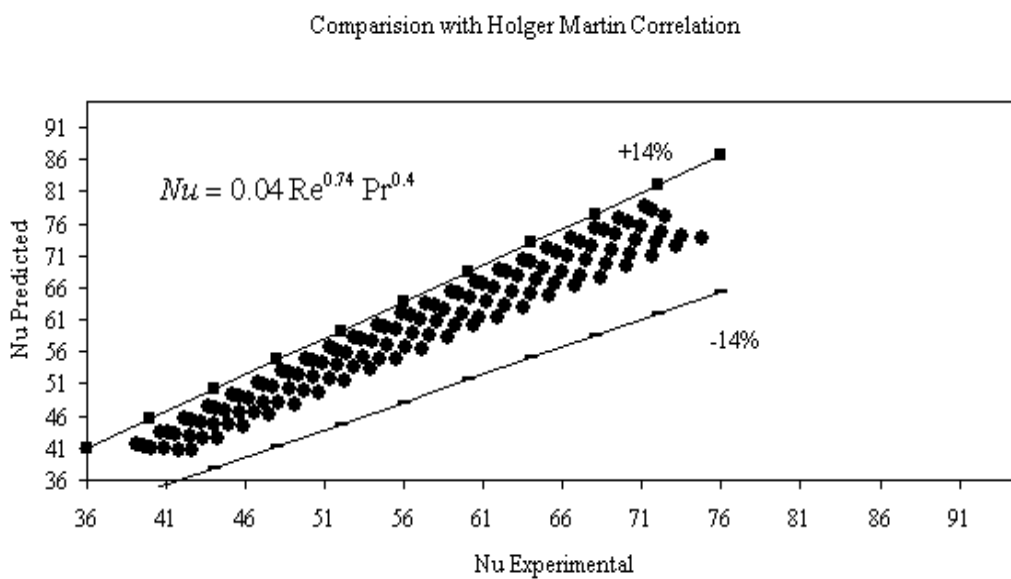


Figure 4.8 Comparison of Experimental data with Holger Martin correlation



The Shapley Value for Stochastic Cooperative Game

Ying Ma(Corresponding author)

Department of Science, Yanshan University

438 west of He Bei Avenue, Qin Huangdao 066004, China

E-mail: mymy82@163.com

Zuofeng Gao, Wei Li, Ning Jiang, Lei Guo

Department of Science, Yanshan University

438 west of He Bei Avenue, Qin Huangdao 066004, China

The research is financed by the foundation for the edbiz of He Bei province of China(2004468)and the foundation for the natural science of He Bei province of China(A2005000301)

Abstract

In this paper we extend the notion of Shapley value to the stochastic cooperative games. We give the definition of marginal vector to the stochastic cooperative games and we define the Shapley value for this game. Furthermore, we discuss the axioms of the Shapley value and give the proofs of these axioms.

Keywords: Stochastic cooperative game, Shapley value, Marginal vector, Carrier

1. Introduction

In general, the payoffs of a coalition in cooperative games are assumed to be known with certainty. In many cases, however, payoffs to coalitions are uncertain. If the formation of coalitions and allocations has to take place before the payoffs are realized, standard cooperative game theory can not be applied.

Suijs et al. (1995) considered cooperative games with stochastic payoffs, the model introduced by Suijs et al. (1995) is explicitly incorporates preferences on stochastic payoffs for each agent and allows each coalition to choose from several actions.

Suijs et al. (1999) continue on the model introduced by Suijs et al. (1995). They extend the definitions of superadditivity and convexity for TU games to stochastic cooperative games. Furthermore, they show that a stochastic cooperative game has a nonempty core.

In this paper we take the model introduced by Suijs et al. (1999) as a basis. We define the Shapley value of stochastic cooperative games. Furthermore, we discuss the axioms of the Shalely value.

This paper is organized as follows. In section2 we introduce basic definitions concerning stochastic cooperative games. Section3 presents our main results. The axioms for Shapley value of stochastic cooperative game.

2. Stochastic cooperative games

Let us first recall some of the definitions concerning stochastic cooperative games as introduced by Suijs et al. (1999). A stochastic cooperative game is described by a tuple

$$\Gamma = (N, \{A_S\}_{S \subseteq N}, \{X_S\}_{S \subseteq N}, \{\geq_i\}_{i \in N})$$

where N is the set of agents, A_S the nonempty and finite set of actions a coalition S can take, $X_S : A_S \rightarrow L^1(R)$ the payoff function of coalition S , assigning to each action $a \in A_S$ a stochastic payoff $X_S(a) \in L^1(R)$ with finite expectation, and \geq_i the preference relation of agent i over the set $L^1(R)$ of stochastic payoffs with finite expectation.

We assume that for each player the preferences are complete, transitive and continuous. Furthermore, we assume that $P(X_\emptyset(a) = 0) = 1$ for all $a \in A_\emptyset$. The class of all cooperative games with stochastic payoffs with agent set N is denoted by $SG(N)$. To simplify notation, however, we restrict our attention to the case that each coalition only has one action to take, that is, $|A_S| = 1$ for all $S \subseteq N$. So we can denote a stochastic cooperative game by $\Gamma = (N, \{X_S\}_{S \subseteq N}, \{\geq_i\}_{i \in N})$.

For our definition of the Shapley value of stochastic cooperative game, we first give the definition of marginal vector.

Let (N, v) be a game and let Π_N be the set of all permutations of N . Then the k th coordinate of the marginal vector $m^\pi(v), \pi \in \Pi_N$, is defined by

$$m_k^\pi(v) = v(\langle j | \pi(j) \leq \pi(k) \rangle) - v(\langle j | \pi(j) < \pi(k) \rangle)$$

Now we extend the notion of marginal vector to the stochastic cooperative games.

Let $\Gamma = (N, \{X_S\}_{S \subseteq N}, \{\geq_i\}_{i \in N})$ be a stochastic cooperative game, and let Π_N be the set of all permutations of N . Then the k th coordinate of the marginal vector $m^\pi(\Gamma), \pi \in \Pi_N$ is defined by

$$m_k^\pi(\Gamma) = X_{\langle j | \pi(j) \leq \pi(k) \rangle} - X_{\langle j | \pi(j) < \pi(k) \rangle}$$

Before we give the definition of Shapley value of stochastic cooperative game, we define some useful notions.

1. (Carrier) Let $\Gamma = (N, \{X_S\}_{S \subseteq N}, \{\geq_i\}_{i \in N})$ be a stochastic cooperative game, $T \subseteq N$ is called a carrier for the game if $X_S = X_{S \cap T}$ for all $S \subseteq N$.

There have two properties of the carrier:

(1). Let T be the carrier of Γ , then for all $T \subseteq T' \subseteq N$, T' is the carrier of Γ too.

Because, for all $S \subseteq N$, we have

$$\begin{aligned} X_{S \cap T'} &= X_{(S \cap T') \cap T} \\ &= X_{S \cap T} \\ &= X_S \end{aligned}$$

(2). Let T be the carrier of Γ , $i \notin T$, then for all $S \subseteq N$, we have

$$\begin{aligned} X_{S \cup \{i\}} &= X_{(S \cup \{i\}) \cap T} \\ &= X_{S \cap T} \\ &= X_S \end{aligned}$$

2. (Dummy player) The player $k \in N$ is a dummy in the stochastic cooperative game $\Gamma = (N, \{X_S\}_{S \subseteq N}, \{\geq_i\}_{i \in N})$ if for every $S \subseteq N$ such that $k \notin S$ and $S \cup \{k\} \in N$, we have

$$X_{S \cup \{k\}} = X_S = 0$$

We can describe the Shapley value as the average of the marginal vectors of the player i to the coalitions.

Then we extend the Shapley value to the stochastic cooperative games.

If $\Gamma = (N, \{X_S\}_{S \subseteq N}, \{\geq_i\}_{i \in N})$ is a stochastic cooperative game, then the Shapley value for the player $i (i \in N)$ is

$$\varphi_i(\Gamma) = \sum_{S \subseteq N \setminus \{i\}} \frac{|S|!(n-|S|-1)!}{n!} m_i^\pi(\Gamma) \tag{1}$$

3. Axioms for the Shapley value

We give one axiomatization for the Shapley value of stochastic cooperative game. We consider the axioms:

1. (Efficiency) If T is a carrier of Γ , then $\sum_{i \in T} \varphi_i(\Gamma) = X_T(\Gamma)$.

2. (Symmetry) If π is a permutation of N , such that $X_{\pi S} = X_S$ for all $S \subseteq N$. (2)

Then $\varphi_{\pi i}(\Gamma) = \varphi_i(\Gamma)$ for all $i \in N$.

3. (Additivity) If Φ and $\Psi \in SG(N)$, we have $\varphi_i(\Phi + \Psi) = \varphi_i(\Phi) + \varphi_i(\Psi)$

for all $i \in N$.

Then the Shapley value of stochastic cooperative game is the vector that satisfies the axioms above.

$$\varphi(\Gamma) = (\varphi_1(\Gamma), \varphi_2(\Gamma), \dots, \varphi_n(\Gamma)) \tag{3}$$

Lemma1. The definition of (1)

$$\varphi(\Gamma) = (\varphi_1(\Gamma), \varphi_2(\Gamma), \dots, \varphi_n(\Gamma))$$

is the Shapley value of $SG(N)$.

Proof. (1) Efficiency axiom. Let T be the carrier of Γ , according to the property (2) of the carrier, we have $X_{S \cup \{i\}} = X_S$, for all $i \in N \setminus T$, for all $S \subseteq N$, then for all $i \in N \setminus T$, we get

$$\varphi_i(\Gamma) = \sum_{S \subseteq N \setminus \{i\}} \frac{|S|!(n-|S|-1)!}{n!} m_i^\pi(\Gamma) = 0$$

such that

$$\begin{aligned} X_T &= X_{N \cap T} \\ &= X_N \\ &= \sum_{i \in N} \varphi_i(\Gamma) \\ &= \sum_{i \in T} \varphi_i(\Gamma) \end{aligned}$$

(2). Symmetry axiom. Let π be a permutation of N , which satisfies formula (2), then we have $|\pi S| = |S|$, and for each $i \in N$, such that

$$\begin{aligned} \varphi_{\pi i}(\Gamma) &= \sum_{\pi S \subseteq N \setminus \{\pi i\}} \frac{|\pi S|!(n-|\pi S|-1)!}{n!} m_{\pi i}^\pi(\Gamma) \\ &= \sum_{S \subseteq N \setminus \{i\}} \frac{|S|!(n-|S|-1)!}{n!} m_i^\pi(\Gamma) \\ &= \varphi_i(\Gamma) \end{aligned}$$

(3). Additivity axiom. Because $\varphi_i(\Gamma)$ is the linear function of Γ , $i = 1, 2, \dots, n$, $\varphi(\Gamma)$ satisfies the additivity axiom obviously.

Above all, $\varphi(\Gamma)$ is the Shapley value of Γ .

Lemma2. Define the function X^T :

$$X_S^T = \begin{cases} 1 & S \supseteq T \\ 0 & \text{otherwise} \end{cases} \text{ for all } T \subseteq N, T \neq \emptyset.$$

then for each constant $c \geq 0$, cX^T is the characteristic function, and each Shapley value Φ of cX^T satisfies

$$\varphi_i(cX^T) = \begin{cases} 0 & i \notin T \\ \frac{c}{|T|} & i \in T \end{cases}$$

Proof. It is easy to prove that cX^T is the characteristic function, and T is a carrier of cX^T .

While $i \in N \setminus T$, T and $T \cup \{i\}$ are carriers of cX^T , then according to efficiency axiom, we have

$$\begin{aligned} \sum_{j \in T} \varphi_j(cX^T) &= cX_T^T = cX_{T \cup \{i\}}^T = \sum_{j \in T \cup \{i\}} \varphi_j(cX^T) \\ &= \sum_{j \in T} \varphi_j(cX^T) + \varphi_i(cX^T) \end{aligned}$$

Hence $\varphi_i(cX^T) = 0$, for all $i \notin T$.

While $i, j \in T$, and $i \neq j$, let π be a permutation of N , such that

$$\pi k = \begin{cases} j, & k = i, \\ i, & k = j, \\ k, & k \neq i, j. \end{cases}$$

First we prove $cX_{\pi S}^T = cX_S^T$ for all $S \subseteq N$.

The reason is: If $S \supseteq T$, then $\pi S \supseteq \pi T = T$, such that $cX_{\pi S}^T = c = cX_S^T$.

Otherwise, then while $i \notin S$, we have $j \notin \pi S$;

while $j \notin S$, we have $i \notin \pi S$;

while $k \notin S$ and $k \in T \setminus \{i, j\}$, we have $k \notin \pi S$, such that $\pi S \supseteq N \setminus T$.

Hence $cX_{\pi S}^T = 0 = cX_S^T$.

According to the symmetry axiom, we have $\varphi_j(cX^T) = \varphi_{\pi j}(cX^T) = \varphi_i(cX^T)$, then from the efficiency axiom, we know $|T|\varphi_i(cX^T) = \sum_{i \in T} \varphi_i(cX^T) = cX^T = c$, for all $i \in T$, hence

$$\varphi_i(cX^T) = \frac{c}{|T|}, \text{ for all } i \in T$$

Lemma3. The characteristic function of stochastic cooperative game Γ can describe as

$$X^{cT} = \sum_{\emptyset \neq T \subseteq N} c_T X^T, \tag{4}$$

where X^T is defined in Lemma2, and $c_T = \sum_{U \subseteq T} (-1)^{|T|-|U|} X_U$. (5)

Proof. According to the definitions of X^T and c_T , for all $S \subseteq N$, we have

$$\begin{aligned} (\sum_{\emptyset \neq T \subseteq N} c_T X^T)(S) &= \sum_{\emptyset \neq T \subseteq N} c_T X_S^T \\ &= \sum_{\emptyset \neq T \subseteq N} c_T \\ &= \sum_{\emptyset \neq T \subseteq N} \sum_{U \subseteq T} (-1)^{|T|-|U|} X_U \\ &= \sum_{U \subseteq S} (\sum_{U \neq T \subseteq S} (-1)^{|T|-|U|}) X_U \\ &= \sum_{U \subseteq S} \sum_{t=|U|}^{|S|} (-1)^{t-|U|} \binom{|S|-|U|}{t-|U|} X_U \end{aligned}$$

Then according to the binomial theorem of combinatorial mathematics, we have

$$\sum_{i=0}^r (-1)^i \binom{r}{i} = 0 \text{ for all } r \in N_+, \text{ then } \sum_{t=|U|}^{|S|} (-1)^{t-|U|} \binom{|S|-|U|}{t-|U|} = 0, \text{ for all } U \subset S.$$

So $(\sum_{\emptyset \neq T \subseteq N} c_T X^T)(S) = X_S$, for all $S \subseteq N$. We have proved formula (4).

Theorem1. If $\Gamma \in SG(N)$ is a stochastic cooperative game, then the definition of $\varphi(\Gamma)$ in formula (3) is the only Shapley value of Γ .

Proof. From Lemma1. we know that $\varphi(\Gamma)$ which defined in formula (3) is indeed the Shapley value of Γ .

Then by Lemma3. we have that

$$X_S = \sum_{\substack{\emptyset \neq T \subseteq N \\ c_T \geq 0}} c_T X_S^T - \sum_{\substack{\emptyset \neq T \subseteq N \\ c_T < 0}} (-c_T) X_S^T$$

According to Lemma2. the two polynomials of the upper formula both are characteristic functions. And their difference X_S is also a characteristic function. Hence it can be proved by the additivity axiom that each Shapley value $\Phi(\Gamma)$ of Γ satisfies

$$\varphi_i(\Gamma) = \sum_{\substack{\emptyset \neq T \subseteq N \\ c_T \geq 0}} \varphi_i(c_T X^T) - \sum_{\substack{\emptyset \neq T \subseteq N \\ c_T < 0}} \varphi_i(-c_T X^T)$$

for all $i \in N$. So from Lemma2. we know that

$$\varphi_i(\Gamma) = \sum_{\substack{i \in T \subseteq N \\ c_T \geq 0}} \frac{c_T}{|T|} - \sum_{\substack{i \in T \subseteq N \\ c_T < 0}} \frac{-c_T}{|T|} = \sum_{i \in T \subseteq N} \frac{c_T}{|T|}$$

for all $i \in N$. And we know the number c_T is unique derived by T and X_S , hence $\varphi_i(\Gamma)$ is unique derived by X_S , N and i , that is to say the Shapley value $\Phi(\Gamma)$ is unique derived by X_S and N .

References

- Suijs, J., & Borm, P. (1999). Stochastic Cooperative Games: Superadditivity, Convexity and Certainty Equivalents. *Games and Economic Behavior*. 27, 331-345.
- Suijs, J., Borm, P., De Waegenaere A., & Tijs S. (1999). Cooperative Games with Stochastic payoffs. *European Journal of Operational Research*. 113, 193-205.
- Khmelnitskaya B.A. (1999). Marginalist and Efficient Value for TU Games. *Mathematical Social Sciences*. 38, 45-54.
- Hamers. H., Suijs. J., Tijs S., & Borm. P. (1996). The Split Core of Sequencing Games. *Games and Economic Behavior*. 15, 165-176.
- Bilbao. J.M., & Edelman. P.H. (2000). The Shapley Value on Convex Geometries. *Discrete Applied Mathematics*. 103, 33-40.
- Bilbao. J.M., (1998). Axioms for the Shapley Value on Convex Geometries. *European Journal of Operational Research*. 110, 368-376.
- Rothschild. R., (2001). On The Use of a Modified Shapley Value to Determine The Optimal Size of a Cartel. *Journal of Economic Behavior & Organization*. 45, 37-47.
- Xie Zheng., (2004),. *Game Theory*. Chang Sha: The press of national university of defense technology. pp. 234-239.